
Electronic Thesis and Dissertation Repository

8-9-2019 10:00 AM

Differentiating the Substantia Nigra and Ventral Tegmental Area in Early-stage Parkinson's Disease Using Iron Imaging

Erind Alushaj, *The University of Western Ontario*

Supervisor: MacDonald, Penny A., *The University of Western Ontario*

Co-Supervisor: Khan, Ali R., *The University of Western Ontario*

Co-Supervisor: Owen, Adrian M., *The University of Western Ontario*

A thesis submitted in partial fulfillment of the requirements for the Master of Science degree in Neuroscience

© Erind Alushaj 2019

Follow this and additional works at: <https://ir.lib.uwo.ca/etd>



Part of the [Nervous System Diseases Commons](#)

Recommended Citation

Alushaj, Erind, "Differentiating the Substantia Nigra and Ventral Tegmental Area in Early-stage Parkinson's Disease Using Iron Imaging" (2019). *Electronic Thesis and Dissertation Repository*. 6345.
<https://ir.lib.uwo.ca/etd/6345>

This Dissertation/Thesis is brought to you for free and open access by Scholarship@Western. It has been accepted for inclusion in Electronic Thesis and Dissertation Repository by an authorized administrator of Scholarship@Western. For more information, please contact wlsadmin@uwo.ca.

Abstract

Excessive midbrain iron accumulation in Parkinson's Disease (PD) contributes to degeneration of the substantia nigra pars compacta (SNc) and ventral tegmental area (VTA). Despite this understanding, there are no validated PD biomarkers. Magnetic resonance imaging (MRI) can localize and quantify brain iron for diagnosis of PD. Seventeen early-stage PD patients and twenty-one controls were scanned with 3-Tesla and 7-Tesla MRI. Using quantitative susceptibility mapping (QSM) and R2* relaxometry, we analyzed the average iron content in the SNc, substantia nigra pars reticulata (SNr), and VTA. QSM detected significantly higher SNc iron content in PD patients compared to controls at both field strengths. R2* only detected differences at 7-Tesla and showed lower sensitivity and diagnostic accuracy in diagnostic biomarker analyses. As predicted, the SNr and VTA were spared from iron accumulation. SNc iron overload in early-stage PD, best detected using QSM, could be the first diagnostic biomarker of PD following validation.

Keywords

Parkinson's disease; iron; MRI; QSM; R2*; biomarker; substantia nigra; ventral tegmental area

Summary for Lay Audience

Parkinson's disease (PD) is a neurodegenerative disorder that impacts movement and thinking. Loss of cells in a brain area called the substantia nigra contributes to PD. When neurologists diagnose PD based on clinical symptoms, up to 80% of these cells have already degenerated. Therapy becomes less effective with progressing degeneration, which means early diagnosis is vital for more effective treatment and improved patient outcome.

Excessive iron buildup in the substantia nigra cells in PD could potentially identify the degeneration based on previous research findings. This highlights an importance to precisely locate and measure brain iron for potential uses in early diagnosis. Magnetic resonance imaging (MRI) can image brain iron and look for excessive iron buildup. This study aimed to use iron imaging based on MRI methods to determine if this technique can improve diagnosis of PD.

Our study used two different iron imaging techniques in two MRI scanners to measure brain iron in early-stage PD patients and healthy elderly adults. Excessive iron buildup was detected only in a subregion called the substantia nigra pars compacta (SNc), which is the first area affected by PD. The other two areas had no changes in brain iron because they are affected in later stages of PD. Consequently, iron imaging is most effective when using SNc iron levels for early diagnosis of PD. The newer iron imaging technique had better diagnostic accuracy when using SNc iron to sort PD patients from healthy adults. Our research suggests newer iron imaging techniques could diagnose PD though more work is needed to determine its accuracy and reliability in clinical settings. This research could have a major impact on our understanding of PD, the way it is diagnosed, and ultimately the improvement of patients' lives.

Acknowledgements

First off, I would like to thank my supervisors Dr. Penny MacDonald, Dr. Ali Khan, and Dr. Adrian Owen for their guidance throughout this project. I want to thank Dr. MacDonald for providing assistance and guidance in all aspects of my academic, professional, and personal life. You are an incredible mentor who leads by example and somehow manages to do all of this without any sleep. A huge thank you to Dr. Khan for answering all of my methodological and technical questions, no matter how simple they may have been. With your help, I was able to acquire the neuroimaging processing skills necessary to complete this work. In addition, I would like to thank Dr. Adrian Owen for his backing and support of my research project.

I am also grateful for the feedback and support that I received from my advisory committee members: Dr. Jody Culham and Dr. Derek Mitchell. I would like to thank my lab members and friends for always being by my side. Chad, Mark, and Sonia these two years flew by with our adventures and all the laughs we shared together. I would like to thank Nick for his assistance and friendship; you are the other half of the Basal Ganglia Gemini, the Aquaman to my Ironman.

Funding was generously provided by a Canada Institutes for Health Research (CIHR) Frederick Banting and Charles Best Canada Graduate Scholarship – Masters and Parkinson Society Southwestern Ontario Graduate Student Scholarship awarded to Erind Alushaj; along with several grants from Natural Sciences and Engineering Research Council of Canada (NSERC), CIHR, Canada Research Chairs (CRC), Canada Excellence Research Chairs (CERC), and Canada First Research Excellence Fund (CFREF) BrainsCAN awarded to my supervisors.

Së fundi, dua të falënderoj familjen time për mbështetjen dhe dashurin e tyre. Newton tha: “Nëse kam parë më larg se burrat e tjerë, është për shkak se kam qëndruar mbi supet e gjigantëve.” Ju jeni gjigandët e mi.

Table of Contents

Abstract	i
Summary for Lay Audience.....	ii
Acknowledgements	iii
Table of Contents	iv
List of Tables	vi
List of Figures	vii
List of Appendices	viii
List of Abbreviations	ix
Chapter 1: Introduction	1
1.1.1 Parkinson’s Disease Pathology in the Midbrain	1
1.1.2 The Role of Iron in Parkinson’s Disease Pathology	2
1.1.3 The Need for Biomarkers of Parkinson’s Disease	8
1.2.1 Iron Imaging Using Magnetic Resonance Imaging	9
1.2.2 Relaxometry and Susceptibility Weighted Imaging	10
1.2.3 Quantitative Susceptibility Mapping	11
1.3.1 Rationale	12
1.3.2 Objectives	13
1.3.3 Predictions	13
Chapter 2: Methods	14
2.1 Participants	14
2.2 Questionnaires	14
2.3 MRI Data Acquisition	15
2.4 MRI Data Postprocessing	16
2.5 Statistical Analyses	19
Chapter 3: Results	21
3.1.1 Demographics	21
3.2.1 QSM in the SNc	21
3.2.2 R2* in the SNc	24

3.2.3 ROC Curve Analyses in the SNc	26
3.3.1 QSM in the SNr	28
3.3.2 R2* in the SNr	30
3.4.1 QSM in the VTA	32
3.4.2 R2* in the VTA	34
3.5.1 Dice Similarity Coefficients between Scanners	36
 Chapter 4: Discussion	 37
4.1 General Summary of Results	37
4.2 Assessment of Iron Imaging as a Diagnostic Biomarker of PD	38
4.3 Comparison of Iron Imaging with Other Imaging Biomarkers	41
4.4 Limitations	42
4.5 Future Directions	43
4.6 Conclusions	45
 References	 46
Appendices	69
Curriculum Vitae	93

List of Tables

Table 1: Demographics and clinical information for early-stage PD patients and controls 21

List of Figures

Figure 1: Neurotoxicity of iron-dopamine interactions underlying PD pathology in dopaminergic neurons	7
Figure 2: Segmentation of midbrain nuclei on QSM and R2* maps of a healthy control	18
Figure 3: Average susceptibility for the SNc of early-stage PD patients and healthy controls at 3T and 7T	23
Figure 4: Average R2* values for the SNc of early-stage PD patients and healthy controls at 3T and 7T	25
Figure 5: ROC curves for MAH and LAH of SNc average susceptibility at 3T and 7T	27
Figure 6: ROC curves for MAH and LAH of SNc average R2* value at 3T and 7T	27
Figure 7: Average susceptibility for the SNr of early-stage PD patients and healthy controls at 3T and 7T	29
Figure 8: Average R2* values for the SNr of early-stage PD patients and healthy controls at 3T and 7T	31
Figure 9: Average susceptibility for the VTA of early-stage PD patients and healthy controls at 3T and 7T	33
Figure 10: Average R2* values for the VTA of early-stage PD patients and healthy controls at 3T and 7T	35
Figure 11: Dice similarity coefficients between scanners for midbrain structures of PD patients and controls	36

List of Appendices

Appendix A: Participant Inclusion/Exclusion Criteria	69
Appendix B: Consent Form	70
Appendix C: Health & Demographics Questionnaire	81
Appendix D: Montreal Cognitive Assessment	83
Appendix E: Montreal Cognitive Assessment Evaluation Scale	84
Appendix F: UPDRS-III Protocol	88
Appendix G: Covariate Analysis for Age and Sex	89
Appendix H: ROC Curve Analyses of Left and Right Hemisphere SNc	91
Appendix I: Ethics Approval	92

List of Abbreviations

PD	Parkinson's Disease
SN	Substantia nigra
SNC	Substantia nigra pars compacta
SNr	Substantia nigra pars reticulata
VTA	Ventral tegmental area
6-OHDA	6-hydroxydopamine
MPTP	1-methyl-4-phenyl-1,2,3,6-tetrahydropyridine
MRI	Magnetic resonance imaging
GRE	Gradient echo
SWI	Susceptibility weighted imaging
QSM	Quantitative susceptibility mapping
CIT168	California Institute of Technology 168
T	Tesla
ROC	Receiver operating characteristic
MoCA	Montreal Cognitive Assessment
UPDRS-III	Unified Parkinson's Disease Rating Scale Part III
T1w	T1-weighted
MPRAGE	Magnetization-prepared rapid gradient echo
TR	Repetition time
TE	Echo time
FoV	Field of view
MP2RAGE	Magnetization-prepared 2 rapid gradient echo

FSL	FMRIB Software Library
ANTs	Advanced Normalization Tools
BEaST	Brain Extraction based on nonlocal Segmentation Technique
FLIRT	FMRIB's Linear Image Registration Tool
ANOVA	Analysis of variance
ppb	parts per billion
RM-ANCOVA	Repeated measures analysis of covariance
MAH	More affected hemisphere
LAH	Less affected hemisphere
AUC	Area under the curve
RM-ANOVA	Repeated measures analysis of variance
DWI	Diffusion-weighted imaging
CSF	Cerebrospinal fluid
REM	Rapid eye movement
RBD	Rapid eye movement sleep behaviour disorder
MSA	Multiple system atrophy
LBD	Lewy body dementia

Chapter 1: Introduction

1.1.1 Parkinson's Disease Pathology in the Midbrain

Dr. James Parkinson first described Parkinson's disease (PD) in his work titled, 'An Essay on the Shaking Palsy' (Parkinson, 1817). While he described the motor symptoms of PD, he stated that the senses and intellects are uninjured in the disease (Parkinson, 1817). Since then, research has shown that PD does in fact present with non-motor symptoms such as anxiety, depression, and difficulty with concentration (Barone et al., 2009; Pfeiffer, 2016). These non-motor symptoms occur in almost all PD patients (98.6%) with about eight symptoms per patient based on a large-scale multi-centre study (Barone et al., 2009). To better understand the symptomology of PD, we must assess the underlying pathology that causes this progressive, neurodegenerative disorder.

The substantia nigra (SN) is composed of two distinct subregions: the substantia nigra pars compacta (SNc) and the substantia nigra pars reticulata (SNr; Gibb & Lees, 1991). The cardinal feature of PD is the loss of midbrain dopaminergic neurons in the SNc (Hornykiewicz, 1998). Degeneration of the SNc neurons produces the core motor symptoms of PD: resting tremor, rigidity, postural instability, and bradykinesia or slowness of movement (Fahn & Sulzer, 2004; Jankovic, 2008). Using histological assessment of PD brains, Gibb and Lees (1991) found the ventral tier of the SNc had few surviving neurons with cell preservation in the dorsal tier. In humans, the ventral SNc neurons project to the putamen and dorsal caudate regions of the striatum (Smith & Parent, 1986). Thus, loss of ventral SNc neurons results in greater dopamine depletions in these striatum regions, creating an uneven pattern of dopamine depletion in PD (Gibb & Lees, 1991; Kish, Shannak, & Hornykiewicz, 1988).

At disease onset, PD will impact one side of the body more than the other, thus presenting in an asymmetric fashion (Verreyt, Nys, Santens, & Vingerhoets, 2011). A demographic study of over 300 PD patients found that about 85% showed asymmetric symptom presentation (Yust-Katz, Tesler, Treves, Melamed, & Djaldetti, 2008). This asymmetry remains throughout the disease course and is associated with uneven dopaminergic degeneration in the ventral SNc (Verreyt et al., 2011). Asymmetry is an important clinical feature in early-stage PD and further highlights the uneven dopamine depletion (Jankovic, 2008). This pattern of selective neuron degeneration is unrelated to ageing processes, which preferentially affect the dorsal SNc (Scherman et al., 1989). In addition, post-mortem ageing studies found an SNc neuronal loss of 5-6% per decade, which

cannot account for the degeneration of 60-80% of neurons at the time of PD diagnosis (Fearnley & Lees, 1991; Scherman et al., 1989). It is evident that degeneration in the SNc is central to PD pathology, with vulnerability differences in dorsal and ventral tiers, as well as brain hemispheres.

Early research into the ventral tegmental area (VTA) assumed this dopaminergic midbrain nucleus was spared in PD due to: the different neuronal population (Nair-Roberts et al., 2008), differences in calcium channel expression (Mosharov et al., 2009), lower expression of dopamine transporters (Lammel et al., 2008), and the different levels of α -synuclein (Pan & Ryan, 2012). A literature review later revealed the VTA unequivocally degenerates in PD and its dopaminergic neuronal loss can explain the non-motor symptoms of PD (Alberico, Cassell, & Narayanan, 2015). For example, loss of VTA projections to the ventral striatum and prefrontal cortex could explain why 25% of PD patients experience anxiety or depression (Aarsland et al., 2010) and nearly 30% have executive dysfunction (Elgh et al., 2009). Though this is made with caution as dopaminergic systems are not the only ones affected in PD progression (Narayanan, Rodnitzky, & Uc, 2013).

Recognition of the vulnerability of the VTA helped researchers appreciate why the area is affected later on and to a lesser extent than the SNc (Alberico et al., 2015). Reyes and colleagues (2012) found higher co-expression of calbindin and tyrosine hydroxylase, the dopamine producing enzyme, in the VTA. This co-expression results in lower dopamine release, which may result in less oxidative stress and neurotoxicity (Alberico et al., 2015). In a recent study, Hare and colleagues (2014) assessed an iron-dopamine co-expression index as a marker of PD susceptibility to oxidative stress. In their mouse model of PD, the SNc had a significantly higher iron-dopamine index than the VTA when accounting for differences in nucleus size, which suggests a higher susceptibility to oxidative stress in the SNc (Hare et al., 2014). The properties of iron, its abundance in the midbrain, and its involvement in generation of oxidative stress make iron a useful tool for understanding these nuclei and their role in PD pathophysiology.

1.1.2 The Role of Iron in Parkinson's Disease Pathology

Research has provided evidence supporting an oxidative stress hypothesis playing a major role in PD pathology (Chinta & Andersen, 2008). The brain is most susceptible to oxidative stress because of the presence of high amounts of polyunsaturated fatty acids, low levels of antioxidants such as glutathione, and elevated iron content (Chinta & Andersen, 2008; Sies & Cadenas, 1985). Oxidative damage in PD includes increased lipid peroxidation products, protein oxidation

including cross-linking, fragmentation and carbonyl group formation, as well as DNA oxidation products (Jenner, 2003). It is not clear, however, if oxidative stress in PD is a primary event or consequent to other cellular dysfunctions (Chinta & Andersen, 2008).

Oxidative stress is essential for the generation of PD symptomology in established animal models of the disorder (Chinta & Andersen, 2008). For example, 6-hydroxydopamine (6-OHDA), a common neurotoxin is known to destroy dopaminergic neurons through free radical-mediated mechanisms (Blum et al., 2001; Hare et al., 2014). Similarly, 1-methyl-4-phenyl-1,2,3,6-tetrahydropyridine (MPTP) inhibits mitochondrial complex I which enhances superoxide formation that initiates neuronal death (Blum et al., 2001; Pennathur, Jackson-Lewis, Przedborski, & Heinecke, 1999). These observations lend support to oxidative stress being a primary event as two well-established PD animal models require the presence of oxidants for symptom generation.

Furthermore, antioxidants such as glutathione are drastically depleted in the SNc of PD patients (Bharath, Hsu, Kaur, Rajagolapan, & Andersen, 2002; Sofic, Lange, Jellinger, & Riederer, 1992). Glutathione depletion parallels PD severity and is the earliest known indicator of SNc degeneration, reportedly preceding changes in striatal dopamine and mitochondrial complex I (Jenner, 1993; Jenner & Olanow, 1996). Decreased glutathione promotes mitochondrial damage, protein oxidation, protein aggregation, and reduced mitochondrial complex I activity (Albers & Beal, 2000; Haas et al., 1995). The depleted glutathione is specific to the SNc of PD patients, with no major alterations to other dopaminergic neurons (Bharath et al., 2002). Research suggests this depletion is caused by increased removal of SNc glutathione because synthesis of glutathione and its oxidation are intact in early-stage PD (Sian et al., 1994). These observations suggest an early redox imbalance exists in PD with reduced antioxidants, which promote oxidative stress. Therefore, oxidative stress could exist as both an initiator of neurodegeneration and a component of the pathogenetic process accelerating neuronal loss (Berg, Youdim, & Reiderer, 2004).

As an abundant oxidant in the SNc, iron also plays a role in the redox imbalance, which could explain PD pathology. The first investigations of brain iron were conducted by Spatz (1922) who found the SN and globus pallidus gave the strongest iron reaction when using histology (Friedman & Galazka-Friedman, 2012). Regions of the brain associated with motor behaviour tend to have higher iron than non-motor areas (Crichton & Ward, 2014). Hallgren and Sourander (1958) followed up this work by assessing the effects of age on iron in the brain. Rapid increases occur in the first two decades, followed by a slower increase in these 'high iron' structures throughout the

lifespan (Hallgren & Sourander, 1958). The majority of brain iron is stored in the protein ferritin that forms a large protein cage in which thousands of Fe(3+) atoms are sequestered in mineral ferrihydrite form (Honarmand Ebrahimi, Hagedoorn, & Hagen, 2015). Looking at post-mortem iron and ferritin levels, Dexter and colleagues (1991) found elevated iron and reduced ferritin in the SNc of PD patients. The authors proposed that the release of iron from ferritin causes oxidative stress and cell death through free radical generation (Dexter et al., 1991).

Another iron-binding molecule linked with PD vulnerability is the pigment neuromelanin (Zucca et al., 2017). Neuromelanin is the major iron storage molecule in dopaminergic neurons of human SNc where it also acts as an 'iron sink' and a potential source of toxic iron if its capacity becomes saturated (Hirsch, Graybiel, & Agid, 1988; Zecca et al., 2001a; Zecca et al., 2001b; Zecca, Youdim, Riederer, Conner, & Crichton, 2004; Zucca et al., 2014). Neuromelanin has a ferritin-like center that binds iron with high affinity, where iron is stabilized (Aime et al., 1997; Shima et al., 1997), and another site which binds iron with lower affinity (Zucca et al., 2017). It may be that once high affinity sites of neuromelanin are saturated, the excess iron in PD may bind lower affinity sites from where it can be released as 'free' iron (Zucca et al., 2017).

Interestingly, glutathione is the natural ligand for 'free' iron found in the labile iron pool (Guiney, Adlard, Bush, Finkelstein, & Ayton, 2017). This labile iron pool is defined as a pool of chelatable and redox-active iron in complexes of low stability that is between uptake and long-term storage (Guiney et al., 2017; Zucca et al., 2017). The depletion of glutathione in PD leads to an increase in free iron within the labile iron pool, which could have neurotoxic effects (Kaur, Lee, Ragapolan, & Andersen, 2009). With ageing and degenerative processes such as PD, there is an abnormal, progressive deposition of iron and increased free iron concentration in the SNc of PD patients (Sian-Hulsman, Mandel, Youdim, & Riederer, 2011).

In PD, there is also a change in the type of free iron that is found in cells. The ratio of Fe(2+) to Fe(3+) increases from 1:2 to almost 2:1, which allows Fe(2+) to form hydroxyl radicals via the Fenton and Haber-Weiss reactions, ultimately causing oxidative stress (Dexter et al. 1991; Riederer et al. 1989; Sofic et al. 1988). In the presence of reduced metals such as Fe(2+), hydrogen peroxide can be converted into hydroxyl radicals by the Fenton reaction and Haber-Weiss reaction (Youdim & Riederer, 1993). The hydroxyl radical is highly reactive and extremely toxic, making it the most harmful of all reactive oxygen species in oxidative stress (Crichton & Ward, 2014; Dlouhy & Outten, 2013; Sian-Hulsmann et al., 2011). Unsaturated fatty acids in cell membranes

donate electrons to hydroxyl radicals causing destruction of membranal lipids through the accumulation of lipid peroxides (Sian-Hulsmann et al., 2011). Iron accumulation can also facilitate neurotoxic processes through mechanisms apart from this Fenton chemistry (Zucca et al. 2017).

It was thought that the majority of regulated cell death in neurons resulted from caspase-dependent apoptosis, which could explain the underlying cause of PD (Fuchs & Steller, 2011; Thompson, 1995). In fact, neurodegenerative mechanisms originating from iron toxicity can eventually lead to classical apoptosis (Ott, Gogyadze, Orrenius, & Zhivotovsky, 2007). Recently, our understanding of PD pathology has incorporated non-apoptotic mechanisms and a unique iron-dependent form of cell death was termed ferroptosis by Dixon and colleagues (2012). Ferroptosis is initiated by the failure of glutathione-dependent antioxidant defense mechanisms and an excessive iron build-up resulting in lipid peroxide accumulation and eventual cell death (Cao & Dixon, 2016; Dixon & Stockwell, 2014). Notably, the key difference between ferroptosis and apoptosis is the release of intracellular fluid and lipid metabolites as neurons degrade through ferroptosis pathways (Hambright, Fonesca, Chen, Na, & Ran, 2017). This release leads to inflammation, which is another prominent feature of PD and other neurodegenerative diseases (Tufekci, Meuwissen, Genc, & Genc, 2012). It is evident that depleted glutathione, excess iron accumulation, and pro-oxidant redox imbalances causing oxidative stress could all worsen SNC degeneration through ferroptosis and other cell death pathways in PD.

The hypothesis of ‘iron-facilitated’ neurodegeneration is supported by *in vitro* studies showing aggregation of α -synuclein and hyper-phosphorylated tau, both of which are involved in neurodegeneration, can be triggered by iron accumulation (Hashimoto et al., 1999; Li, Jiang, Song, & Xie, 2010; Yamamoto et al., 2002). Furthermore, iron can directly promote the aggregation of amyloid- β (House et al., 2004; Schubert & Chevion, 1995) and modulate amyloid precursor protein pathways (Exley, House, Polwart, & Esiri, 2012; Silvestri & Camaschella, 2008). While ferroptosis clearly has explanatory potential for neuronal changes in PD, a concern remains regarding its ability to explain the cell type-specificity of the disorder (Zucca et al., 2017). In other words, can excess iron accumulation explain midbrain dopaminergic neuronal degeneration in PD.

First, iron is essential in the synthesis of catecholamine neurotransmitters like dopamine, epinephrine, and serotonin because these molecules are produced by iron-dependent enzymes (Beard, 2003; Flydal & Martinez, 2013; Windahl, Petersen, Christensen, & Harris, 2008). Iron also affects other steps of catecholamine metabolism, such as uptake, synaptic concentration,

receptor interaction, and catabolism (Beard, Chen, Connor, & Jones, 1994; Bianco et al., 2008; Burhans et al., 2005; Youdim, Ben-Shachar, & Yehuda, 1989; Zucca et al., 2017). Given these observations, there is already an apparent connection between iron and dopamine.

Importantly, dopamine can be oxidized to form highly toxic quinones and the rate of quinone formation greatly increases in the presence of excess iron (Figure 1; Billings et al., 2019; Paris et al., 2005; Sulzer & Zecca, 2000). Aminochrome is a quinone that under normal conditions is necessary for the formation of neuromelanin, which has neuroprotective effects and accumulates with age in SN dopaminergic neuron cell bodies (Figure 1; Bisaglia, Mammi, & Bubacco, 2007; Zecca et al., 2002). However, dopamine quinones can also participate in neurotoxic reactions. Dopamine-*o*-quinone is likely the most reactive *o*-quinone species responsible for the oxidative stress induced by DA oxidation (Bisaglia, Soriano, Arduini, Mammi, & Bubacco, 2010). The depletion of glutathione in dopaminergic neurons would be the consequence of the rapid nucleophilic addition of glutathione to dopamine-*o*-quinone (Tse, McCreery, & Adams, 1976).

Aminochrome interacts with human α -synuclein, inducing and stabilizing the formation of neurotoxic oligomers (Figure 1; Munoz et al., 2015; Norris et al., 2005). The neurotoxicity of α -synuclein oligomers depends on the silencing of DT-diaphorase enzyme, which reduces aminochrome to leukoaminochrome (Munoz et al., 2015). Aminochrome also induces protein degradation dysfunction by impairing proteasomes *in vitro* (Figure 1; Xiong, Siegel, & Ross, 2014; Zafar, Siegel, & Ross, 2006), inhibiting autophagy (Paris et al., 2010), and inducing lysosomal dysfunction (Huenchuguala et al., 2014). In addition, aminochrome forms adducts with mitochondrial complex I in dopaminergic cells, inducing mitochondria dysfunction and inhibiting ATP production (Figure 1; Aguirre et al., 2012). Lastly, aminochrome can induce oxidative stress through superoxide formation in a redox cycling between aminochrome and leukoaminochrome-*o*-semiquinone radical (Figure 1; Arriagada et al., 2004).

Clearly, there is substantial evidence to suggest that oxidative stress derived from the combined presence of low glutathione, excessive free iron, and dopamine contribute to dopaminergic neuronal loss in PD and the pathology of this disorder. Regardless of the status of iron accumulation as either a primary or secondary neurodegenerative event, the overload is a potential marker of the parkinsonian disease state (Ayton & Lei, 2014).

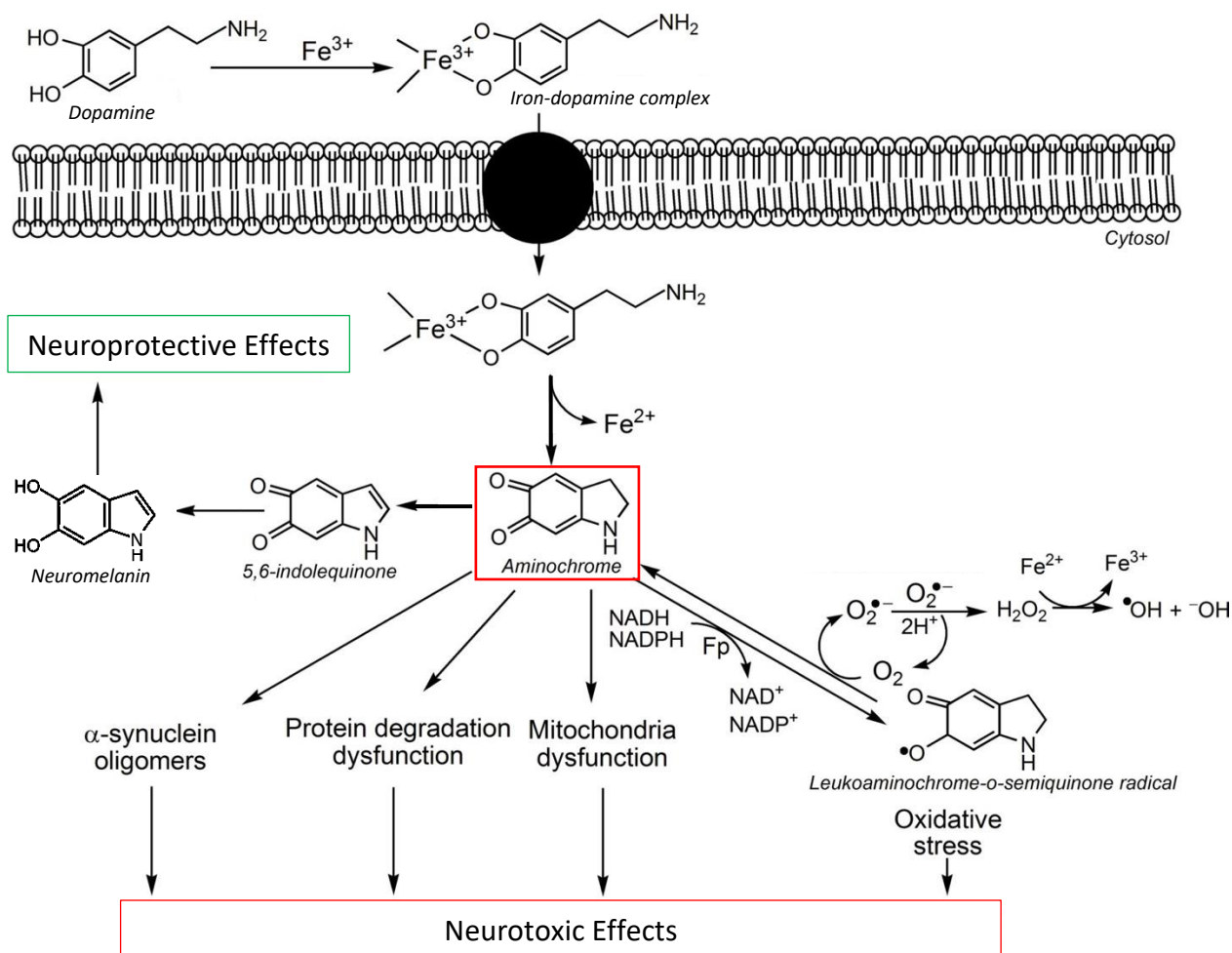


Figure 1. Neurotoxicity of iron-dopamine interactions underlying PD pathology in dopaminergic neurons. Dopamine forms a complex with Fe^{3+} that is taken up into the cell where iron oxidizes dopamine to aminochrome. Then aminochrome can polymerize to neuromelanin via 5,6-indolequinone affording neuroprotection. Aminochrome-induced neurotoxic reactions include: α -synuclein oligomerization, protein degradation dysfunction, mitochondria dysfunction, and oxidative stress caused by redox cycling between aminochrome and leukoaminochrome-o-semiquinone radical. This redox cycling forms superoxide then hydrogen peroxide, which in the presence of ferrous iron forms hydroxyl radical leading to high oxidative stress. (Adapted from Zucca et al., 2017).

1.1.3 The Need for Biomarkers of Parkinson's Disease

Biomarkers are a broad subcategory of medical signs, which reflect a characteristic of biological processes and can be measured accurately and reproducibly (Strimbu & Tavel, 2011). Currently, there are no validated biomarkers of PD, but many groups have searched for reliable and objective biomarkers of the disease (Du, Lewis, Sica, Kong, & Huang, 2019; Khan et al., 2019; Pyatigorskaya et al., 2018; Saeed et al., 2017). Several magnetic resonance imaging (MRI) biomarkers have been used to detect SNc neurodegeneration (Pyatigorskaya et al., 2018). MRI techniques such as diffusion tensor imaging, neuromelanin imaging, R2* relaxometry and susceptibility mapping have shown ability to distinguish PD patients from healthy controls (Pyatigorskaya et al., 2018). Although several candidates have been discovered, important challenges remain in translation to clinical practice and clinical trials research (Du et al., 2019).

Biomarkers of PD can be classified into *diagnostic*, *progression*, and *preclinical* categories (He et al., 2018; Khan et al., 2019). Diagnostic biomarkers can distinguish PD patients from controls and ideally other Parkinsonian disorders, as they enter the clinical phase of the disease. Progression biomarkers change over the course of the disease allowing us to distinguish between early-stage and late-stage PD, as well as provide objective endpoints for assessing the potential of treatments to modify disease course (Khan et al., 2019). Lastly, preclinical biomarkers index biological changes in patients who are in the preclinical and prodromal stages before the onset of motor symptoms when they are actually diagnosed with PD. Preclinical biomarkers would allow us to predict the development of PD in a healthy population and to potentially intervene at earlier stages when therapy could be most effective (He et al., 2018; Postuma & Berg, 2016).

The development of reliable biomarkers is critical to aid diagnosis, improve clinical trials, and measure the efficacy of novel disease-modifying treatments (Miller & O'Callaghan, 2015; Tuite, 2016). Without diagnostic biomarkers, patients require time-consuming clinical assessment by clinicians with specialized training to diagnose PD. Furthermore, individuals without PD are inadvertently enrolled in clinical trials, which compromises their findings. Without progression biomarkers that can track disease advancement, the efficacy of disease-modifying treatments cannot be ascertained. Clinical response is highly subjective and variable due to fluctuating symptoms, making it an unreliable endpoint in clinical trials. In addition, clinical response confounds symptom alleviation with actual disease-modifying effects of a treatment that is under investigation (Strimbu & Tavel, 2010). Lastly, without preclinical biomarkers, diagnosis occurs

too late in the disease course for potential neuroprotective or therapeutic treatment as the majority of SNc neurons are compromised (Postuma & Berg, 2016). Preclinical biomarkers would improve clinical trials by inclusion of patients who are most likely to develop PD (Postuma, 2017). It is clear that biomarkers are important for diagnosis, prognosis, and prediction of PD. Biomarkers are needed to improve clinical practice along with clinical trials in PD. The discovery of PD biomarkers can lead to enhanced diagnosis, accurate tracking of disease advancement, and most importantly the improvement in patients' quality of life.

1.2.1 Iron Imaging using Magnetic Resonance Imaging

MRI allows for non-invasive, *in vivo* imaging of brain iron based on the interaction of atoms with the magnetic field (Ward, Zucca, Duyn, Crichton, & Zecca, 2014). MRI is the most powerful and sensitive imaging technique for detecting iron (Dusek, Dezortova, & Wuerfel, 2013). The interaction is based on susceptibility, a measure of the extent to which a substance becomes magnetized when placed in an external magnetic field (Duyn, 2013). Normally, susceptibility is responsible for the artefacts in MRI; however, this property can serve as the signal rather than noise and provide valuable information (Acosta-Cabronero et al., 2018; Li & Leigh, 2004).

When a substance interacts with a magnetic field, an internal magnetization or polarization is created that either opposes or augments the external field. If the polarization opposes the field, the substance is diamagnetic as is observed with water, fat and calcium (Haacke et al., 2015). If the polarization is in the same direction as the external field, then depending on the degree of this augmentation the substance is said to be paramagnetic (eg. iron salts), superparamagnetic (eg. ferritin), or ferromagnetic (eg. pure iron; Ghassaban, Liu, Jiang, & Haacke, 2019). Most biological tissues are weakly diamagnetic, but tissues with focal accumulation of iron are paramagnetic, such as the midbrain nuclei (Ropele & Langkammer, 2017).

Using conventional magnitude imaging, the findings of most neurodegenerative diseases are negative (Zhang et al., 2010). Typically, a gradient echo (GRE) sequence is used given that these sequences are more affected by susceptibility (Elster, 1993). A GRE is produced by a single radiofrequency pulse in conjunction with a gradient reversal, which refocuses only the spins that have been dephased by action of the initial radiofrequency pulse itself (Winkler, 1988). Thus, phase shifts resulting from static tissue susceptibility are not cancelled meaning these sequences are influenced by susceptibility, which allows for iron imaging (Sethi et al., 2019).

1.2.2 Relaxometry and Susceptibility Weighted Imaging

Determination of relaxation times through MRI relaxometry is most frequently used for iron quantification (Dusek et al., 2013). Following a radiofrequency pulse, nuclei lose their transverse magnetization to return to a more ‘relaxed’ state after a short period of time called T2 (Pooley, 2005). In practice, the inherent inhomogeneity of the magnetic field in each voxel accelerates this loss of transverse magnetization and the real relaxation time is T2* (Huettel, Song, & McCarthy, 2014; Pooley, 2005). Differences in magnetic susceptibility can increase field inhomogeneity (Pooley, 2005). With differences in iron concentration between regions, one can expect greater field inhomogeneities and thus T2* relaxation and its inverse parameter R2* can be used to measure iron content (Storey et al., 2007).

T2* relaxometry has shown significant increases in nigral iron content due to ageing (Sohmiya, Tanaka, Aihara, Hirai, & Okamoto, 2001) and PD (Baudrexel et al., 2010; Du et al., 2019; Martin, Wieler, & Gee, 2008). However, T2* has difficulties due to other local background sources of inhomogeneity that cause signal loss unrelated to the iron content (Haacke et al., 2005; Reichenbach et al., 1997). R2* relaxometry has also detected PD-related iron content increases *in vivo* (Gelman et al., 1999; Péran et al., 2009; Yao et al., 2009). Post-mortem validation found R2* relaxometry in grey matter linearly correlates with brain iron determined using chemical methods (Langkammer et al., 2010). However, R2* maps are affected by intravoxel spin dephasing near steep phase gradients (e.g. focal iron or air-tissue interfaces; Fernández-Seara & Wehrli, 2000).

Susceptibility weighted imaging (SWI) also relies on spin dephasing from local field inhomogeneities but independently incorporates phase information along with the magnitude data (Dusek et al., 2013). In the past, phase images were rarely used because artefacts from the background field masked the changes in biological tissue (Zhang et al., 2010). Modern SWI sequences incorporate several features to outperform traditional T2*-weighted GRE sequences: acquired in 3D mode to reduce time, flow compensated to reduce artefacts, and employed parallel imaging to reduce time (Dusek et al., 2013; Manova et al., 2009). SN iron was increased in PD patients as determined by SWI and correlated with motor symptom severity (Zhang et al., 2010). Much like previous techniques, SWI is influenced by the susceptibility of surrounding tissue in addition to the local iron content, which can impact iron measurement (Chen et al., 2010; Hammond et al., 2008). The need for local susceptibility measurement culminated in the development of quantitative susceptibility mapping (Bilgic et al., 2012; Li & Leigh, 2004).

1.2.3 Quantitative Susceptibility Mapping

Quantitative susceptibility mapping (QSM) is a novel post-processing technique that allows calculation of bulk magnetic susceptibility from GRE phase images (Li & Leigh, 2004; Reichenbach, 2012). QSM requires the following steps: phase unwrapping, background field removal, and solving the ill-posed phase inverse problem (Robinson et al., 2017). Spatial phase unwrapping algorithms remove 2π phase discontinuities from wrapped phase thus making it usable for QSM (Abdul-Rahman et al., 2007). The background field is then removed to allow for estimates of susceptibility solely related to the region of interest (ie. brain tissue) and eliminate superimposed fields to avoid any degrading effect on susceptibility maps (Schweser et al., 2017). Lastly, the ill-posed inverse problem relating brain tissue phase to the unknown magnetic susceptibility distribution (dipole inversion) must be solved (Chatnuntawech et al., 2017).

QSM generates relative susceptibility rather than absolute values, which requires normalization to a reference region (usually cerebrospinal fluid or white matter) to allow between-subject comparisons (Langkammer et al., 2012). Findings in controls suggest that high correlations exist between susceptibility measured using QSM and regional iron concentration (Bilgic et al., 2012; Wu, Du, Xue, Wu, & Zhou, 2012) based on the gold standard histochemical experiment of Hallgren and Sourander (1958). Furthermore, QSM was validated using a post-mortem tissue analysis of iron with MRI and Perl's staining (Langkammer et al., 2012; Sun et al., 2015).

Looking at PD patients, QSM has consistently shown elevations in iron in the whole SN (Barbosa et al., 2015; Langkammer et al., 2016; Lotfipour et al., 2012; Sethi et al., 2019) and just the SNc (Du et al., 2016; Guan et al., 2017; Takahashi et al., 2018a,b). QSM also correlated well with $R2^*$ and with iron content in deep gray matter nuclei (Deistung et al., 2013). QSM also correlated with clinical features of PD including disease duration (Du et al., 2016; He et al., 2015), motor symptom severity (Langkammer et al., 2016; Wang et al., 2016), and levodopa equivalent daily dosage (Du et al., 2016; Langkammer et al., 2016). Taken together, this suggests that QSM has potential to provide a diagnostic biomarker of PD and clinically relevant measure. To date, no study has measured VTA iron *in vivo*, but an animal model of PD found VTA iron increases were not comparable to those observed in the SNc (Hare et al., 2014; Lv, Jiang, Xu, Song, & Xie, 2010).

QSM recently became feasible following computational power improvement, novel algorithm development, and artefact reduction through improved susceptibility reconstruction (Schweser et al., 2012; Wharton & Bowtell, 2010). At high fields, contrast-to-noise characteristics

of GRE phase images exceed magnitude images (Duyn et al., 2007), which means QSM could be more sensitive to magnetic tissue properties than relaxometry and SWI (Haacke et al., 2005; Langkammer et al., 2012). There are several differences between susceptibility mapping and relaxometry (Langkammer et al., 2012). Areas containing diamagnetic and paramagnetic substances would counteract in bulk susceptibility, but have an additive effect in $R2^*$, which confounds interpretation of $R2^*$ in low iron regions (Langkammer et al., 2012). QSM also reduces the object orientation dependence of susceptibility in GRE images (Li et al., 2012). While research suggests that QSM is more sensitive than $R2^*$ to estimate brain iron in PD (Barbosa et al., 2015; Yang, Burciu, & Vaillancourt, 2018), work by Du and colleagues (2018), found QSM measures in SNc did not change over 18 months, whereas $R2^*$ measures did increase in late-stage PD. This suggests a need to compare both methods for both diagnostic and prognostic purposes in PD. While relaxometry has been applied in numerous clinical studies, QSM is a recent technique with ongoing methodological improvements, which may overcome its limitations (Langkammer et al., 2012).

1.3.1 Rationale for Current Study

Although the previous studies detected iron elevation in PD patients relative to controls using QSM and $R2^*$, the current research aimed to assess whether iron accumulation was specific in the SNc relative to the entire SN and the VTA. No studies have previously contrasted iron levels in SNc relative to SNr using objective atlas-based segmentation and instead relied on hand-drawn segmentation which presents with bias and lacks replicability (Guan et al., 2017; Shin, Lee, Lee, Rhim, & Park, 2018; Xuan et al., 2017). Further, no previous investigations have assessed iron accumulation in VTA *in vivo* in humans due to the structure's small size, low contrast and lack of atlases. The recently developed California Institute of Technology 168 (CIT168) probabilistic subcortical atlas includes the VTA and will be used to outline the structure so that we can assess its iron levels in early-stages of PD (Alberico et al., 2015; Pauli, Nili, & Tyszka, 2018).

Our understanding of PD pathophysiology leads to the prediction that iron accumulation, particularly in early stages, will be selectively enhanced in the SNc relative to the SNr and VTA. This has not been explicitly investigated empirically. Particularly the assessment of VTA in early-stage PD patients is expected to provide a negative control, given that degenerative changes in VTA are expected in later stages of PD only. If this pattern is borne out, this would suggest that focusing on SNc iron measures provides a more sensitive diagnostic biomarker of PD and would

justify the effort of obtaining of sub-regional measurement of iron content rather than simply assessing whole SN iron levels. Lastly, no studies have compared the differences between field strengths such as 3 Tesla (T) versus 7T using QSM and R2*. These assessments in the same patients will allow us to determine any potential advantages of ultra-high field imaging (i.e. 7T) when measuring iron in midbrain dopaminergic nuclei, and whether this advantage is more important for QSM or R2* relaxometry (Deistung et al., 2013). The availability of 3T scanners far exceeds 7T scanners; therefore, biomarkers at 3T are more impactful and relevant in clinic, thus necessitating separate analyses (Springer et al., 2016).

1.3.2 Objectives

The present study has several objectives which aim to diagnostically tease apart early-stage PD patients from healthy elderly controls using quantitative MRI of iron. First, it will individually assess the iron content profiles of the SNc and SNr to determine if researchers should continue to image the whole SN for QSM and R2* relaxometry. Second, this study will be the first to perform an *in vivo* assessment of VTA iron in humans given the importance of this structure in the later stages of PD. Third, it will compare the diagnostic ability of the two iron-imaging methods: QSM and R2* relaxometry using receiver operating characteristic (ROC) curve analysis. Lastly, the study will assess the different field strengths: 3T and 7T to determine if ultra-high field 7T MRI is necessary for detection of iron overload in early-stage PD.

1.3.3 Predictions

Given the literature on early-stage PD, we predict iron elevation will exist to a greater degree and perhaps only in the SNc of patients, which will be detected using both imaging methods. Correspondingly, the SNr and VTA will be spared from iron overload in early stages of PD and measures that focus on the SNc will provide more sensitive diagnostic biomarkers. Because it has been suggested that QSM is more sensitive, we expect QSM to outperform R2* relaxometry in terms of diagnostic ability when assessing the elevated SNc iron as a biomarker. Lastly, the use of 7T MRI will have a diagnostic advantage over 3T MRI given increased signal-to-noise ratio, but we expect that this advantage will be small and perhaps outweighed by the lack of access to 7T and patients' and elderly controls' poorer tolerability of 7T imaging.

Chapter 2: Methods

2.1 Participants

Seventeen early-stage PD patients and twenty-one elderly healthy controls were recruited for this study. Each patient was matched with a healthy control within three years of age. Early-stage PD patients were diagnosed within the last five years and had no co-existing diagnosis of dementia or any other neurological or psychiatric disease, save for mild depression or anxiety. Disease duration was calculated from the date of physician-confirmed PD diagnosis to the first imaging session. All PD patients were optimized medically and receiving some form of dopamine therapy under the management of a movement disorder specialist to be included in the study. Participants abusing alcohol, prescription or illicit drugs, or taking cognitive-enhancing medications were excluded, as were patients who were diagnosed before the age of 45, had more than two first-degree relatives with PD, or had contraindication to MRI. The Health Sciences Research Ethics Board of the University of Western Ontario approved this study. All participants provided informed written consent to the approved protocol before beginning the experiment, according to the Declaration of Helsinki (2013).

2.2 Questionnaires

The Montreal Cognitive Assessment (MoCA) was conducted in all participants to rule out impaired cognition, such as dementias or mild cognitive impairment (Nasreddine et al., 2005). MoCA total score was used to rule out global cognitive deficits in early-stage PD patients and elderly controls and any participants falling into the cognitive impairment test score range was removed from further analyses.

The Unified Parkinson Disease Rating Scale Part III (UPDRS-III) was conducted on all participants (Martinez-Martin et al., 1987; Ramaker, Marinus, Stiggelbout, & Van Hilten, 2002). This neurological assessment was used to measure disease severity, to verify the presence of motor symptoms in the PD patients' OFF medication state, and to verify the absence of motor symptoms in the healthy controls. The UPDRS-III was recorded and later evaluated by a movement disorders neurologist, PM for interpretation of motor behaviour and symptoms.

2.3 MRI Data Acquisition

MRI data was collected using a high field 3T Siemens MAGNETOM Prisma whole-body scanner and an ultra-high field 7T Siemens MAGNETOM scanner at Robarts Research Institute at the University of Western Ontario. A 32-channel head coil was used in both scanners. Participants were scanned once on each scanner with up to a maximum of seven days between sessions using a random counterbalanced design for scanner order.

On the 3T scanner, we first obtained a localizer image for positioning participants. T1-weighted (T1w) anatomical scans were obtained for structural information, registration of quantitative maps and the segmentation of midbrain nuclei using the CIT168 probabilistic subcortical atlas (Pauli et al., 2018). T1w anatomical images were acquired using a magnetization-prepared rapid gradient echo (MPRAGE) sequence (repetition time (TR) = 2300 ms, echo time (TE) = 2.98 ms, flip angle = 9°, Field of View (FoV) = 256×256 mm², 159 slices, voxel size = 1×1×0.9 mm³, receiver bandwidth = 160 Hz/Px, acquisition time = 5:35 min). High resolution GRE images (Deistung et al., 2008) were acquired with an rf-spoiled, flow compensated 3D gradient echo sequence with six echoes (TE ranging from 8.09 ms to 40.49 ms and an equal interval of 6.48 ms), and (TR = 52 ms, flip angle = 20°, FoV = 224×224 mm², 96 slices, voxel size = 0.5×0.5×2 mm³, receiver bandwidth = 160 Hz/Px, acquisition time = 8:30 min).

On the 7T scanner, we obtained a localizer image for positioning participants. T1w images were acquired with a magnetization-prepared 2 rapid gradient echo (MP2RAGE) sequence (TR = 6000 ms, TE = 2.73 ms, flip angle₁ = 4°, flip angle₂ = 5°, FoV = 240×240 mm², 224 slices, voxel size = 0.7×0.7×0.7 mm³, receiver bandwidth = 150 Hz/Px, acquisition time = 10:14 min). High resolution GRE images were acquired with an rf-spoiled, flow compensated 3D gradient echo sequence with four echoes (TE ranging from 4.61 ms to 15.50 ms and an equal interval of 3.63 ms), and (TR = 35 ms, flip angle = 13°, FoV = 220×220 mm², 128 slices, voxel size = 0.8×0.8×0.8 mm³, receiver bandwidth = 310 Hz/Px, acquisition time = 9:07 min).

2.4 MRI Data Postprocessing

T1w Postprocessing – T1w image processing was performed using FMRIB Software Library (FSL) 5.0.11 (<https://fsl.fmrib.ox.ac.uk/fsl/fslwiki/>) and Advanced Normalization Tools (ANTs) 2.2 (<http://picsl.upenn.edu/software/ants>). Brain Extraction based on nonlocal Segmentation

Technique (BEaST) was used for skull-stripping T1w images from both field strengths (Eskildsen et al., 2013) using code from: <<https://github.com/khanlab/beast>>. Then bias fields for skull-stripped 3T and 7T T1w images were corrected using N4BiasFieldCorrection, followed by intensity normalization.

Gradient Echo Magnitude Postprocessing – GRE magnitude images from all echoes were averaged then skull-stripped using BEaST. Skull-stripped averaged GRE magnitude images were then linearly registered to the final postprocessed T1w images using FMRIB's Linear Image Registration Tool (FLIRT).

R2 Relaxometry Image Generation* – Non-linear least squares estimation of R2* was calculated at each voxel using the Levenberg–Marquardt algorithm (<http://netlib.org/minpack/>; Levenberg, 1944; Marquardt, 1963) on the complex signal. All code for R2* image generation is available at (https://github.com/AlanKuurstra/qsm_sstv).

Quantitative Susceptibility Map Generation – An in-house singular value decomposition algorithm based on Walsh, Gmitro, and Marcellin (2000) was employed to reconstruct the GRE raw data, described in (<https://cds.ismrm.org/protected/13MProceedings/files/3739.PDF>). This algorithm gives the least squares best estimate of the magnetization and avoids phase singularities. QSM processing was performed as follows: spatial phase unwrapping was accomplished using a 3D best path algorithm (Abdul-Rahman et al., 2007). The frequency at each voxel was then estimated by weighted least squares; each phase echo was weighted by the local signal-to-noise ratio in the corresponding T2* image. Finally, background removal and dipole inversion were performed simultaneously using a single-step QSM algorithm (Chatnuntawech et al., 2017). Since susceptibility values calculated by dipole inversion are relative with unknown offset, an offset was set by forcing the average value within the brain to be zero parts per billion (ppb). All code for QSM image generation is available at (https://github.com/AlanKuurstra/qsm_sstv).

Quantitative Map Postprocessing – The transformation matrices from the average GRE magnitude to T1w image registrations were used to perform linear registration of both QSM and R2* images onto T1w images using FLIRT. QSM images were then offset using the average susceptibility in

the cerebrospinal fluid of each participant as a reference, which allows for between subject comparisons to be performed given that the susceptibility values are relativistic and not absolute (Langkammer et al., 2012).

Atlas-Based Segmentation – The CIT168 probabilistic subcortical atlas developed by Pauli and colleagues (2018) available at (<https://neurovault.org/collections/3145/>) was used for single atlas-based segmentation. This high-resolution atlas clearly demarcates the SNc, SNr, and VTA based on data from young controls in the Human Connectome Project database. The limitations of this atlas are its use of only 3T data being non-ideal for use in our 7T data and the young population, which may not account for age-related anatomical changes in our sample. Nevertheless, this is one of the better available atlases for subcortical segmentation.

Atlas-based segmentation of each participant was performed using the NiftyReg linear and deformable b-spline registration tools to the CIT168 atlas in MNI152 space (Non-linear 2009c 1mm) as shown in Figure 2 (Modat et al., 2014). Volumes of the midbrain nuclei: SNc, SNr, and VTA were extracted from these segmentations. Quality assurance for each registration was performed.

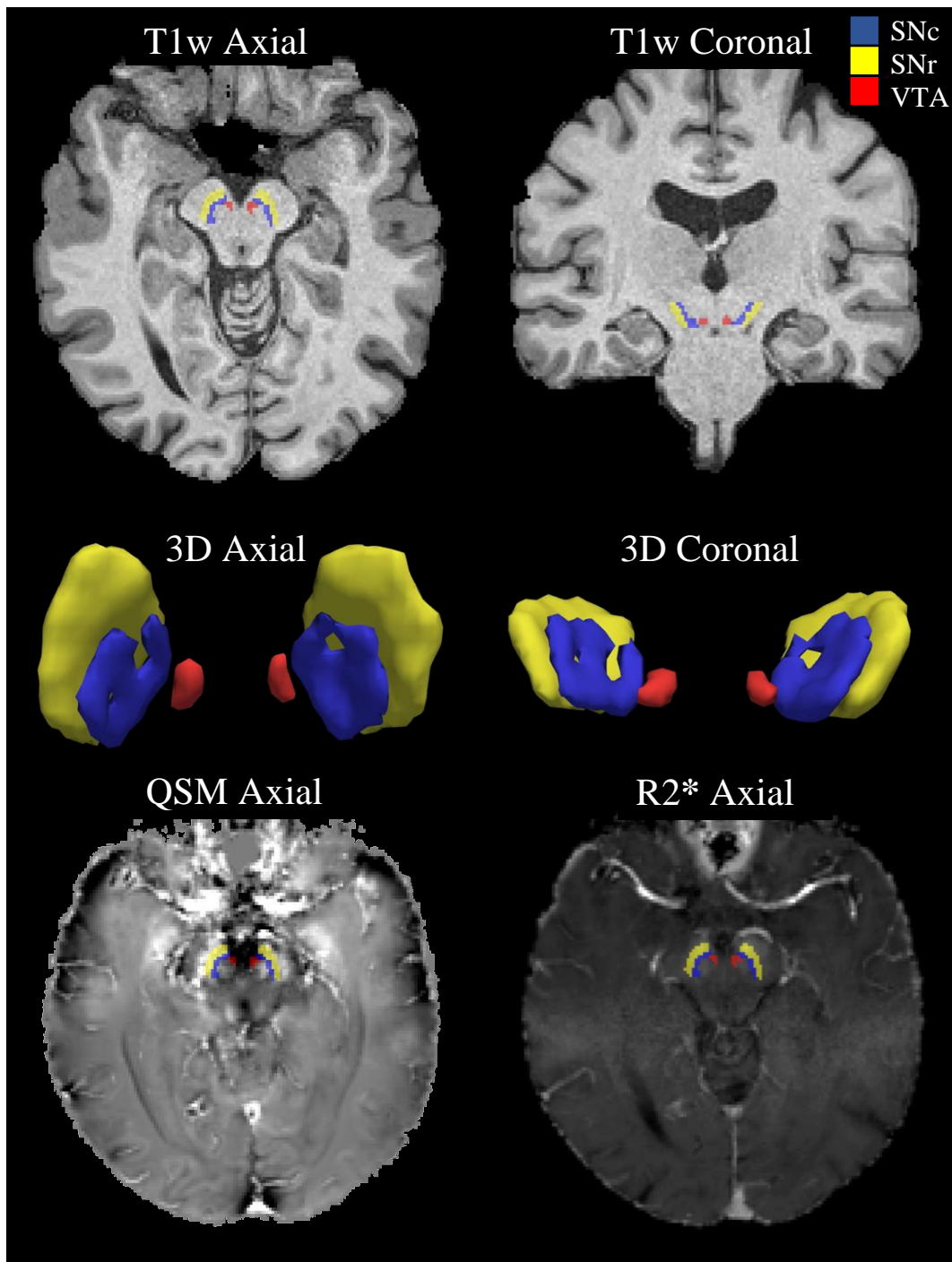


Figure 2. Segmentation of midbrain nuclei on QSM and R2* maps of a healthy control. Top row shows SNc, SNr, and VTA from CIT168 atlas mapped onto T1w images in axial and coronal planes. Middle row shows a 3D model of the midbrain nuclei in axial plane, superior view (left) and coronal plane, posterior view (right). Bottom row shows midbrain nuclei on QS map (left) and R2* map (right) of the same healthy control in axial planes. SNc is shown in blue, SNr in yellow and VTA in red for all images.

2.5 Statistical Analysis

Demographic data for all participants was compared between groups using a one-way analysis of variance (ANOVA) looking at age and MoCA total scores, along with a chi-square test for sex. For the three midbrain nuclei, early-stage PD patients were compared to healthy controls for the average susceptibility in ppb in QSM images and average R2* values (1/s) in R2* images. All measures were considered separately in each hemisphere given the asymmetrical presentation of symptoms in early-stage PD.

To assess the effects of early-stage PD on the QSM and R2* relaxometry measures of the SNc, a $2 \times 2 \times 2$ repeated measures analysis of covariance (RM-ANCOVA) was conducted with Group (PD versus Control) as the between-subjects factor and Hemisphere (Left versus Right) and Scanner (3T versus 7T) as within-subjects variables controlling for age and sex as covariates. Subcortical iron deposits increase with age and males display higher iron levels than females, even when accounting for age, thus warranting both as covariates for our analyses (Persson et al., 2015). Separate 2×2 RM-ANCOVAs were performed at each of the two field strengths (3T and 7T) to assess for biomarker potential at each field strength individually. The 2×2 RM-ANCOVAs were conducted for QSM and R2* measures of the SNc at both field strengths using Group as the between-subjects factor and Hemisphere as the within-subjects variable controlling for age and sex as covariates. For all statistical analyses, $p < 0.05$ was used as the statistical threshold. Benjamini-Hochberg correction (1995) was used to control the false discovery rate at $q = .05$ and to avoid stringent approaches such as Bonferroni family wise error correction. All RM-ANCOVAs were then repeated using the QSM and R2* averages of the SNr and the VTA with identical factors, variables, and covariates as those previously described.

ROC curves were constructed for any measures showing significant group differences between early-stage PD patients and healthy controls to assess for their potential to discriminate between groups at a participant level. To optimally test for discriminatory ability, average susceptibility and R2* values were sorted based on the more affected or less affected hemisphere as defined by the UPDRS-III motor assessment rather than using left and right hemispheres. This allows us to account for the asymmetric presentation associated with early-stage PD. The more affected hemisphere (MAH) was defined as being contralateral to the more affected body side and the less affected hemisphere (LAH) was contralateral to the less affected body side based on the UPDRS-III. The area under the ROC curve (AUC) was calculated to compare the diagnostic

accuracy between measures. The highest Youden index was also used to determine the best diagnostic cut-off value based on sensitivity and specificity for each of the measures.

The AUCs of the MAH and LAH were compared within the same method to test for significant differences in diagnostic accuracy using the method established by Hanley and McNeil (1983). The AUC of the MAH was compared between the different iron imaging methods to test if any method significantly outperformed others based on diagnostic accuracy of early-stage PD patients compared to healthy controls.

To assess the nuclei volumes being sampled at each field strength, the 7T T1w image whole brain volume was registered to the 3T T1w image whole brain volume of each participant using FLIRT. The translation matrix of this registration was then applied to the respective segmented volumes of the SNc, SNr, and VTA to register the 3T volumes onto the 7T volumes using FLIRT. The percentage of overlap between the “3T onto 7T” volumes and the original 7T volumes was computed using Dice similarity coefficient for the SNc, SNr, and VTA (Dice, 1945). To assess if similar volumes were sampled between scanners, Dice similarity coefficients were then compared using a 3×2 repeated measures analysis of variance (RM-ANOVA) using Group (PD versus Control) as between-subjects factor and Nucleus (SNc, SNr, and VTA) as within-subjects variable. All statistical analyses were performed using IBM SPSS Statistics (version 23, IBM Corp., Armonk, NY, USA). The Hanley-McNeil method for AUC comparison was performed using MedCalc (version 18, MedCalc Software).

Chapter 3: Results

3.1.1 Demographics

For general demographics, early-stage PD patients did not differ significantly in age ($F(1,36) = 1.480$, $MSe = 71.8$, $p_{adj} = .23$) or sex ($\chi^2(1) = 1.799$, $p_{adj} = .18$) from the healthy controls (Table 1). No significant differences were found on the MoCA total scores between groups ($F(1,36) = 2.014$, $MSe = 14.5$, $p_{adj} = .17$), indicating similar general cognitive ability and a lack of global cognitive impairment in these groups. The early-stage PD patients had an average disease duration of 2.50 ± 1.80 years with six patients having had PD for 0-1 years, six for 2-3 years and five for 4-5 years indicating an even spread of patients across our selected disease duration range.

Table 1. Demographics and clinical information for early-stage PD patients and controls. Cells show ratio of female to male for sex, age in years, PD duration in years, ratio for more affected hemisphere in PD patients and MoCA total scores. Averages reported as means \pm standard error mean (NS = not significant).

	Control	PD	<i>p</i> -value
Sex	12 F : 9 M	6 F : 11 M	NS
Age	65.0 \pm 1.5	67.8 \pm 1.7	NS
PD Duration	-	2.5 \pm 0.4	-
MAH	-	14 L : 3 R	-
MoCA Total	28.1 \pm 0.5	27.1 \pm 0.7	NS

3.2.1 QSM in the SNc

A $2 \times 2 \times 2$ RM-ANCOVA of SNc average susceptibility from QSM data was performed using Group as the between-subjects factor with Hemisphere and Scanner as the within-subjects variables controlling for age and sex as covariates. A significant main effect of Group was found [$F(1,31) = 16.137$, $MSe = 2930$, $p_{adj} = .002$], which suggests early-stage PD patients had higher iron deposition regardless of scanner field strength (Figure 3). There was no significant main effect of Hemisphere [$F(1,31) = 3.090$, $MSe = 607$, $p_{adj} = .26$] or Scanner [$F(1,31) < 1$]. No significant interactions were found for Hemisphere*Group [$F(1,31) = 2.123$, $MSe = 607$, $p_{adj} = .31$], Scanner*Group [$F(1,31) < 1$], Hemisphere*Scanner [$F(1,31) = 2.891$, $MSe = 581$, $p_{adj} = .26$], or Hemisphere*Scanner*Group [$F(1,31) < 1$].

Separate 2×2 RM-ANCOVAs were performed at the two field strengths (3T and 7T) to assess for biomarker potential at each field strength individually. Again, using Group as the

between-subjects factor with Hemisphere as the within-subjects variable controlling for age and sex as covariates. For 3T data, a significant main effect of Group was found [$F(1,34) = 13.051$, $MSe = 2475$, $p_{adj} = .01$] with PD patients showing higher average susceptibility than controls, suggesting increased iron deposition (Figure 3A). No significant main effect of Hemisphere was found [$F(1,34) = 6.476$, $MSe = 666$, $p_{adj} = .08$], suggesting similar iron deposition in both hemispheres overall (Figure 3A). Lastly, no significant Hemisphere*Group interaction was found [$F(1,34) = 1.973$, $MSe = 666$, $p_{adj} = .29$].

For 7T data, a significant main effect of Group was found [$F(1,31) = 11.134$, $MSe = 1830$, $p_{adj} = .01$] with PD patients showing higher susceptibility and iron deposition again (Figure 3B). Looking at Hemisphere, no significant main effect of Hemisphere was found [$F(1,31) < 1$] with no significant Hemisphere*Group interaction [$F(1,31) < 1$]. Taken together, these results suggest that QSM at both 3T and 7T detected bilateral elevated iron content in the SNc of early-stage PD patients when compared to age-matched healthy controls.

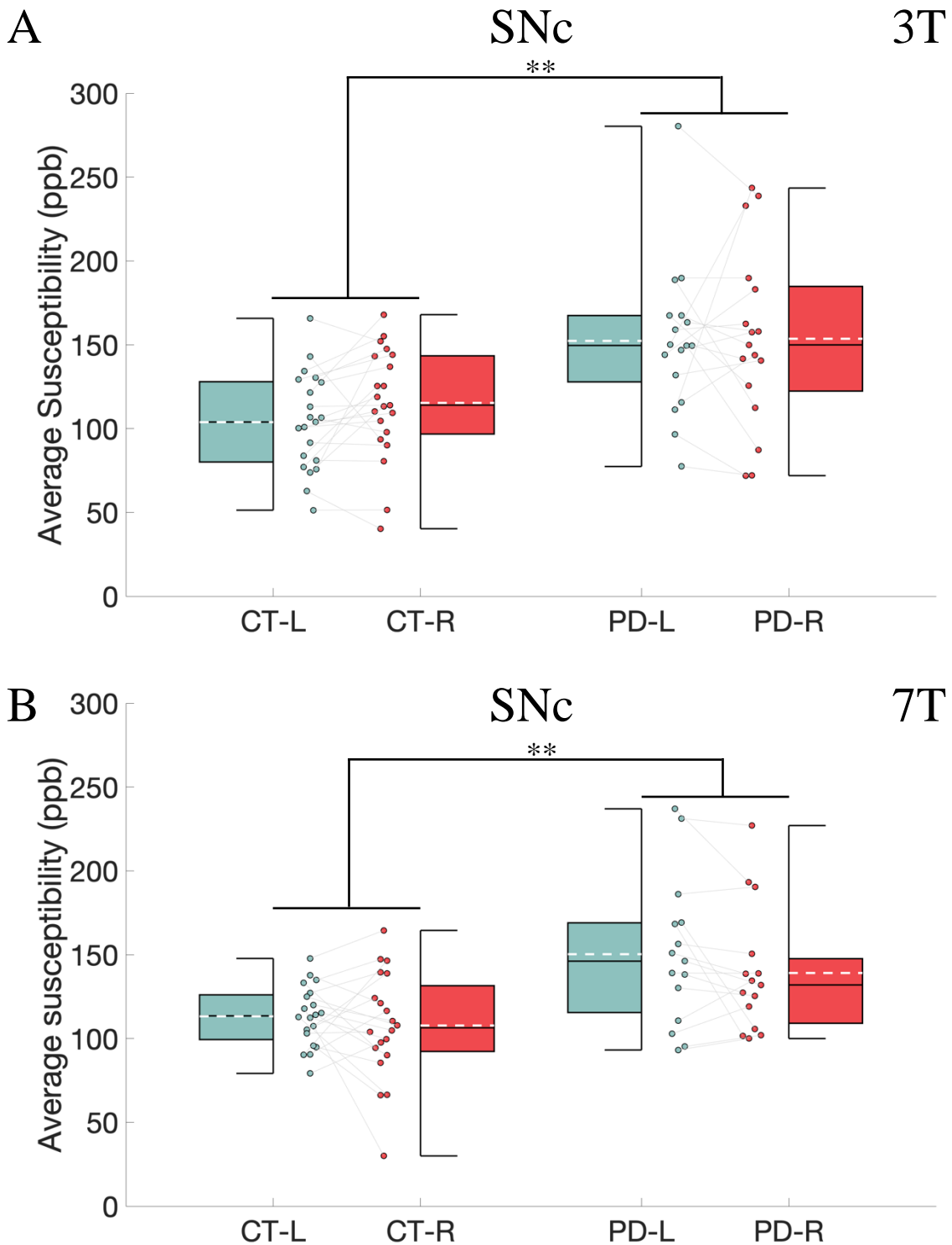


Figure 3. Average susceptibility for the SNc of early-stage PD patients and healthy controls at 3T and 7T. Data show paired hemispheric averages for all participants in scatterplots with corresponding boxplots demonstrating median and interquartile range in black lines. SNc average susceptibility in ppb from QSM at both field strengths are shown as dashed white lines. Significant group differences were found at both field strengths with PD showing increased iron deposition. $n_{CT} = 21$, $n_{PD} = 17$. * $p \leq .05$, ** $p \leq .01$

3.2.2 R2* in the SNc

A $2 \times 2 \times 2$ RM-ANCOVA of SNc average R2* value from R2* relaxometry was performed using Group as the between-subjects factor with Hemisphere and Scanner as the within-subjects variables controlling for age and sex as covariates. There was a significant main effect of Scanner [$F(1,31) = 11.289$, $MSe = 80.5$, $p_{adj} = .01$] suggesting 7T R2* values were higher than 3T showing field strength dependence (Figure 4). No significant main effect of Group was found [$F(1,31) = 5.901$, $MSe = 159$, $p_{adj} = .08$], which suggests early-stage PD patients had similar iron deposition to elderly controls regardless of scanner field strength (Figure 4). No significant main effect of Hemisphere was found [$F(1,31) < 1$]. In addition, no significant interactions were found for Hemisphere*Group [$F(1,31) = 1.035$, $MSe = 23.2$, $p_{adj} = .52$], Scanner*Group [$F(1,31) = 2.127$, $MSe = 80.5$, $p_{adj} = .29$], Hemisphere*Scanner [$F(1,31) < 1$], or Hemisphere*Scanner*Group [$F(1,31) = 2.608$, $MSe = 40.4$, $p_{adj} = .27$].

Separate 2×2 RM-ANCOVAs were again performed at both field strengths using Group as the between-subjects factor with Hemisphere as the within-subjects variable controlling for age and sex as covariates. For 3T data, no significant main effect of Group was found [$F(1,34) = 2.265$, $MSe = 90.0$, $p_{adj} = .29$] with PD patients showing similar R2* values as controls, suggesting similar iron deposition (Figure 4A). No significant main effect of Hemisphere was found [$F(1,34) < 1$], suggesting no difference in iron deposition between hemispheres (Figure 4A). No significant Hemisphere*Group interaction was found [$F(1,34) = 5.262$, $MSe = 22.4$, $p_{adj} = .09$].

For 7T data, a marginally significant main effect of Group was found [$F(1,31) = 7.465$, $MSe = 148$, $p_{adj} = .052$] with PD patients showing higher iron deposition (Figure 4B). No significant main effect of Hemisphere was found [$F(1,31) < 1$] with no significant Hemisphere*Group interaction [$F(1,31) < 1$]. Taken together, these results suggest that R2* only detected elevated iron content in the SNc of early-stage PD patients at 7T and not at 3T.

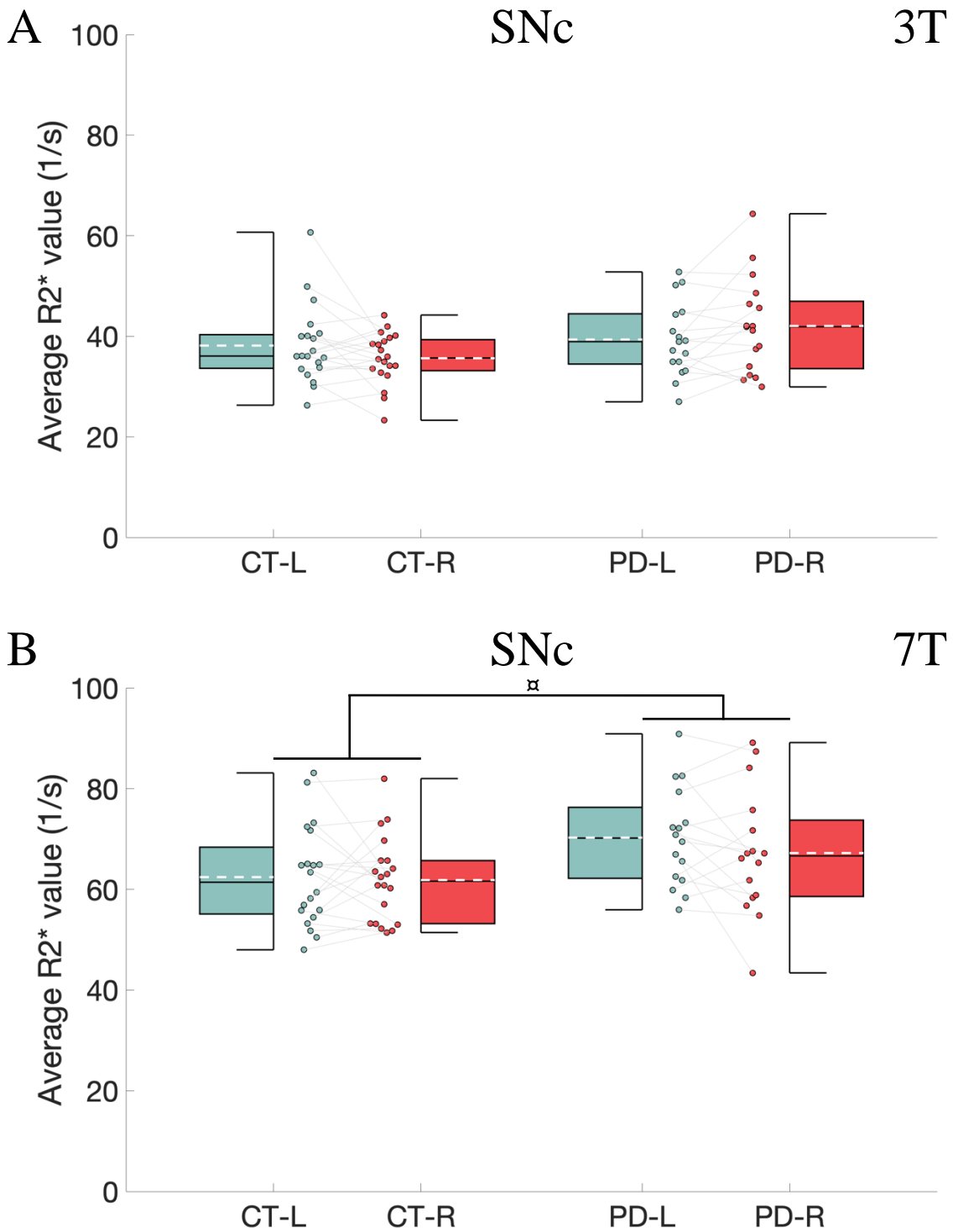


Figure 4. Average R2* values for the SNc of early-stage PD patients and healthy controls at 3T and 7T. Data show paired hemispheric averages for all participants in scatterplots with corresponding boxplots demonstrating median and interquartile range in black lines. SNc average R2* values in 1/s from R2* at both field strengths are shown as dashed white lines. Marginally significant differences were found between groups at 7T with PD showing increased iron deposition. $n_{CT} = 21$, $n_{PD} = 17$. ✕ $p_{adj} = .052$

3.2.3 ROC Curve Analyses in the SNc

For diagnostic biomarker assessments, the MAH and LAH were used instead of the right and left hemisphere conventions to better account for early-stage PD asymmetry. The MAH based on the more symptomatic body side from the UPDRS-III is of greater clinical relevance; therefore, results from only this hemisphere are reported here.

Looking at QSM 3T data, the ROC curves for SNc average susceptibility show the MAH is a significant predictor for distinguishing PD patients ($AUC = .871$, $p < .001$; Figure 5). Based on the highest Youden index, the optimal cut-off value for distinguishing PD patients in the MAH is 137.5 ppb (Sensitivity = 0.824, Specificity = 0.905). Similarly, ROC curves for the SNc average susceptibility at 7T show that the MAH is a significant predictor ($AUC = .807$, $p = .002$) with an optimal cut-off value of 137.9 ppb (Sensitivity = 0.667, Specificity = 0.95; Figure 5). Both field strengths had almost identical optimal cut-off values.

For R2* data at 3T, ROC curves show that the average R2* values of the MAH SNc was not a significant predictor ($AUC = .565$, $p = .503$) with an optimal cut-off value of 36.3 s⁻¹ (Sensitivity = .647, Specificity = .550; Figure 6). Looking at the SNc average R2* values at 7T, however, the MAH was a significant predictor ($AUC = .725$, $p = .022$) with an optimal cut-off value of 65.2 s⁻¹ (Sensitivity = .750, Specificity = .750; Figure 6).

Using the Hanley-McNeil method (1983), we compared the AUC of the measures with significant diagnostic accuracy which were QSM at 3T, QSM at 7T and R2* at 7T. This method allows comparison of AUCs which are based on the same sample of participants. Comparing the MAH SNc to LAH SNc, QSM at 3T had a significant difference between hemispheres ($Z = 2.307$, $p = .02$; Figure 5), whereas QSM at 7T ($Z = 0.924$, $p = .36$; Figure 5) and R2* at 7T ($Z = 1.023$, $p = .31$) did not (Figure 6). This suggests that QSM at 3T was somewhat sensitive to the asymmetry of early-stage PD, given that the MAH outperformed the LAH in terms of diagnostic accuracy.

Comparing the MAH SNc between the three different methods, QSM 3T versus R2* 7T was marginally significant ($Z = 1.514$, $p = .065$) suggesting QSM 3T out-performed R2* 7T based on diagnostic accuracy. No significant differences were found between QSM 3T versus QSM 7T ($Z = 0.643$, $p = .52$) and QSM 7T versus R2* 7T ($Z = 0.707$, $p = .48$). Taken together, this suggests that QSM outperforms R2* relaxometry in terms of diagnostic accuracy using iron in the SNc of early-stage PD patients compared to controls.

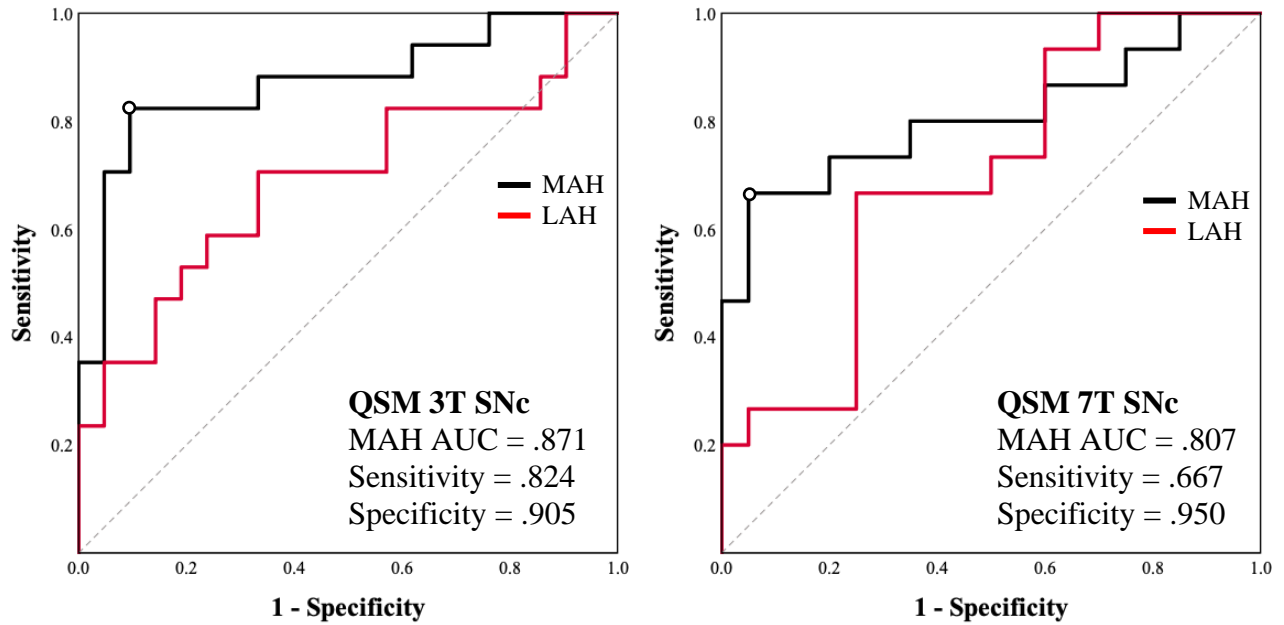


Figure 5. ROC curves for MAH and LAH of SNc average susceptibility at 3T and 7T. Data show more affected (black) and less affected (red) hemispheres from QSM at 3T and 7T with the optimal cut-off point (white circle) based on the highest Youden index. MAH AUC and optimal cut-off sensitivity and specificity are shown. $n_{CT} = 21$, $n_{PD} = 17$

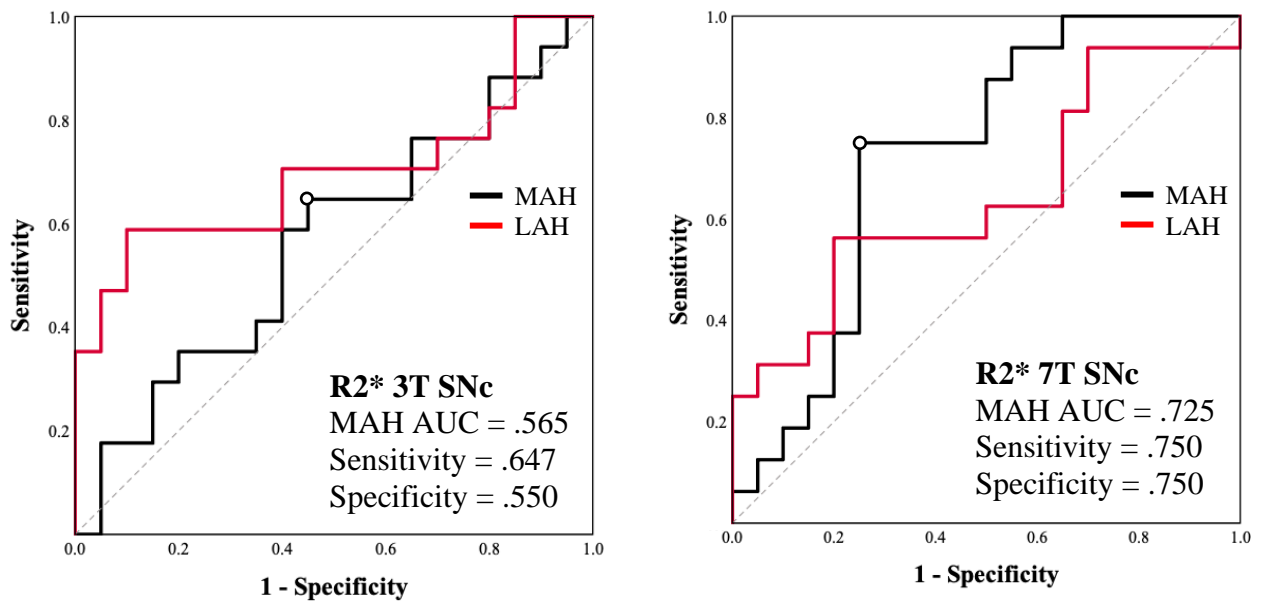


Figure 6. ROC curves for MAH and LAH of SNc average $R2^*$ value at 3T and 7T. Data show more affected (black) and less affected (red) hemispheres of from $R2^*$ relaxometry at 3T and 7T with the optimal cut-off point (white circle) based on the highest Youden index. MAH AUC and optimal cut-off sensitivity and specificity are shown. $n_{CT} = 21$, $n_{PD} = 17$

3.3.1 QSM in the SNr

A $2 \times 2 \times 2$ RM-ANCOVA of SNr average susceptibility from QSM was performed using Group as the between-subjects factor with Hemisphere and Scanner as the within-subjects variables controlling for age and sex as covariates. No significant main effect of Group was found [$F(1,31) < 1$], which suggests early-stage PD patients had similar iron deposition to elderly controls regardless of scanner field strength (Figure 7). There was no significant main effect of Scanner [$F(1,31) < 1$] suggesting similar values between field strengths (Figure 7). No significant main effect of Hemisphere was found [$F(1,31) < 1$]. Lastly, no significant interactions were found for Hemisphere*Group [$F(1,31) = 1.000$, $MSe = 572$, $p_{adj} = .85$], Scanner*Group [$F(1,31) < 1$], Hemisphere*Scanner [$F(1,31) < 1$], or Hemisphere*Scanner*Group [$F(1,31) < 1$].

Separate 2×2 RM-ANCOVAs were performed at 3T and 7T using Group as the between-subjects factor with Hemisphere as the within-subjects variable controlling for age and sex as covariates. For 3T data, no significant main effect of Group was found [$F(1,34) < 1$] with PD patients showing similar average susceptibility as elderly controls, suggesting similar iron deposition (Figure 7A). No significant main effect of Hemisphere was found [$F(1,34) < 1$], suggesting no difference in iron deposition between hemispheres (Figure 7A) and no significant Hemisphere*Group interaction was found [$F(1,34) < 1$].

For 7T data, no significant main effect of Group was found [$F(1,31) < 1$] with PD patients showing similar average susceptibility and iron deposition (Figure 7B). No significant main effect of Hemisphere was found [$F(1,31) < 1$] along with no significant Hemisphere*Group interaction [$F(1,31) < 1$]. Taken together, these observations suggest no differences in SNr iron content were found between early-stage PD patients and controls using QSM at 3T and 7T. Given that the main effect of Group was not significant for SNr iron content imaged using QSM, the ROC curve analyses were not performed on our SNr measures.

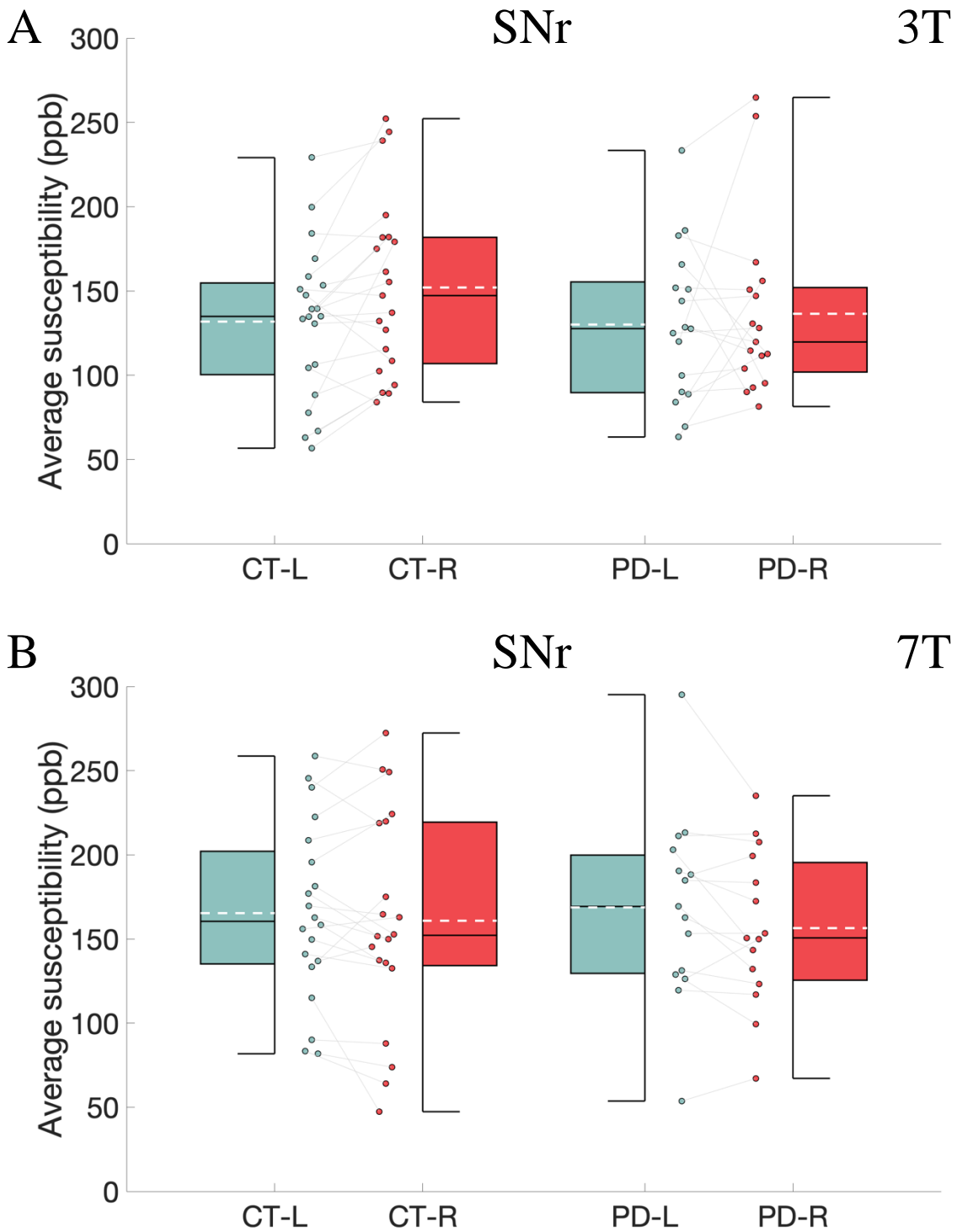


Figure 7. Average susceptibility for the SNr of early-stage PD patients and healthy controls at 3T and 7T. Data show paired hemispheric averages for all participants in scatterplots with corresponding boxplots demonstrating median and interquartile range in black lines. SNr average susceptibility values in ppb from QSM at both field strengths are shown as dashed white lines. No significant differences were found between groups at both field strengths. $n_{CT} = 21$, $n_{PD} = 17$

3.3.2 R2* in the SNr

A $2 \times 2 \times 2$ RM-ANCOVA of SNr average R2* values was performed using Group as the between-subjects factor with Hemisphere and Scanner as within-subjects variables controlling for age and sex as covariates. There was a significant main effect of Scanner [$F(1,31) = 12.875$, $MSe = 78.2$, $p_{adj} = .01$] suggesting higher R2* values at 7T overall (Figure 8). No significant main effect of Group was found [$F(1,31) = 1.020$, $MSe = 281$, $p_{adj} = .77$], which suggests early-stage PD patients have similar iron to controls regardless of scanner field strength (Figure 8). No significant main effect of Hemisphere was found [$F(1,31) < 1$]. Lastly, no significant interactions were found for Hemisphere*Group [$F(1,31) = 1.079$, $MSe = 54.8$, $p_{adj} = .77$], Scanner*Group [$F(1,31) = 2.457$, $MSe = 89.3$, $p_{adj} = .41$], Hemisphere*Scanner [$F(1,31) < 1$], or Hemisphere*Scanner*Group [$F(1,31) < 1$].

Separate 2×2 RM-ANCOVAs were performed at 3T and 7T using Group as the between-subjects factor with Hemisphere as the within-subjects variable controlling for age and sex as covariates. For 3T data, no significant main effect of Group was found [$F(1,34) < 1$] with PD patients showing similar average R2* values as elderly controls, suggesting similar iron deposition (Figure 8A). No significant main effect of Hemisphere was found [$F(1,34) < 1$], suggesting no difference in iron deposition between hemispheres (Figure 8A) and no significant Hemisphere*Group interaction was found [$F(1,34) = 1.170$, $MSe = 24.1$, $p_{adj} = .77$].

For 7T data, no significant main effect of Group was found [$F(1,31) = 2.066$, $MSe = 244$, $p_{adj} = .46$] with PD patients showing similar average susceptibility and iron deposition (Figure 8B). No significant main effect of Hemisphere was found [$F(1,31) < 1$] along with no significant Hemisphere*Group interaction [$F(1,31) < 1$]. Taken together, these observations suggest no differences in SNr iron content were found between early-stage PD patients and controls using R2* at 3T and 7T. Given that the main effect of Group was not significant for SNr iron content imaged using R2* relaxometry, the ROC curve analyses were not performed on our SNr measures.

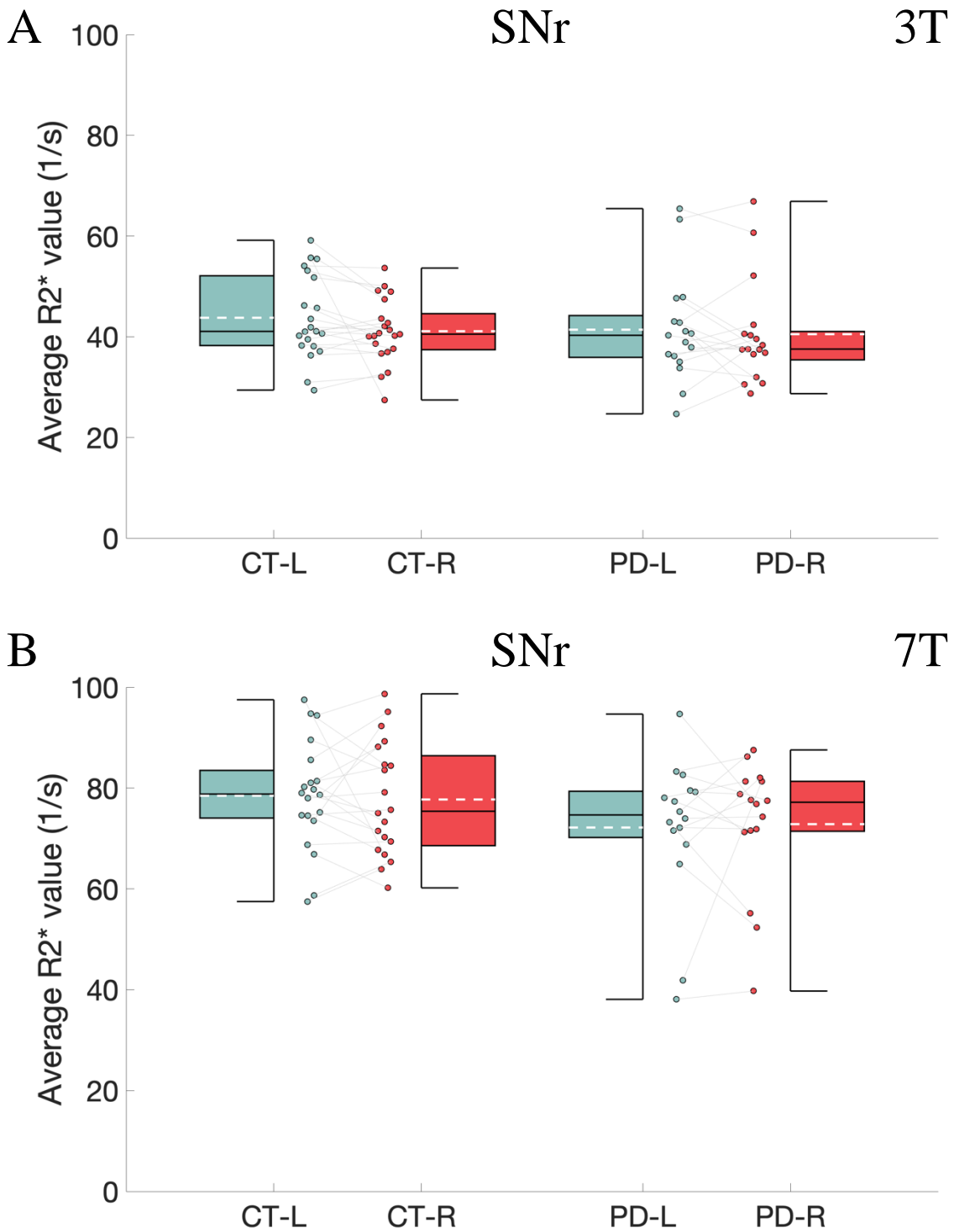


Figure 8. Average R2* values for the SNr of early-stage PD patients and healthy controls at 3T and 7T. Data show paired hemispheric averages for all participants in scatterplots with corresponding boxplots demonstrating median and interquartile range in black lines. SNr average R2* values in 1/s from R2* at both field strengths are shown as dashed white lines. No significant differences were found between groups at both field strengths with PD showing similar averages to controls. $n_{CT} = 21$, $n_{PD} = 17$

3.4.1 QSM in the VTA

A $2 \times 2 \times 2$ RM-ANCOVA of VTA average susceptibility was performed using Group as the between-subjects factor with Hemisphere and Scanner as within-subjects variables controlling for age and sex as covariates. No significant main effect of Group was found [$F(1,31) = 2.530$, $MSe = 2040$, $p_{adj} = .37$], which suggests PD patients had similar VTA iron deposition to controls regardless of scanner (Figure 9). There was no significant main effect of Scanner [$F(1,31) = 2.262$, $MSe = 1925$, $p_{adj} = .40$] suggesting similar values between field strengths (Figure 9). No significant main effect of Hemisphere was found [$F(1,31) < 1$]. Lastly, no significant interactions were found for Hemisphere*Group [$F(1,31) < 1$], Scanner*Group [$F(1,31) < 1$], Hemisphere*Scanner [$F(1,31) = 3.514$, $MSe = 159$, $p_{adj} = .34$], or Hemisphere*Scanner*Group [$F(1,31) < 1$].

Separate 2×2 RM-ANCOVAs were performed at 3T and 7T using Group as the between-subjects factor and Hemisphere as the within-subjects variable controlling for age and sex. For 3T, no significant main effect of Group was found [$F(1,34) = 2.457$, $MSe = 1972$, $p_{adj} = .37$] with PD patients showing similar average susceptibility as elderly controls, suggesting similar iron deposition (Figure 9A). No significant main effect of Hemisphere was found [$F(1,34) = 3.437$, $MSe = 438$, $p_{adj} = .34$], suggesting no difference in iron deposition between hemispheres with no significant Hemisphere*Group interaction [$F(1,34) < 1$; Figure 9A].

For 7T data, no significant main effect of Group was found [$F(1,31) < 1$] with PD patients showing similar average susceptibility and iron deposition (Figure 9B). No significant main effect of Hemisphere was found [$F(1,31) = 2.675$, $MSe = 149$, $p_{adj} = .36$] along with no significant Hemisphere*Group interaction [$F(1,31) < 1$]. Taken together, these observations suggest no elevation in VTA iron was found in early-stage PD patients using QSM at 3T and 7T. Given that the main effect of Group was not significant for VTA iron content imaged using QSM, the ROC curve analyses were not performed on our VTA measures.

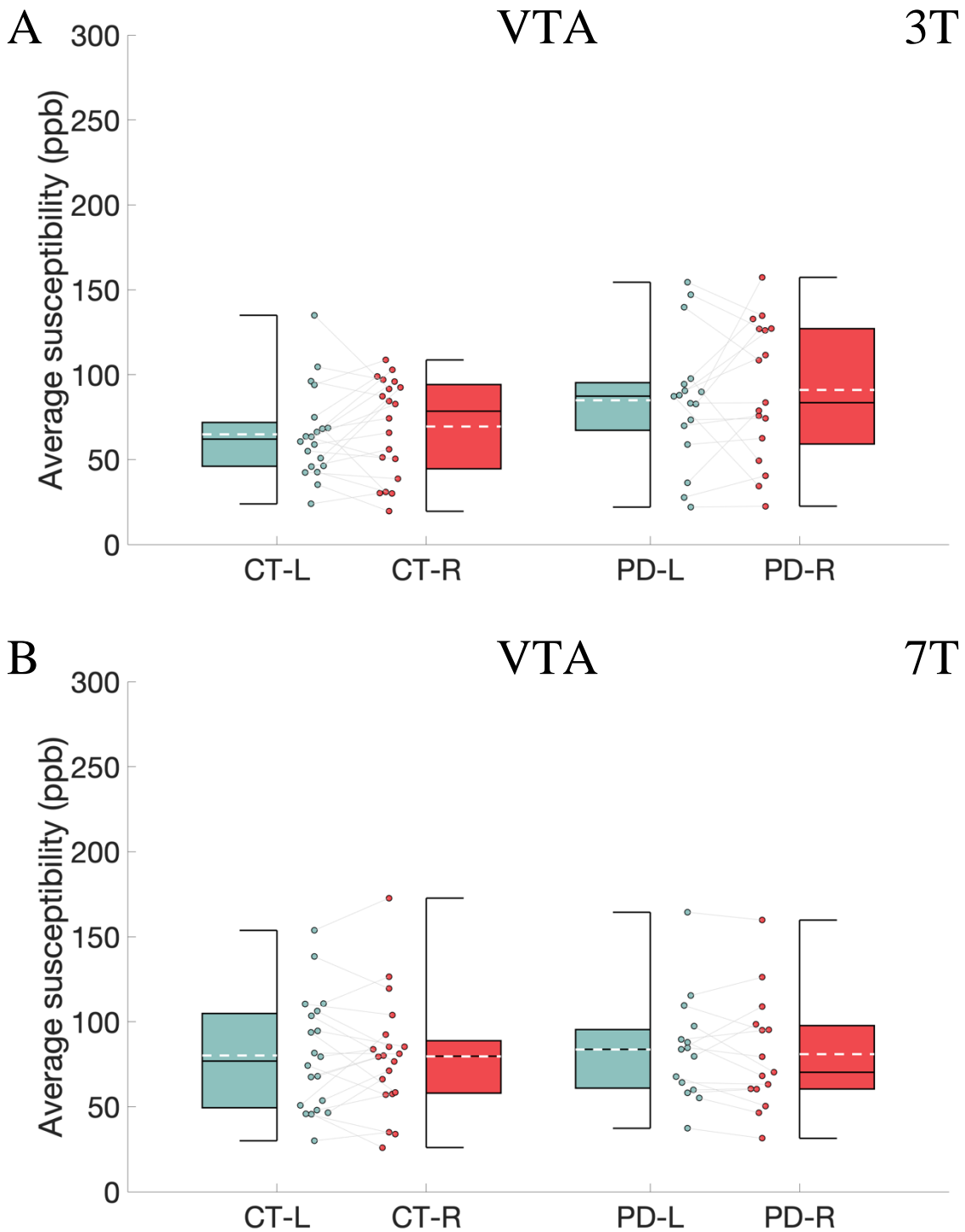


Figure 9. Average susceptibility for the VTA of early-stage PD patients and healthy controls at 3T and 7T. Data show paired hemispheric averages for all participants in scatterplots with corresponding boxplots demonstrating median and interquartile range in black lines. VTA average susceptibility values in ppb from QSM at both field strengths are shown as dashed white lines. No significant differences were found between groups at both field strengths. $n_{CT} = 21$, $n_{PD} = 17$

3.4.2 R2* in the VTA

A $2 \times 2 \times 2$ RM-ANCOVA of VTA average R2* value was performed using Group as the between-subjects factor with Hemisphere and Scanner as within-subjects variables controlling for age and sex as covariates. There was a significant main effect of Scanner [$F(1,31) = 9.635$, $MSe = 9.31$, $p_{adj} = .02$] suggesting higher R2* values at 7T versus 3T (Figure 10). No significant main effect of Group was found [$F(1,31) < 1$], which suggests PD patients had similar VTA iron deposition to controls regardless of scanner (Figure 10). No significant main effect of Hemisphere was found [$F(1,31) < 1$], suggesting similar iron levels between hemispheres. Lastly, no significant interactions were found for Hemisphere*Group [$F(1,31) < 1$], Scanner*Group [$F(1,31) = 2.679$, $MSe = 59.6$, $p_{adj} = .36$], Hemisphere*Scanner [$F(1,31) < 1$], or Hemisphere*Scanner*Group [$F(1,31) = 4.511$, $MSe = 15.8$, $p_{adj} = .27$].

Separate 2×2 RM-ANCOVAs were performed at 3T and 7T using Group as the between-subjects factor and Hemisphere as the within-subjects variable controlling for age and sex. For 3T, no significant main effect of Group was found [$F(1,34) = 1.465$, $MSe = 71.7$, $p_{adj} = .56$] with PD patients showing similar average R2* values as elderly controls, suggesting similar iron deposition (Figure 10A). No significant main effect of Hemisphere was found [$F(1,34) = 1.279$, $MSe = 16.7$, $p_{adj} = .58$], suggesting no difference in iron deposition between hemispheres with no significant Hemisphere*Group interaction [$F(1,34) = 5.581$, $MSe = 16.7$, $p_{adj} = .27$; Figure 10A].

For 7T data, no significant main effect of Group was found [$F(1,31) < 1$] with PD patients showing similar average R2* values and iron deposition (Figure 10B). No significant main effect of Hemisphere was found [$F(1,31) < 1$] along with no significant Hemisphere*Group interaction [$F(1,31) = 1.422$, $MSe = 19.2$, $p_{adj} = .57$]. Taken together, these observations suggest no elevation in VTA iron was found in early-stage PD patients using R2* relaxometry at 3T and 7T. Given that the main effect of Group was not significant for VTA iron content using R2* relaxometry, the ROC curve analyses were not performed on our VTA measures.

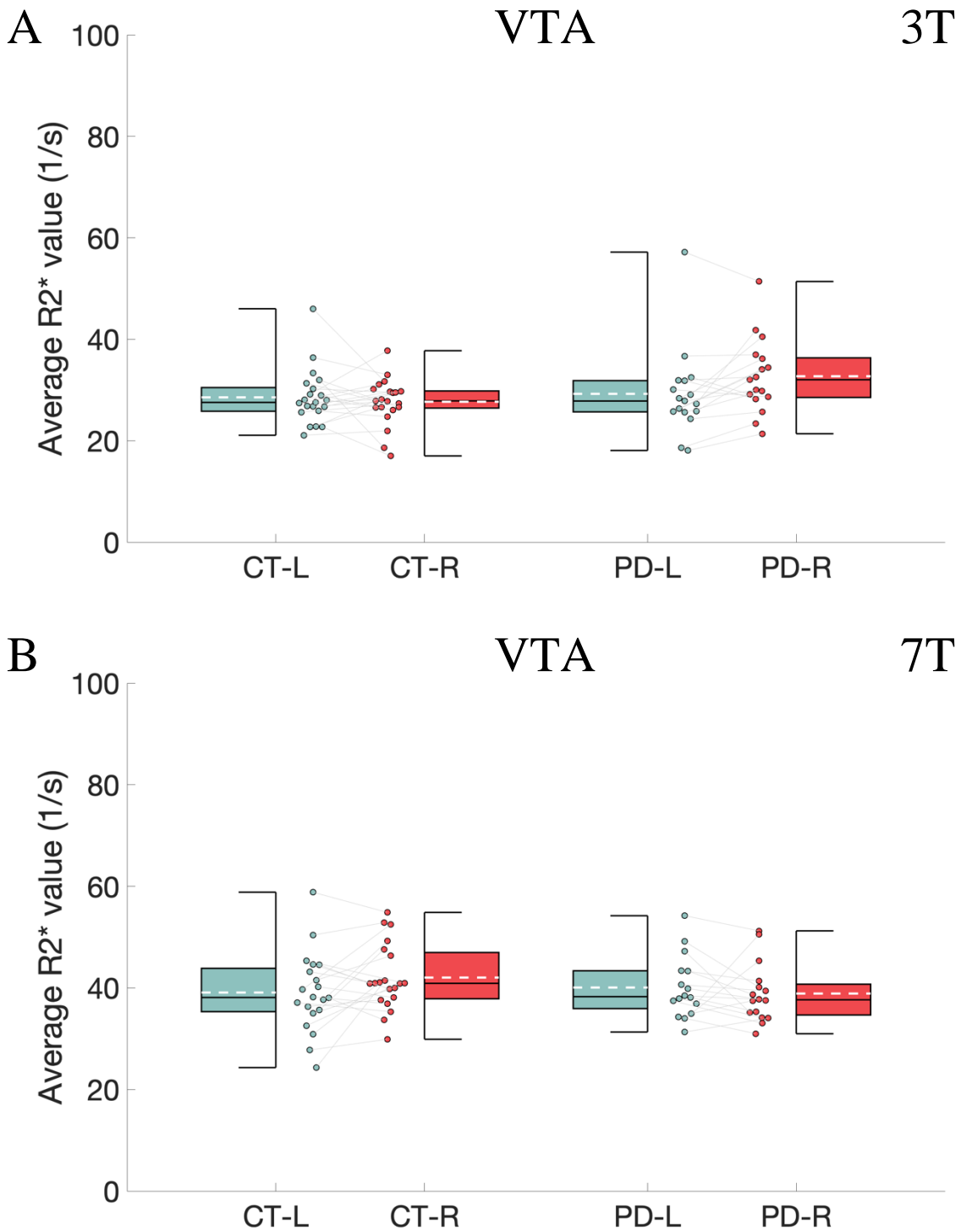


Figure 10. Average R2* values for the VTA of early-stage PD patients and healthy controls at 3T and 7T. Data show paired hemispheric averages for all participants in scatterplots with corresponding boxplots demonstrating median and interquartile range in black lines. VTA average R2* values in 1/s from R2* at both field strengths are shown as white dashed lines. No significant differences were found between groups at both field strengths with PD showing similar iron deposition to controls. $n_{CT} = 21$, $n_{PD} = 17$

3.5.1 Dice Similarity Coefficients between Scanners

To assess if similar volumes were being sampled between scanners, Dice similarity coefficients were calculated for the midbrain nuclei in each participant (Figure 11). Despite their small volumes, there was good overlap (Range of average Dice similarity coefficients: 0.67 - 0.82). A 3×2 RM-ANOVA using Group as between-subjects factor and Nucleus (SNc, SNr, and VTA) as within-subjects variable was performed. Mauchly's test of sphericity for Dice similarity coefficients indicated that the assumption of sphericity was violated ($\chi^2(2) = 10.984, p = .004$). Following Greenhouse-Geisser correction, a significant main effect of Nucleus was found [$F(1.56, 53.0) = 302, MSe = .254, p_{adj} < .001$] suggesting differences in between-scanner overlap across the midbrain nuclei (Figure 11). No significant main effect of Group [$F(1, 34) < 1$] or Nucleus*Group interaction [$F(1.56, 53.0) = 1.458, MSe = .001, p_{adj} = .24$] was found suggesting similar between-scanner overlap between PDs and controls across midbrain nuclei (Figure 11).

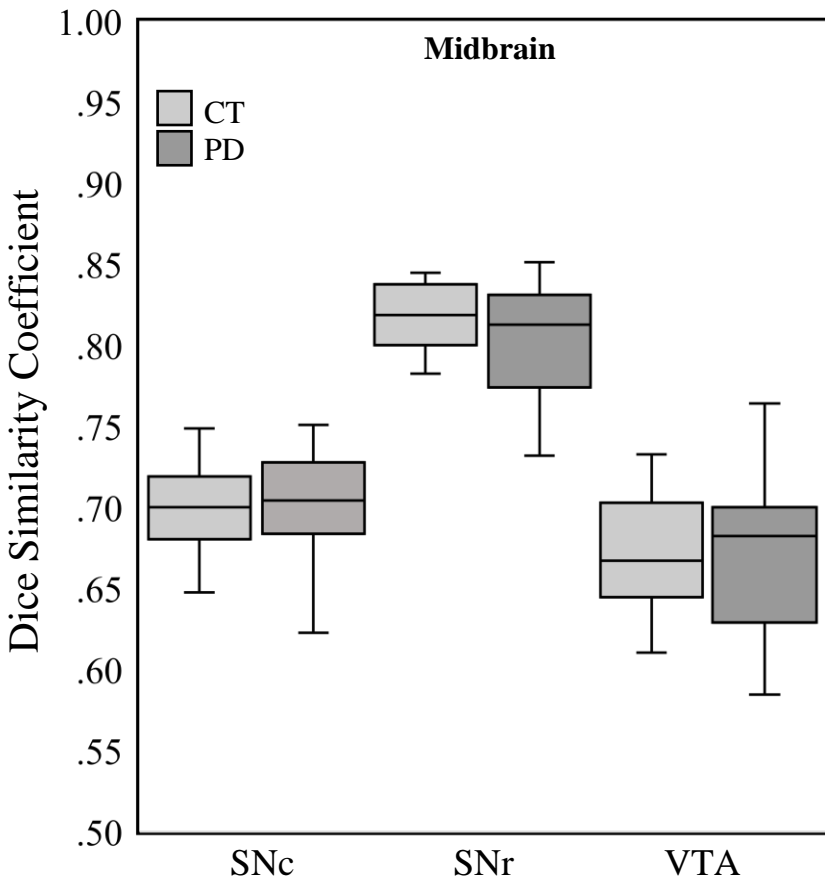


Figure 11. Dice similarity coefficients between scanners for midbrain structures of PD patients and controls. Data shows the overlap of bilateral ROIs between scanners after linear registration of 3T ROIs onto 7T ROIs. No significant differences were found between groups. $n_{CT} = 21, n_{PD} = 17$

Chapter 4: Discussion

4.1 General Summary of Results

In the present study, iron in the dopaminergic midbrain nuclei was successfully quantified in early-stage PD patients and healthy, age-matched elderly controls using QSM and R2* relaxometry at 3T and 7T MRI. Using the recently developed CIT168 probabilistic subcortical atlas, we bilaterally segmented the SNc, SNr, and VTA to measure average susceptibility and R2* values in these nuclei as proxies for iron concentration (Pauli et al., 2018). Additionally, the first *in vivo* assessment of human VTA iron was performed.

As predicted, SNc iron was significantly elevated bilaterally in early-stage PD patients based on average susceptibility from QSM at 3T and 7T. Using R2*, SNc iron elevation was not detected at 3T, but showed marginal significance at 7T, which suggests lower potential for clinical translation given the lack of sensitivity at the common 3T field strength. For diagnostic biomarker assessment of SNc iron, ROC curve analyses found QSM in the MAH of the SNc had diagnostic accuracy in the good to excellent range with AUCs from 0.81-0.87 at both field strengths. Conversely, R2* at 3T failed to reach significance for diagnostic accuracy while R2* at 7T was significant with an AUC of 0.73, which is still below the “good biomarker” cut-off of AUC = 0.80. These observations support the notion that QSM is more sensitive and accurate diagnostically than R2* relaxometry regarding SNc iron elevation in PD (Langkammer et al., 2016).

No significant group differences were detected in the SNr and VTA for either iron imaging technique at both field strengths. This suggests similar SNr and VTA iron content in early-stage PD patients and controls, as well as sparing of these structures from iron overload in early-stage PD as predicted. These observations highlight the need to separate the two SN subregions and measure SNc iron content in isolation to enhance sensitivity and diagnostic accuracy. The VTA succeeded as a negative control since iron elevation would be expected in late stage PD.

Looking between field strengths, no apparent advantage of 7T was found over 3T for QSM in the SNc. QSM was independent of field strength while R2* demonstrated dependence and proportionality with field strength as expected (Langkammer et al., 2016). Lastly, Dice similarity coefficients showed no differences in between-scanner overlap between groups. There was good overlap despite Dice score bias for small structures such as the SNc and VTA (Pauli et al., 2018).

Taken together, these findings suggest that QSM is a better diagnostic imaging tool for detecting the increased SNc iron content observed in PD when compared to R2* relaxometry.

4.2 Assessment of Iron Imaging as a Diagnostic Biomarker of PD

Iron content in the SNc successfully differentiated early-stage PD patients from age-matched controls. Given that iron elevation was noted only in the SNc in early-stage PD, it is beneficial to split the SN into its two constituents to improve sensitivity and diagnostic accuracy (Barbosa et al., 2015; Martin et al., 2008; Sofic, Paulus, Jellinger, Riederer, & Youdim, 1991). Our QSM and R2* averages in the SNc and SNr agree with previous findings (Barbosa et al., 2015; Du et al., 2016; Guan et al., 2017; Sethi et al., 2019). Furthermore, the relationship of higher iron in SNr compared to SNc is upheld in our findings, though only SNc iron could differentiate PD patients from controls (Good, Olanow & Perl, 1992; Kwon et al., 2012; Sofic et al., 1991). Our findings support previous work which suggests that whole SN iron measures are not sensitive to early-stage PD and control differences (Barbosa et al., 2015; He et al., 2015). This suggests that proper demarcation of the SNc/SNr border is imperative to isolate SNc and derive the most sensitive and accurate biomarker of early-stage PD. To date, segmentation algorithms have had difficulty delineating the subtle difference between the SNc and SNr, let alone providing boundaries of the much smaller VTA (Eapen et al., 2011; Pauli et al., 2018). In fact, the CIT168 subcortical atlas is the first to include the SNc, SNr, and importantly the VTA (Pauli et al., 2018).

To our knowledge, this study is the first to report *in vivo* measurements of iron in the VTA using MRI. The VTA had the lowest average values on both imaging techniques, which suggests that this nucleus has lower overall iron content than the SN regions (Hare et al., 2014; Hare & Double, 2016). This observation fits in line with histology that reports higher iron in the SNc and SNr relative to other dopaminergic midbrain nuclei (Dexter et al., 1991; Hare et al., 2014). The finding of statistically equivalent VTA iron between early-stage PD and controls was entirely predicted given that VTA degeneration occurs in later stages (Alberico et al., 2015). We tested only early-stage PD patients, with less than five years disease duration and who did not have cognitive impairment. VTA degeneration at later stages of PD is presumed to cause non-motor symptoms, particularly cognitive impairment (Alberico et al., 2015). The absence of VTA differences between our PD and control groups provided an important negative control. Furthermore, these differences in overall iron content could potentially explain the differences in

vulnerability between both nuclei in PD, given that the VTA is affected at later stages. However, this is made with caution as further analyses must rule out other differences between these nuclei that could contribute to differences in vulnerability to neurodegeneration (Hare et al., 2014).

Previous work comparing the two iron imaging techniques of QSM and R2* has led to similar results as those reported here. Using the Hanley-McNeil method (1983), we found that QSM had superior diagnostic sensitivity and accuracy, making it the preferred *in vivo* iron quantification technique (Barbosa et al., 2015; Du et al., 2016; Langkammer et al., 2016; Murakami et al., 2015). For example, Deistung and colleagues (2013) found only QSM provided qualitative discrimination of the SNc and SNr boundary when compared to magnitude and R2* images. This superior boundary demarcation could potentially have contributed to QSM's greater ability to detect iron overload in the SNc of PD patients compared to healthy controls in our study. QSM has also shown potential to detect unique iron "fingerprints" for differential diagnosis of parkinsonian syndromes (Ito et al., 2017). Furthermore, the effects of phase differences with non-local tissue is not accounted for in R2* relaxometry, which introduces noise from surrounding structures (e.g., from the SNr to the SNc and vice versa), which reduces sensitivity (Dusek et al., 2013; Sethi et al., 2019). The lower sensitivity of R2* relaxometry to detect SNc iron elevation in PD has been previously reported (Barbosa et al., 2015; Du et al., 2016; Guan et al., 2015; Langkammer et al., 2013; Sethi et al., 2019). QSM also shows stronger correlation with clinical severity scores in patients with PD than R2* relaxometry (Du et al., 2016; Langkammer et al., 2016). The advantages of using susceptibility for iron quantification, instead of using phase directly, is that susceptibility is not dependent on imaging parameters such as main field strength, object orientation, and echo time (Haacke et al., 2015; Liu, Li, Tong, Yeom, & Kuzminski, 2014, Liu et al., 2017). Furthermore, susceptibility has shown a linear relationship with iron content using ferritin phantoms and post-mortem analyses (Langkammer et al., 2010; Zheng et al., 2013). A recent paper suggests that 1 ppb in susceptibility is equivalent to a value close to 1 μg of iron per g of wet tissue (Ghasaban et al., 2018; Liu et al., 2016). Although R2* has been heavily utilized to quantify iron content, QSM is clearly a more promising method in terms of sensitivity and specificity (Barbosa et al., 2015; Du et al., 2016; Haacke et al., 2015; Langkammer et al., 2016).

This study found no apparent diagnostic advantage of 7T MRI over 3T MRI when using the average susceptibility or R2* value features of the three midbrain nuclei in direct comparisons. Any between-field strength comparison, however, is made with caution given the different voxel

sizes and shapes of the sequences between scanners. The smaller axial in-plane voxel size of the GRE scan at 3T could provide better discriminatory ability of boundaries than the larger isometric voxel size at 7T (Springer et al., 2016). Furthermore, different image features such as variance and entropy were not analyzed, which may prove a clear advantage for 7T MRI over 3T MRI. Lastly, there were differences in overlap based on the Dice coefficients, which tend to be biased for smaller structures, which can further limit between scanner comparisons (Pauli et al., 2018). The purpose of the between-field strength comparisons was strictly to determine if the diagnostic capability of QSM and R2* was sufficiently sensitive at lower field strengths (i.e. 3T). QSM in the SNc held up at 3T, although the between-group difference in SNc iron assessed with R2* was only marginally significant at 7T (Sethi et al., 2019). This observation is important for clinical translation as 3T scanners are more widely available than 7T scanners. Consequently, imaging biomarkers that are sensitive and accurate at 3T hold much more clinical potential than those discovered at 7T (Springer et al., 2016).

Looking at the ROC curves, the diagnostic accuracy of our iron imaging methods falls in line with previous reports (Barbosa et al., 2015; Du et al., 2016; Li et al., 2019). QSM falls in the good to excellent range of diagnostic accuracy with an AUC from 81 – 87%. R2* relaxometry was not significant at 3T and reached a diagnostic accuracy of 73% at 7T. Du and colleagues (2016) reported a diagnostic accuracy of 83% for QSM and 78% for R2* relaxometry when looking at the hand-drawn SNc at 3T MRI. Their R2* results have slightly higher diagnostic accuracy at 3T than ours, but this can be explained by the longer disease duration in their PD patients compensating for the lower sensitivity of R2*. The disease duration in their study was 5.5 years whereas it was only 2.5 years in ours.

A study by Li and colleagues (2019) at 3T, found only QSM and not R2* could significantly distinguish between PD patients and controls when looking at average values in the SN. They found that second-order features like entropy of QSM and R2* images had better results with diagnostic accuracies of 88-89% and 73-77%, respectively. The discriminatory ability of their SN second-order values falls in line with our SNc first-order values, which further highlights the improved sensitivity achieved when looking at the SNc in isolation rather than the whole SN in PD. Their work also suggests that features other than the mean value of the image could prove useful in future for detecting ideal diagnostic features, or perhaps generating a more sensitive combinatorial measure (Li et al., 2019). It is therefore evident that iron imaging, especially QSM,

demonstrates great potential as a diagnostic biomarker of PD. Though this novel structural imaging technique is still being developed and perfected, it demonstrates an ability to distinguish PD patients from healthy controls with strong diagnostic accuracy.

4.3 Comparison of Iron Imaging with Other Imaging Biomarkers

Although this study focused on iron imaging, other measures have been explored in trying to identify PD biomarkers. As mentioned earlier, neuromelanin is a pigment which has neuroprotective effects through iron chelation. Neuromelanin is lost as a result of PD and patients have about 50% of the neuromelanin of an age-matched control, which has been visualized using *in vivo* imaging (Sasaki et al., 2006). Recently, neuromelanin-sensitive T1w MRI has been developed that can discriminate neuromelanin loss in the SN of PD patients compared to controls. Further, neuromelanin MRI is sensitive to PD progression (Fabbri et al., 2017; Yang et al., 2018).

The ‘swallow-tail’ sign describes the normal axial imaging appearance of the nigrosome-1 within the SN using high resolution MRI (Schwarz et al., 2014). The loss of the ‘swallow-tail’ sign in PD has a reported diagnostic accuracy above 90% using susceptibility imaging (Schwarz et al., 2014). This change can be detected with QSM using the elevated iron content and neuromelanin-sensitive MRI using the decreased neuromelanin, which suggests a point of comparison and conversion between these two diagnostic techniques (Li et al., 2019). Takahashi and colleagues (2018a,b) reported on two occasions that neuromelanin imaging outperformed QSM (NM AUC = 0.86 versus QSM AUC = 0.68), but their methods used neuromelanin images to segment regions-of-interest and had lower quality segmentations and GRE sequences than those reported here. Nevertheless, both techniques have potential for combinatorial analyses to better understand structural changes in the SNc using T1w and T2w sequences.

Diffusion-weighted imaging (DWI) has shown some promise as a PD biomarker (Khan et al., 2019). Given that nigrostriatal pathway degeneration is a cardinal feature of early PD, followed by mesolimbic and mesocortical pathway abnormality, DWI measurement can provide insight into changes in these pathways for diagnosis and staging (Khan et al., 2019; Tuite, 2016). Good diagnostic accuracy using reduced fractional anisotropy in the SN of PD patients has been reported using DWI (Deng, Wang, Yang, Li, & Yu., 2018; He et al., 2018; Huddleston et al., 2017). However, there is noticeable variation in results among DWI studies, so an understanding of the full potential of DWI in PD is not yet established (Schwarz et al., 2013). Nonetheless, DWI can

differentially diagnose PD from other Parkinsonian syndromes like multiple system atrophy (Chung et al., 2009) and progressive supranuclear palsy (Seppi et al., 2003). In white matter, iron imaging underperforms diagnostically in PD patients because myelin content confounds the signal of the iron content (Langkammer et al., 2012; Guan et al., 2018). In this way, DWI might complement iron imaging to provide a measure of white matter degeneration whereas QSM can index gray-matter abnormalities in early-stage PD (Yang et al., 2018). Clearly, MRI biomarkers are multi-faceted in the analysis of PD features, with each technique showing benefits and costs relative to the others (Tuite, 2016). Despite all these investigations, MRI structural biomarkers of PD are only beginning to be developed with novel approaches and analysis techniques.

4.4 Limitations

The CIT168 probabilistic subcortical atlas used in this study has several limitations. The atlas is derived using a younger cohort, is based only on 3T MRI data, and uses averaging of numerous brains to raise the contrast-to-noise ratio between regions for delineation (Pauli et al., 2018). The atlas cohort is roughly 35 years younger than that of our sample, which means structural changes related to ageing are likely unaccounted for in these midbrain structures. However, since both PD patients and controls are age-matched and we have used the same atlas in both groups, this moderates any disadvantages based on using an atlas derived in healthy young controls. The atlas was derived in 3T MRI, which likely has reduced resolution compared to 7T MRI and altered boundary delineation; ideally a 7T version should be employed in our 7T data. Lastly, averaging results in the loss of some small-scale individual features such as the SNc/SNr boundary, which despite registration accuracy results in boundaries that can no longer be mapped back to the individual exactly (Pauli et al., 2018). This inherent limitation of atlases impacts the delineation of these midbrain nuclei, which can only be practically solved by having repeated scans of the same person, a costly solution (Pauli et al., 2018).

Other limitations include the implementation of cerebrospinal fluid (CSF) as a reference structure in QSM (Deistung et al., 2013). This structure was chosen based on its frequent appearance in the QSM literature (Acosta-Cabronero et al., 2018). Studies have reported that the inter-subject variability of susceptibility is higher in CSF relative to frontal white matter or cortical grey matter and propose that one of the latter be used instead (Betts, Acosta-Cabronero, Cardenas-Blanco, Nestor, & Duzel, 2016; Feng, Deistung, & Reichenbach, 2018). We ran an exploratory

analysis of cortical grey matter and found no major differences in the relationships compared to CSF. The CSF is a more generalizable reference structure given that tissue types are differentially affected by neurological diseases (Acosta-Cabronero et al., 2018). This would suggest that the CSF reference structure is sufficient for our analyses, but frontal white matter could be implemented as a second reference structure in future studies (Ropele & Langkammer, 2017).

Given the novelty of QSM, more work needs to be done regarding the ideal method for generating the susceptibility maps (Yu et al., 2019). Although we showed one technique, others may be more or less successful in a diagnostic capacity, thus warranting consortia to compare the various techniques (Acosta-Cabronero et al., 2018). Our technique could be further improved upon through prospective motion correction for QSM at 7T and using identical isometric voxel sizes to allow for between field strength comparison (Karsa, Punwani, & Shmueli, 2019; Mattern et al., 2019). Lastly, there are some white matter fibres and calcium deposits in these deep grey matter nuclei which could be reducing our sensitivity and estimation of iron values (Buch et al., 2015; Deistung, Schweser, & Reichenbach, 2017; Lancione et al., 2017). Looking at iron in white matter presents with difficulties using QSM due to the influence of myelin content on susceptibility, which reduces the ability of QSM to detect nigrostriatal degeneration (Langkammer et al., 2012).

4.5 Future Directions

The single atlas employed in this study could be improved upon through multi-atlas segmentation or segmentation algorithm approaches to better define nuclei boundaries. To our knowledge, no other atlases include all three midbrain nuclei hence our single atlas approach. With the development of better subcortical atlases, a multi-atlas approach could be conducted to better determine accurate structural boundaries. Furthermore, the development of novel segmentation algorithms that can accurately segment these small subcortical structures could bypass the need for atlases. Work by Eapen and colleagues (2011) found some success with SN segmentation at 7T, however, the VTA was more difficult to define and required manual tracing using the SNc and red nucleus as boundaries for the structure. Some segmentation algorithms have been developed to segment the striatum directly in QSM images, but more work is needed before they can accurately define the SNc/SNr boundary and delineate the elusive VTA nucleus. Being able to segment directly on QSM and R2* images would remove the step of registration to T1w images, reducing any alignment concerns.

Another avenue worth pursuing is the parcellation of the SNc as previous work has shown an important distinction between dorsal and ventral tiers of SNc in PD (Gibb & Lees, 1991; Haber, Fudge, & MacFarland, 2000). Though it is not possible to clearly distinguish these tiers *in vivo* using individual structural MRI, combining QSM and DWI could be employed to overcome this limitation (Pauli et al., 2018). Acosta-Carbenero and colleagues (2015) have shown iron elevation in the SNc and ventral lateral SN using whole brain QSM. A region-of-interest analysis of the ventral lateral SNc is warranted given this area is first affected by PD (Gibb & Lees, 1991). Our lab intends to parcellate the SNc using probabilistic tractography from DWI to better localize SNc iron accumulation and develop an understanding of the potential functional impacts based on reciprocal connections with the striatum and cortex (Khan et al., 2019).

Given that QSM has been shown here to detect early-stage PD, further experimentation is needed in even earlier stages of PD. We aim to look at *de novo* PD patients, immediately upon diagnosis, as well as in pre-clinical populations such as in patients with Rapid eye movement (REM) sleep behaviour disorder (RBD) to verify QSM's potential as an early diagnostic or pre-clinical biomarker, respectively (Postuma, 2017). Imaging *de novo* patients could provide insight about structural changes in the brain at the time of PD diagnosis. This could be used in combination with or in place of neurological assessment depending upon biomarker accuracy (Kim et al., 2018; Vaillancourt et al., 2009). Patients with RBD have become a major focus in neurodegeneration research as they present a unique opportunity to study changes that precede the onset of motor symptoms of alpha-synucleinopathies, such as PD. A majority of RBD patients will convert to PD or another alpha-synucleinopathy, such as multiple system atrophy (MSA) and Lewy body dementia (LBD) within ten years of their RBD diagnosis making it the strongest predictor of neurodegeneration (Postuma et al., 2009; Postuma et al., 2015). If changes in SNc iron content can be found in patients with RBD who later convert to PD, such a biomarker would allow trials of medications at earlier stages when these interventions have a better chance of efficacy.

Neuropathology investigations have reported the spatial patterns of dopaminergic neuron loss and iron accumulation within the SNc occur in parallel during PD (Massey et al., 2017). Following advancements and improvements to segmentation and QSM methodology, we can expect more accurate estimates of the true iron content in PD patients and increased sensitivity to subregions within the SNc, suggesting promise for iron imaging in clinical settings.

4.6 Conclusions

The present study found excessive iron accumulation in the SNc of early-stage PD patients with sparing of the SNr and VTA. This fits with our understanding of the pathophysiology of PD. This SNc iron overload was detected using QSM and R2* relaxometry. QSM in the SNc had higher diagnostic accuracy and outperformed R2* as a diagnostic biomarker of PD at both 3T and 7T. R2* of SNc did not distinguish PD patients from controls at 3T though QSM showed this difference strongly. Using QSM, there was no detectable advantage of using 7T relative to 3T. In this way, QSM demonstrated superior potential for clinical translation given its efficacy at 3T MRI. Capitalizing on our understanding of iron accumulation in the specific brain regions in early-stage PD and across disease progression, iron imaging could provide valuable biomarkers of PD, enabling accurate and reproducible diagnosis and prognosis of the disease. Finally, establishing sensitive and specific biomarkers of PD is a necessary step toward developing the first disease-modifying therapies in this neurodegenerative disorder, first described over 200 years ago.

References

- Aarsland, D., Bronnick, K., Williams-Gray, C., Weintraub, D., Marder, K., Kulisevsky, J., . . . Emre, M. (2010). Mild cognitive impairment in Parkinson disease: A multicenter pooled analysis. *Neurology*, *75*(12), 1062-1069. doi:10.1212/WNL.0b013e3181f39d0e
- Abdul-Rahman, H. S., Gdeisat, M. A., Burton, D. R., Lalor, M. J., Lilley, F., & Moore, C. J. (2007). Fast and robust three-dimensional best path phase unwrapping algorithm. *Applied Optics*, *46*(26), 6623-6635. doi:10.1364/AO.46.006623
- Acosta-Cabronero, J., Milovic, C., Mattern, H., Tejos, C., Speck, O., & Callaghan, M. F. (2018). A robust multi-scale approach to quantitative susceptibility mapping. *Neuroimage*, *183*, 7-24. doi:10.1016/j.neuroimage.2018.07.065
- Aime, S., Bergamasco, B., Biglino, D., Digilio, G., Fasano, M., Giamello, E., & Lopiano, L. (1997). EPR investigations of the iron domain in neuromelanin. *Biochimica et Biophysica Acta (BBA) - Molecular Basis of Disease*, *1361*(1), 49-58. doi:https://doi.org/10.1016/S0925-4439(97)00014-8
- Aguirre, P., Urrutia, P., Tapia, V., Villa, M., Paris, I., Segura-Aguilar, J., & Nunez, M. T. (2012). The dopamine metabolite aminochrome inhibits mitochondrial complex I and modifies the expression of iron transporters DMT1 and FPN1. *Biometals*, *25*(4), 795-803. doi:10.1007/s10534-012-9525-y
- Alberico, S. L., Cassell, M. D., & Narayanan, N. S. (2015). The vulnerable ventral tegmental area in Parkinson's Disease. *Basal Ganglia*, *5*(2-3), 51-55. doi:10.1016/j.baga.2015.06.001
- Albers, D. S., & Beal, M. F. (2000). Mitochondrial dysfunction and oxidative stress in aging and neurodegenerative disease. *Journal of Neural Transmission. Supplementa*, *59*, 133-154.
- Arriagada, C., Paris, I., Sanchez de las Matas, M. J., Martinez-Alvarado, P., Cardenas, S., Castaneda, P., . . . Segura-Aguilar, J. (2004). On the neurotoxicity mechanism of leucoaminochrome o-semiquinone radical derived from dopamine oxidation: Mitochondria damage, necrosis, and hydroxyl radical formation. *Neurobiology of Disease*, *16*(2), 468-477. doi:10.1016/j.nbd.2004.03.014
- Atherton, J. F., & Bevan, M. D. (2005). Ionic mechanisms underlying autonomous action

- potential generation in the somata and dendrites of GABAergic substantia nigra pars reticulata neurons in vitro. *Journal of Neuroscience*, 25(36), 8272-8281.
doi:10.1523/JNEUROSCI.1475-05.2005
- Ayton, S., & Lei, P. (2014). Nigral iron elevation is an invariable feature of Parkinson's disease and is a sufficient cause of neurodegeneration. *Biomed Research International*, 2014, 581256. doi:10.1155/2014/581256
- Barbosa, J. H., Santos, A. C., Tumas, V., Liu, M., Zheng, W., Haacke, E. M., & Salmon, C. E. (2015). Quantifying brain iron deposition in patients with Parkinson's disease using quantitative susceptibility mapping, R2 and R2*. *Magnetic Resonance Imaging*, 33(5), 559-565. doi:10.1016/j.mri.2015.02.021
- Barone, P., Antonini, A., Colosimo, C., Marconi, R., Morgante, L., Avarello, T. P., . . . group, P. s. (2009). The PRIAMO study: A multicenter assessment of nonmotor symptoms and their impact on quality of life in Parkinson's disease. *Movement Disorders*, 24(11), 1641-1649. doi:10.1002/mds.22643
- Baudrexel, S., Nurnberger, L., Rub, U., Seifried, C., Klein, J. C., Deller, T., . . . Hilker, R. (2010). Quantitative mapping of T1 and T2* discloses nigral and brainstem pathology in early Parkinson's disease. *Neuroimage*, 51(2), 512-520.
doi:10.1016/j.neuroimage.2010.03.005
- Beard, J. (2003). Iron deficiency alters brain development and functioning. *The Journal of Nutrition*, 133(5 Suppl 1), 1468s-1472s. doi:10.1093/jn/133.5.1468S
- Beard, J. L., Chen, Q., Connor, J., & Jones, B. C. (1994). Altered monoamine metabolism in caudate-putamen of iron-deficient rats. *Pharmacology Biochemistry and Behavior*, 48(3), 621-624.
- Benjamini, Y., & Hochberg, Y. (1995). Controlling the False Discovery Rate: A Practical and Powerful Approach to Multiple Testing. *Journal of the Royal Statistical Society: Series B (Methodological)*, 57(1), 289-300. doi:10.1111/j.2517-6161.1995.tb02031.x
- Berg, D., Youdim, M. B., & Riederer, P. (2004). Redox imbalance. *Cell and Tissue Research*, 318(1), 201-213. doi:10.1007/s00441-004-0976-5
- Betts, M. J., Acosta-Cabronero, J., Cardenas-Blanco, A., Nestor, P. J., & Duzel, E. (2016). High-resolution characterisation of the aging brain using simultaneous quantitative

- susceptibility mapping (QSM) and R2* measurements at 7T. *Neuroimage*, 138, 43-63.
doi:10.1016/j.neuroimage.2016.05.024
- Bharath, S., Hsu, M., Kaur, D., Rajagopalan, S., & Andersen, J. K. (2002). Glutathione, iron and Parkinson's disease. *Biochemical Pharmacology*, 64(5), 1037-1048.
doi:https://doi.org/10.1016/S0006-2952(02)01174-7
- Bianco, L. E., Wiesinger, J., Earley, C. J., Jones, B. C., & Beard, J. L. (2008). Iron deficiency alters dopamine uptake and response to L-DOPA injection in Sprague-Dawley rats. *Journal of Neurochemistry*, 106(1), 205-215. doi:10.1111/j.1471-4159.2008.05358.x
- Bilgic, B., Pfefferbaum, A., Rohlfing, T., Sullivan, E. V., & Adalsteinsson, E. (2012). MRI estimates of brain iron concentration in normal aging using quantitative susceptibility mapping. *Neuroimage*, 59(3), 2625-2635. doi:10.1016/j.neuroimage.2011.08.077
- Billings, J. L., Gordon, S. L., Rawling, T., Doble, P. A., Bush, A. I., Adlard, P. A., . . . Hare, D. J. (2019). L-DOPA modulates brain iron, dopaminergic neurodegeneration and motor dysfunction in iron overload and mutant alpha-synuclein mouse models of Parkinson's disease. *Journal of Neurochemistry*, 150(1), 88-106. doi:10.1111/jnc.14676
- Bisaglia, M., Mammi, S., & Bubacco, L. (2007). Kinetic and structural analysis of the early oxidation products of dopamine: Analysis of the interactions with alpha-synuclein. *Journal of Biological Chemistry*, 282(21), 15597-15605. doi:10.1074/jbc.M610893200
- Bisaglia, M., Soriano, M. E., Arduini, I., Mammi, S., & Bubacco, L. (2010). Molecular characterization of dopamine-derived quinones reactivity toward NADH and glutathione: implications for mitochondrial dysfunction in Parkinson disease. *Biochimica et Biophysica Acta*, 1802(9), 699-706. doi:10.1016/j.bbadis.2010.06.006
- Blum, D., Torch, S., Lambeng, N., Nissou, M., Benabid, A. L., Sadoul, R., & Verna, J. M. (2001). Molecular pathways involved in the neurotoxicity of 6-OHDA, dopamine and MPTP: Contribution to the apoptotic theory in Parkinson's disease. *Progress in Neurobiology*, 65(2), 135-172.
- Buch, S., Liu, S., Ye, Y., Cheng, Y.-C. N., Neelavalli, J., & Haacke, E. M. (2015). Susceptibility mapping of air, bone, and calcium in the head. *Magnetic Resonance in Medicine*, 73(6), 2185-2194. doi:10.1002/mrm.25350

- Burhans, M. S., Dailey, C., Beard, Z., Wiesinger, J., Murray-Kolb, L., Jones, B. C., & Beard, J. L. (2005). Iron deficiency: Differential effects on monoamine transporters. *Nutritional Neuroscience*, 8(1), 31-38. doi:10.1080/10284150500047070
- Cao, J. Y., & Dixon, S. J. (2016). Mechanisms of ferroptosis. *Cellular and Molecular Life Sciences*, 73(11), 2195-2209. doi:10.1007/s00018-016-2194-1
- Chatnuntawech, I., McDaniel, P., Cauley, S. F., Gagoski, B. A., Langkammer, C., Martin, A., . . . Bilgic, B. (2017). Single-step quantitative susceptibility mapping with variational penalties. *NMR in Biomedicine*, 30(4). doi:10.1002/nbm.3570
- Chen, Z., Johnston, L. A., Kwon, D. H., Oh, S. H., Cho, Z.-H., & Egan, G. F. (2010). An optimised framework for reconstructing and processing MR phase images. *Neuroimage*, 49(2), 1289-1300. doi:https://doi.org/10.1016/j.neuroimage.2009.09.071
- Chinta, S. J., & Andersen, J. K. (2008). Redox imbalance in Parkinson's disease. *Biochimica et Biophysica Acta*, 1780(11), 1362-1367. doi:10.1016/j.bbagen.2008.02.005
- Chung, E. J., Kim, E. G., Bae, J. S., Eun, C. K., Lee, K. S., Oh, M., & Kim, S. J. (2009). Usefulness of diffusion-weighted MRI for differentiation between Parkinson's disease and Parkinson variant of multiple system atrophy. *Journal of movement disorders*, 2(2), 64-68. doi:10.14802/jmd.09017
- Crichton, R. R., & Ward, R. J. (2014) *Metal based neurodegeneration: From molecular mechanisms to therapeutic strategies*. 2nd edn. Chichester: John Wiley & Sons.
- Deistung, A., Rauscher, A., Sedlacik, J., Stadler, J., Witoszynskyj, S., & Reichenbach, J. R. (2008). Susceptibility weighted imaging at ultra high magnetic field strengths: Theoretical considerations and experimental results. *Magnetic Resonance in Medicine*, 60(5), 1155-1168. doi:10.1002/mrm.21754
- Deistung, A., Schafer, A., Schweser, F., Biedermann, U., Turner, R., & Reichenbach, J. R. (2013). Toward in vivo histology: a comparison of quantitative susceptibility mapping (QSM) with magnitude-, phase-, and R2*-imaging at ultra-high magnetic field strength. *Neuroimage*, 65, 299-314. doi:10.1016/j.neuroimage.2012.09.055
- Deistung, A., Schweser, F., & Reichenbach, J. R. (2017). Overview of quantitative susceptibility mapping. *NMR in Biomedicine*, 30(4). doi:10.1002/nbm.3569

- Deng, X. Y., Wang, L., Yang, T. T., Li, R., & Yu, G. (2018). A meta-analysis of diffusion tensor imaging of substantia nigra in patients with Parkinson's disease. *Scientific Reports*, *8*(1), 2941. doi:10.1038/s41598-018-20076-y
- Dexter, D. T., Carayon, A., Javoy-Agid, F., Agid, Y., Wells, F. R., Daniel, S. E., . . . Marsden, C. D. (1991). Alterations in the levels of iron, ferritin and other trace metals in Parkinson's disease and other neurodegenerative diseases affecting the basal ganglia. *Brain*, *114*, 1953-1975.
- Dice, L. R. (1945). Measures of the amount of ecologic association between species. *Ecology*, *26*(3), 297-302. doi:10.2307/1932409
- Dixon, S. J., Lemberg, K. M., Lamprecht, M. R., Skouta, R., Zaitsev, E. M., Gleason, C. E., . . . Stockwell, B. R. (2012). Ferroptosis: An iron-dependent form of nonapoptotic cell death. *Cell*, *149*(5), 1060-1072. doi:10.1016/j.cell.2012.03.042
- Dixon, S. J., & Stockwell, B. R. (2014). The role of iron and reactive oxygen species in cell death. *Nature Chemical Biology*, *10*, 9. doi:10.1038/nchembio.1416
- Dlouhy, A. C., & Outten, C. E. (2013). The iron metallome in eukaryotic organisms. *Metal Ions in Life Science*, *12*, 241-278. doi:10.1007/978-94-007-5561-1_8
- Du, G., Liu, T., Lewis, M. M., Kong, L., Wang, Y., Connor, J., . . . Huang, X. (2016). Quantitative susceptibility mapping of the midbrain in Parkinson's disease. *Movement Disorders*, *31*(3), 317-324. doi:10.1002/mds.26417
- Du, G., Lewis, M. M., Sica, C., He, L., Connor, J. R., Kong, L., . . . Huang, X. (2018). Distinct progression pattern of susceptibility MRI in the substantia nigra of Parkinson's patients. *Movement Disorders*. doi:10.1002/mds.27318
- Du, G., Lewis, M. M., Sica, C., Kong, L., & Huang, X. (2019). Magnetic resonance T1w/T2w ratio: A parsimonious marker for Parkinson disease. *Annals of Neurology*, *85*(1), 96-104. doi:10.1002/ana.25376
- Dusek, P., Dezortova, M., & Wuerfel, J. (2013). Chapter Nine - Imaging of Iron. In K. P. Bhatia & S. A. Schneider (Eds.), *International Review of Neurobiology* (Vol. 110, pp. 195-239): Academic Press.
- Duyn, J. (2013). MR susceptibility imaging. *Journal of Magnetic Resonance*, *229*, 198-207. doi:https://doi.org/10.1016/j.jmr.2012.11.013
- Duyn, J. H., van Gelderen, P., Li, T.-Q., de Zwart, J. A., Koretsky, A. P., & Fukunaga, M.

- (2007). High-field MRI of brain cortical substructure based on signal phase. *Proceedings of the National Academy of Sciences*, 104(28), 11796. doi:10.1073/pnas.0610821104
- Eapen, M., Zald, D. H., Gatenby, J. C., Ding, Z., & Gore, J. C. (2011). Using high-resolution MR imaging at 7T to evaluate the anatomy of the midbrain dopaminergic system. *AJNR American Journal of Neuroradiology*, 32(4), 688-694. doi:10.3174/ajnr.A2355
- Elgh, E., Domellof, M., Linder, J., Edstrom, M., Stenlund, H., & Forsgren, L. (2009). Cognitive function in early Parkinson's disease: A population-based study. *European Journal of Neurology*, 16(12), 1278-1284. doi:10.1111/j.1468-1331.2009.02707.x
- Elster, A. D. (1993). Sellar susceptibility artifacts: Theory and implications. *AJNR American Journal of Neuroradiology*, 14(1), 129-136.
- Eskildsen, S. F., Coupé, P., Fonov, V., Manjón, J. V., Leung, K. K., Guizard, N., . . . Collins, D. L. (2012). BEaST: Brain extraction based on nonlocal segmentation technique. *Neuroimage*, 59(3), 2362-2373. doi:https://doi.org/10.1016/j.neuroimage.2011.09.012
- Exley, C., House, E., Polwart, A., & Esiri, M. M. (2012). Brain burdens of aluminum, iron, and copper and their relationships with amyloid-beta pathology in 60 human brains. *Journal of Alzheimer's Disease*, 31(4), 725-730. doi:10.3233/jad-2012-120766
- Fabbri, M., Reimao, S., Carvalho, M., Nunes, R. G., Abreu, D., Guedes, L. C., . . . Ferreira, J. J. (2017). Substantia nigra neuromelanin as an imaging biomarker of disease progression in Parkinson's disease. *Journal of Parkinson's Disease*, 7(3), 491-501. doi:10.3233/jpd-171135
- Fahn, S., & Sulzer, D. (2004). Neurodegeneration and neuroprotection in Parkinson disease. *NeuroRx*, 1(1), 139-154. doi:10.1602/neurorx.1.1.139
- Fearnley, J. M., & Lees, A. J. (1991). Ageing and Parkinson's disease: Substantia nigra regional selectivity. *Brain*, 114 (Pt 5)(Pt 5), 2283-2301.
- Feng, X., Deistung, A., & Reichenbach, J. R. (2018). Quantitative susceptibility mapping (QSM) and R2(*) in the human brain at 3T: Evaluation of intra-scanner repeatability. *Zeitschrift für Medizinische Physik*, 28(1), 36-48. doi:10.1016/j.zemedi.2017.05.003
- Fernandez-Seara, M. A., & Wehrli, F. W. (2000). Postprocessing technique to correct for background gradients in image-based R*(2) measurements. *Magnetic Resonance in Medicine*, 44(3), 358-366.

- Flydal, M. I., & Martinez, A. (2013). Phenylalanine hydroxylase: Function, structure, and regulation. *IUBMB Life*, *65*(4), 341-349. doi:10.1002/iub.1150
- Friedman, A., & Galazka-Friedman, J. (2012). The history of the research of iron in parkinsonian substantia nigra. *Journal of Neural Transmission (Vienna)*, *119*(12), 1507-1510. doi:10.1007/s00702-012-0894-8
- Fuchs, Y., & Steller, H. (2011). Programmed cell death in animal development and disease. *Cell*, *147*(4), 742-758. doi:10.1016/j.cell.2011.10.033
- Gelman, N., Gorell, J. M., Barker, P. B., Savage, R. M., Spickler, E. M., Windham, J. P., & Knight, R. A. (1999). MR imaging of human brain at 3.0 T: Preliminary report on transverse relaxation rates and relation to estimated iron content. *Radiology*, *210*(3), 759-767. doi:10.1148/radiology.210.3.r99fe41759
- Ghassaban, K., Liu, S., Jiang, C., & Haacke, E. M. (2019). Quantifying iron content in magnetic resonance imaging. *Neuroimage*, *187*, 77-92. doi:10.1016/j.neuroimage.2018.04.047
- Gibb, W. R., & Lees, A. J. (1991). Anatomy, pigmentation, ventral and dorsal subpopulations of the substantia nigra, and differential cell death in Parkinson's disease. *Journal of Neurology, Neurosurgery, and Psychiatry*, *54*(5), 388-396.
- Good, P. F., Olanow, C. W., & Perl, D. P. (1992). Neuromelanin-containing neurons of the substantia nigra accumulate iron and aluminum in Parkinson's disease: A LAMMA study. *Brain Research*, *593*(2), 343-346. doi:10.1016/0006-8993(92)91334-b
- Guan, X., Xuan, M., Gu, Q., Huang, P., Liu, C., Wang, N., . . . Zhang, M. (2017). Regionally progressive accumulation of iron in Parkinson's disease as measured by quantitative susceptibility mapping. *NMR in Biomedicine*, *30*(4). doi:10.1002/nbm.3489
- Guan, X., Huang, P., Zeng, Q., Liu, C., Wei, H., Xuan, M., . . . Zhang, M. (2018). Quantitative susceptibility mapping as a biomarker for evaluating white matter alterations in Parkinson's disease. *Brain Imaging and Behavior*. doi:10.1007/s11682-018-9842-z
- Guiney, S. J., Adlard, P. A., Bush, A. I., Finkelstein, D. I., & Ayton, S. (2017). Ferroptosis and cell death mechanisms in Parkinson's disease. *Neurochemistry International*, *104*, 34-48. doi:10.1016/j.neuint.2017.01.004
- Haacke, E. M., Cheng, N. Y., House, M. J., Liu, Q., Neelavalli, J., Ogg, R. J., . . . Obenaus, A. (2005). Imaging iron stores in the brain using magnetic resonance imaging. *Magnetic Resonance Imaging*, *23*(1), 1-25. doi:10.1016/j.mri.2004.10.001

- Haacke, E. M., Liu, S., Buch, S., Zheng, W., Wu, D., & Ye, Y. (2015). Quantitative susceptibility mapping: Current status and future directions. *Magnetic Resonance Imaging*, 33(1), 1-25. doi:10.1016/j.mri.2014.09.004
- Haas, R. H., Nasirian, F., Nakano, K., Ward, D., Pay, M., Hill, R., & Shults, C. W. (1995). Low platelet mitochondrial complex I and complex II/III activity in early untreated Parkinson's disease. *Annals of Neurology*, 37(6), 714-722. doi:10.1002/ana.410370604
- Haber, S. N., Fudge, J. L., & McFarland, N. R. (2000). Striatonigrostriatal pathways in primates form an ascending spiral from the shell to the dorsolateral striatum. *Journal of Neuroscience*, 20(6), 2369-2382.
- Hallgren, B., & Sourander, P. (1958). The effect of age on the non-haemin iron in the human brain. *Journal of Neurochemistry*, 3(1), 41-51.
- Hambright, W. S., Fonseca, R. S., Chen, L., Na, R., & Ran, Q. (2017). Ablation of ferroptosis regulator glutathione peroxidase 4 in forebrain neurons promotes cognitive impairment and neurodegeneration. *Redox Biology*, 12, 8-17. doi:10.1016/j.redox.2017.01.021
- Hammond, K. E., Lupo, J. M., Xu, D., Metcalf, M., Kelley, D. A. C., Pelletier, D., . . . Nelson, S. J. (2008). Development of a robust method for generating 7.0 T multichannel phase images of the brain with application to normal volunteers and patients with neurological diseases. *Neuroimage*, 39(4), 1682-1692.
doi:<https://doi.org/10.1016/j.neuroimage.2007.10.037>
- Hanley, J. A., & McNeil, B. J. (1983). A method of comparing the areas under receiver operating characteristic curves derived from the same cases. *Radiology*, 148(3), 839-843.
doi:10.1148/radiology.148.3.6878708
- Hare, D. J., Lei, P., Ayton, S., Roberts, B. R., Grimm, R., George, J. L., . . . Doble, P. A. (2014). An iron–dopamine index predicts risk of parkinsonian neurodegeneration in the substantia nigra pars compacta. *Chemical Science*, 5(6), 2160-2169.
doi:10.1039/c3sc53461h
- Hare, D. J., & Double, K. L. (2016). Iron and dopamine: A toxic couple. *Brain*, 139(Pt 4), 1026-1035. doi:10.1093/brain/aww022
- Hashimoto, M., Hsu, L. J., Xia, Y., Takeda, A., Sisk, A., Sundsmo, M., & Masliah, E. (1999). Oxidative stress induces amyloid-like aggregate formation of NACP/alpha-synuclein in vitro. *Neuroreport*, 10(4), 717-721.

- He, N., Ling, H., Ding, B., Huang, J., Zhang, Y., Zhang, Z., . . . Yan, F. (2015). Region-specific disturbed iron distribution in early idiopathic Parkinson's disease measured by quantitative susceptibility mapping. *Human Brain Mapping, 36*(11), 4407-4420. doi:10.1002/hbm.22928
- He, R., Yan, X., Guo, J., Xu, Q., Tang, B., & Sun, Q. (2018). Recent advances in biomarkers for Parkinson's disease. *Frontiers in Aging Neuroscience, 10*, 305. doi:10.3389/fnagi.2018.00305
- Hirsch, E., Graybiel, A. M., & Agid, Y. A. (1988). Melanized dopaminergic neurons are differentially susceptible to degeneration in Parkinson's disease. *Nature, 334*(6180), 345-348. doi:10.1038/334345a0
- Honarmand Ebrahimi, K., Hagedoorn, P. L., & Hagen, W. R. (2015). Unity in the biochemistry of the iron-storage proteins ferritin and bacterioferritin. *Chemical Reviews, 115*(1), 295-326. doi:10.1021/cr5004908
- Hornykiewicz, O. (1998). Biochemical aspects of Parkinson's disease. *Neurology, 51*(2 Suppl 2), S2-9.
- House, E., Collingwood, J., Khan, A., Korchazkina, O., Berthon, G., & Exley, C. (2004). Aluminium, iron, zinc and copper influence the in vitro formation of amyloid fibrils of Abeta42 in a manner which may have consequences for metal chelation therapy in Alzheimer's disease. *Journal of Alzheimer's Disease, 6*(3), 291-301.
- Huddleston, D. E., Langley, J., Sedlacik, J., Boelmans, K., Factor, S. A., & Hu, X. P. (2017). In vivo detection of lateral-ventral tier nigral degeneration in Parkinson's disease. *Human Brain Mapping, 38*(5), 2627-2634. doi:10.1002/hbm.23547
- Huenchuguala, S., Munoz, P., Zavala, P., Villa, M., Cuevas, C., Ahumada, U., . . . Segura-Aguilar, J. (2014). Glutathione transferase mu 2 protects glioblastoma cells against aminochrome toxicity by preventing autophagy and lysosome dysfunction. *Autophagy, 10*(4), 618-630. doi:10.4161/auto.27720
- Huettel, S. A., Song, A. W., & McCarthy, G. (2014). *Functional magnetic resonance imaging*. Sunderland, MA: Sinauer Associates.
- Ito, K., Ohtsuka, C., Yoshioka, K., Kameda, H., Yokosawa, S., Sato, R., . . . Sasaki, M. (2017). Differential diagnosis of parkinsonism by a combined use of diffusion kurtosis imaging

- and quantitative susceptibility mapping. *Neuroradiology*, 59(8), 759-769.
doi:10.1007/s00234-017-1870-7
- Jankovic, J. (2008). Parkinson's disease: Clinical features and diagnosis. *Journal of Neurology, Neurosurgery, and Psychiatry*, 79(4), 368-376. doi:10.1136/jnnp.2007.131045
- Jenner, P. (1993). Altered mitochondrial function, iron metabolism and glutathione levels in Parkinson's disease. *Acta Neurologica Scandinavica Supplementa*, 146, 6-13.
- Jenner, P., & Olanow, C. W. (1996). Oxidative stress and the pathogenesis of Parkinson's disease. *Neurology*, 47(6 Suppl 3), S161-170. doi:10.1212/wnl.47.6_suppl_3.161s
- Jenner, P. (2003). Oxidative stress in Parkinson's disease. *Annals of Neurology*, 53 Suppl 3, S26-36; discussion S36-28. doi:10.1002/ana.10483
- Karsa, A., Punwani, S., & Shmueli, K. (2019). The effect of low resolution and coverage on the accuracy of susceptibility mapping. *Magnetic Resonance in Medicine*, 81(3), 1833-1848. doi:10.1002/mrm.27542
- Kaur, D., Lee, D., Ragapolan, S., & Andersen, J. K. (2009). Glutathione depletion in immortalized midbrain-derived dopaminergic neurons results in increases in the labile iron pool: Implications for Parkinson's disease. *Free Radical Biology and Medicine*, 46(5), 593-598. doi:10.1016/j.freeradbiomed.2008.11.012
- Khan, A. R., Hiebert, N. M., Vo, A., Wang, B. T., Owen, A. M., Seergobin, K. N., & MacDonald, P. A. (2019). Biomarkers of Parkinson's disease: Striatal sub-regional structural morphometry and diffusion MRI. *Neuroimage: Clinical*, 21, 101597. doi:10.1016/j.nicl.2018.11.007
- Kim, E. Y., Sung, Y. H., Shin, H. G., Noh, Y., Nam, Y., & Lee, J. (2018). Diagnosis of early-stage idiopathic Parkinson's disease using high-resolution quantitative susceptibility mapping combined with histogram analysis in the substantia nigra at 3 T. *Journal of Clinical Neurology*, 14(1), 90-97. doi:10.3988/jcn.2018.14.1.90
- Kish, S. J., Shannak, K., & Hornykiewicz, O. (1988). Uneven pattern of dopamine loss in the striatum of patients with idiopathic Parkinson's disease. Pathophysiologic and clinical implications. *New England Journal of Medicine*, 318(14), 876-880. doi:10.1056/NEJM198804073181402

- Kwon, D. H., Kim, J. M., Oh, S. H., Jeong, H. J., Park, S. Y., Oh, E. S., . . . Cho, Z. H. (2012). Seven-Tesla magnetic resonance images of the substantia nigra in Parkinson disease. *Annals of Neurology*, *71*(2), 267-277. doi:10.1002/ana.22592
- Lammel, S., Hetzel, A., Hackel, O., Jones, I., Liss, B., & Roeper, J. (2008). Unique properties of mesoprefrontal neurons within a dual mesocorticolimbic dopamine system. *Neuron*, *57*(5), 760-773. doi:10.1016/j.neuron.2008.01.022
- Lancione, M., Tosetti, M., Donatelli, G., Cosottini, M., & Costagli, M. (2017). The impact of white matter fiber orientation in single-acquisition quantitative susceptibility mapping. *NMR in Biomedicine*, *30*(11). doi:10.1002/nbm.3798
- Langkammer, C., Krebs, N., Goessler, W., Scheurer, E., Ebner, F., Yen, K., . . . Ropele, S. (2010). Quantitative MR imaging of brain iron: A postmortem validation study. *Radiology*, *257*(2), 455-462. doi:10.1148/radiol.10100495
- Langkammer, C., Schweser, F., Krebs, N., Deistung, A., Goessler, W., Scheurer, E., . . . Reichenbach, J. R. (2012). Quantitative susceptibility mapping (QSM) as a means to measure brain iron? A post mortem validation study. *Neuroimage*, *62*(3), 1593-1599. doi:10.1016/j.neuroimage.2012.05.049
- Langkammer, C., Pirpamer, L., Seiler, S., Deistung, A., Schweser, F., Franthal, S., . . . Schwingenschuh, P. (2016). Quantitative susceptibility mapping in Parkinson's disease. *PLoS One*, *11*(9), e0162460. doi:10.1371/journal.pone.0162460
- Levenberg, K. (1944) A method for the solution of certain non-linear problems in least squares. *Quarterly of Applied Mathematics*, *2*, 164-168.
- Li, D. T. H., Hui, E. S., Chan, Q., Yao, N., Chua, S. E., McAlonan, G. M., . . . Mak, H. K. F. (2018). Quantitative susceptibility mapping as an indicator of subcortical and limbic iron abnormality in Parkinson's disease with dementia. *Neuroimage: Clinical*, *20*, 365-373. doi:10.1016/j.nicl.2018.07.028
- Li, J., Chang, S., Liu, T., Wang, Q., Cui, D., Chen, X., . . . Wang, Y. (2012). Reducing the object orientation dependence of susceptibility effects in gradient echo MRI through quantitative susceptibility mapping. *Magnetic Resonance in Medicine*, *68*(5), 1563-1569. doi:10.1002/mrm.24135
- Li, L., & Leigh, J. S. (2004). Quantifying arbitrary magnetic susceptibility distributions with MR. *Magnetic Resonance in Medicine*, *51*(5), 1077-1082. doi:10.1002/mrm.20054

- Li, W. J., Jiang, H., Song, N., & Xie, J. X. (2010). Dose- and time-dependent alpha-synuclein aggregation induced by ferric iron in SK-N-SH cells. *Neuroscience Bulletin*, *26*(3), 205-210. doi:10.1007/s12264-010-1117-7
- Li, X., Chen, L., Kuttan, K., Ceritoglu, C., Li, Y., Kang, N., . . . Faria, A. V. (2019). Multi-atlas tool for automated segmentation of brain gray matter nuclei and quantification of their magnetic susceptibility. *Neuroimage*, *191*, 337-349. doi:10.1016/j.neuroimage.2019.02.016
- Liu, C., Li, W., Tong, K. A., Yeom, K. W., & Kuzminski, S. (2015). Susceptibility-weighted imaging and quantitative susceptibility mapping in the brain. *Journal of Magnetic Resonance Imaging*, *42*(1), 23-41. doi:10.1002/jmri.24768
- Liu, M., Liu, S., Ghassaban, K., Zheng, W., Diccico, D., Miao, Y., . . . Haacke, E. M. (2016). Assessing global and regional iron content in deep gray matter as a function of age using susceptibility mapping. *Journal of Magnetic Resonance Imaging*, *44*(1), 59-71. doi:10.1002/jmri.25130
- Liu, S., Buch, S., Chen, Y., Choi, H. S., Dai, Y., Habib, C., . . . Haacke, E. M. (2017). Susceptibility-weighted imaging: Current status and future directions. *NMR in Biomedicine*, *30*(4). doi:10.1002/nbm.3552
- Lotfipour, A. K., Wharton, S., Schwarz, S. T., Gontu, V., Schafer, A., Peters, A. M., . . . Bajaj, N. P. (2012). High resolution magnetic susceptibility mapping of the substantia nigra in Parkinson's disease. *Journal of Magnetic Resonance Imaging*, *35*(1), 48-55. doi:10.1002/jmri.22752
- Lu, X., Ma, Y., Chang, E. Y., He, Q., Searleman, A., von Drygalski, A., & Du, J. (2018). Simultaneous quantitative susceptibility mapping (QSM) and R2* for high iron concentration quantification with 3D ultrashort echo time sequences: An echo dependence study. *Magnetic Resonance in Medicine*, *79*(4), 2315-2322. doi:10.1002/mrm.27062
- Lv, Z., Jiang, H., Xu, H., Song, N., & Xie, J. (2011). Increased iron levels correlate with the selective nigral dopaminergic neuron degeneration in Parkinson's disease. *Journal of Neural Transmission (Vienna)*, *118*(3), 361-369. doi:10.1007/s00702-010-0434-3

- Manova, E. S., Habib, C. A., Boikov, A. S., Ayaz, M., Khan, A., Kirsch, W. M., . . . Haacke, E. M. (2009). Characterizing the mesencephalon using susceptibility-weighted imaging. *American Journal of Neuroradiology*, *30*(3), 569-574. doi:10.3174/ajnr.A1401
- Marquardt, D. W. (1963). An algorithm for least-squares estimation of nonlinear parameters. *Journal of the Society for Industrial and Applied Mathematics*, *11*(2), 431-441. doi:10.1137/0111030
- Martin, W. R., Wieler, M., & Gee, M. (2008). Midbrain iron content in early Parkinson disease: A potential biomarker of disease status. *Neurology*, *70*(16 Pt 2), 1411-1417. doi:10.1212/01.wnl.0000286384.31050.b5
- Martinez-Martin, P., Garcia Urrea, D., del Ser Quijano, T., Balseiro Gomez, J., Gomez Utrero, E., Pineiro, R., & Andres, M. T. (1997). A new clinical tool for gait evaluation in Parkinson's disease. *Clinical Neuropharmacology*, *20*(3), 183-194.
- Massey, L. A., Miranda, M. A., Al-Helli, O., Parkes, H. G., Thornton, J. S., So, P. W., . . . Yousry, T. A. (2017). 9.4 T MR microscopy of the substantia nigra with pathological validation in controls and disease. *Neuroimage: Clinical*, *13*, 154-163. doi:10.1016/j.nicl.2016.11.015
- Mattern, H., Sciarra, A., Lusebrink, F., Acosta-Cabronero, J., & Speck, O. (2019). Prospective motion correction improves high-resolution quantitative susceptibility mapping at 7T. *Magnetic Resonance in Medicine*, *81*(3), 1605-1619. doi:10.1002/mrm.27509
- Miller, D. B., & O'Callaghan, J. P. (2015). Biomarkers of Parkinson's disease: Present and future. *Metabolism*, *64*(3 Suppl 1), S40-46. doi:10.1016/j.metabol.2014.10.030
- Modat, M., Ridgway, G. R., Taylor, Z. A., Lehmann, M., Barnes, J., Hawkes, D. J., . . . Ourselin, S. (2010). Fast free-form deformation using graphics processing units. *Computer Methods and Programs in Biomedicine*, *98*(3), 278-284. doi:10.1016/j.cmpb.2009.09.002
- Mosharov, E. V., Larsen, K. E., Kanter, E., Phillips, K. A., Wilson, K., Schmitz, Y., . . . Sulzer, D. (2009). Interplay between cytosolic dopamine, calcium, and alpha-synuclein causes selective death of substantia nigra neurons. *Neuron*, *62*(2), 218-229. doi:10.1016/j.neuron.2009.01.033
- Munoz, P., Cardenas, S., Huenchuguala, S., Briceno, A., Couve, E., Paris, I., & Segura-Aguilar,

- J. (2015). DT-Diaphorase prevents aminochrome-induced alpha-synuclein oligomer formation and neurotoxicity. *Toxicological Sciences*, *145*(1), 37-47.
doi:10.1093/toxsci/kfv016
- Murakami, Y., Kakeda, S., Watanabe, K., Ueda, I., Ogasawara, A., Moriya, J., . . . Korogi, Y. (2015). Usefulness of quantitative susceptibility mapping for the diagnosis of Parkinson disease. *AJNR American Journal of Neuroradiology*, *36*(6), 1102-1108.
doi:10.3174/ajnr.A4260
- Nair-Roberts, R. G., Chatelain-Badie, S. D., Benson, E., White-Cooper, H., Bolam, J. P., & Ungless, M. A. (2008). Stereological estimates of dopaminergic, GABAergic and glutamatergic neurons in the ventral tegmental area, substantia nigra and retrorubral field in the rat. *Neuroscience*, *152*(4), 1024-1031. doi:10.1016/j.neuroscience.2008.01.046
- Narayanan, N. S., Rodnitzky, R. L., & Uc, E. Y. (2013). Prefrontal dopamine signaling and cognitive symptoms of Parkinson's disease. *Reviews in Neuroscience*, *24*(3), 267-278.
doi:10.1515/revneuro-2013-0004
- Nasreddine, Z. S., Phillips, N. A., Bedirian, V., Charbonneau, S., Whitehead, V., Collin, I., . . . Chertkow, H. (2005). The Montreal Cognitive Assessment, MoCA: A brief screening tool for mild cognitive impairment. *Journal of the American Geriatrics Society*, *53*(4), 695-699. doi:10.1111/j.1532-5415.2005.53221.x
- Norris, E. H., Giasson, B. I., Hodara, R., Xu, S., Trojanowski, J. Q., Ischiropoulos, H., & Lee, V. M. (2005). Reversible inhibition of alpha-synuclein fibrillization by dopaminochrome-mediated conformational alterations. *Journal of Biological Chemistry*, *280*(22), 21212-21219. doi:10.1074/jbc.M412621200
- Ott, M., Gogvadze, V., Orrenius, S., & Zhivotovsky, B. (2007). Mitochondria, oxidative stress and cell death. *Apoptosis*, *12*(5), 913-922. doi:10.1007/s10495-007-0756-2
- Pan, P. Y., & Ryan, T. A. (2012). Calbindin controls release probability in ventral tegmental area dopamine neurons. *Nature Neuroscience*, *15*(6), 813-815. doi:10.1038/nn.3099
- Paris, I., Martinez-Alvarado, P., Cardenas, S., Perez-Pastene, C., Graumann, R., Fuentes, P., . . . Segura-Aguilar, J. (2005). Dopamine-dependent iron toxicity in cells derived from rat hypothalamus. *Chemical Research in Toxicology*, *18*(3), 415-419. doi:10.1021/tx0497144
- Paris, I., Perez-Pastene, C., Cardenas, S., Iturriaga-Vasquez, P., Munoz, P., Couve, E., . . . Segura-Aguilar, J. (2010). Aminochrome induces disruption of actin, alpha-, and beta-

- tubulin cytoskeleton networks in substantia-nigra-derived cell line. *Neurotoxicity Research*, 18(1), 82-92. doi:10.1007/s12640-009-9148-4
- Parkinson, J. (2002). An essay on the shaking palsy. 1817. *The Journal of Neuropsychiatry and Clinical Neuroscience*, 14(2), 223-236; discussion 222. doi:10.1176/jnp.14.2.223
- Pauli, W. M., Nili, A. N., & Tyszka, J. M. (2018). A high-resolution probabilistic in vivo atlas of human subcortical brain nuclei. *Scientific Data*, 5, 180063. doi:10.1038/sdata.2018.63
- Pennathur, S., Jackson-Lewis, V., Przedborski, S., & Heinecke, J. W. (1999). Mass spectrometric quantification of 3-nitrotyrosine, ortho-tyrosine, and o,o'-dityrosine in brain tissue of 1-methyl-4-phenyl-1,2,3, 6-tetrahydropyridine-treated mice, a model of oxidative stress in Parkinson's disease. *Journal of Biological Chemistry*, 274(49), 34621-34628. doi:10.1074/jbc.274.49.34621
- Péran, P., Cherubini, A., Luccichenti, G., Hagberg, G., Démonet, J.-F., Rascol, O., . . . Sabatini, U. (2009). Volume and iron content in basal ganglia and thalamus. *Human Brain Mapping*, 30(8), 2667-2675. doi:10.1002/hbm.20698
- Persson, N., Wu, J., Zhang, Q., Liu, T., Shen, J., Bao, R., . . . Spincemaille, P. (2015). Age and sex related differences in subcortical brain iron concentrations among healthy adults. *Neuroimage*, 122, 385-398. doi:10.1016/j.neuroimage.2015.07.050
- Pfeiffer, R. F. (2016). Non-motor symptoms in Parkinson's disease. *Parkinsonism and Related Disorders*, 22 Suppl 1, S119-122. doi:10.1016/j.parkreldis.2015.09.004
- Pooley, R. A. (2005). Fundamental Physics of MR Imaging. *RadioGraphics*, 25(4), 1087-1099. doi:10.1148/rg.254055027
- Postuma, R. B., Gagnon, J. F., Vendette, M., Fantini, M. L., Massicotte-Marquez, J., & Montplaisir, J. (2009). Quantifying the risk of neurodegenerative disease in idiopathic REM sleep behavior disorder. *Neurology*, 72(15), 1296-1300. doi:10.1212/01.wnl.0000340980.19702.6e
- Postuma, R. B., Iranzo, A., Hogl, B., Arnulf, I., Ferini-Strambi, L., Manni, R., . . . Montplaisir, J. Y. (2015). Risk factors for neurodegeneration in idiopathic rapid eye movement sleep behavior disorder: A multicenter study. *Annals of Neurology*, 77(5), 830-839. doi:10.1002/ana.24385
- Postuma, R. B., & Berg, D. (2016). Advances in markers of prodromal Parkinson disease. *Nature Reviews Neurology*, 12(11), 622-634. doi:10.1038/nrneuro.2016.152

- Postuma, R. B. (2017). Dopaminergic imaging and prodromal Parkinson disease: A key biomarker arrives. *JAMA Neurology*, 74(8), 901-903. doi:10.1001/jamaneurol.2017.0846
- Pyatigorskaya, N., Magnin, B., Mongin, M., Yahia-Cherif, L., Valabregue, R., Arnaldi, D., . . . Lehericy, S. (2018). Comparative study of MRI biomarkers in the substantia nigra to discriminate idiopathic Parkinson disease. *AJNR American Journal of Neuroradiology*, 39(8), 1460-1467. doi:10.3174/ajnr.A5702
- Ramaker, C., Marinus, J., Stiggelbout, A. M., & Van Hilten, B. J. (2002). Systematic evaluation of rating scales for impairment and disability in Parkinson's disease. *Movement Disorders*, 17(5), 867-876. doi:10.1002/mds.10248
- Reichenbach, J. R. (2012). The future of susceptibility contrast for assessment of anatomy and function. *Neuroimage*, 62(2), 1311-1315.
doi:<https://doi.org/10.1016/j.neuroimage.2012.01.004>
- Reichenbach, J. R., Venkatesan, R., Yablonskiy, D. A., Thompson, M. R., Lai, S., & Haacke, E. M. (1997). Theory and application of static field inhomogeneity effects in gradient-echo imaging. *Journal of Magnetic Resonance Imaging*, 7(2), 266-279.
- Reyes, S., Fu, Y., Double, K., Thompson, L., Kirik, D., Paxinos, G., & Halliday, G. M. (2012). GIRK2 expression in dopamine neurons of the substantia nigra and ventral tegmental area. *The Journal of Comparative Neurology*, 520(12), 2591-2607.
doi:10.1002/cne.23051
- Riederer, P., Sofic, E., Rausch, W. D., Schmidt, B., Reynolds, G. P., Jellinger, K., & Youdim, M. B. (1989). Transition metals, ferritin, glutathione, and ascorbic acid in parkinsonian brains. *Journal of Neurochemistry*, 52(2), 515-520.
- Robinson, S. D., Bredies, K., Khabipova, D., Dymerska, B., Marques, J. P., & Schweser, F. (2017). An illustrated comparison of processing methods for MR phase imaging and QSM: Combining array coil signals and phase unwrapping. *NMR in Biomedicine*, 30(4).
doi:10.1002/nbm.3601
- Ropele, S., & Langkammer, C. (2017). Iron quantification with susceptibility. *NMR in Biomedicine*, 30(4). doi:10.1002/nbm.3534
- Saeed, U., Compagnone, J., Aviv, R. I., Strafella, A. P., Black, S. E., Lang, A. E., & Masellis, M. (2017). Imaging biomarkers in Parkinson's disease and Parkinsonian syndromes: Current

- and emerging concepts. *Translational Neurodegeneration*, 6, 8. doi:10.1186/s40035-017-0076-6
- Sasaki, M., Shibata, E., Tohyama, K., Takahashi, J., Otsuka, K., Tsuchiya, K., . . . Sakai, A. (2006). Neuromelanin magnetic resonance imaging of locus ceruleus and substantia nigra in Parkinson's disease. *Neuroreport*, 17(11), 1215-1218. doi:10.1097/01.wnr.0000227984.84927.a7
- Scherman, D., Desnos, C., Darchen, F., Pollak, P., Javoy-Agid, F., & Agid, Y. (1989). Striatal dopamine deficiency in Parkinson's disease: Role of aging. *Annals of Neurology*, 26(4), 551-557. doi:10.1002/ana.410260409
- Schubert, D., & Chevion, M. (1995). The role of iron in beta amyloid toxicity. *Biochemical and Biophysical Research Communications*, 216(2), 702-707. doi:10.1006/bbrc.1995.2678
- Schwarz, S. T., Abaei, M., Gontu, V., Morgan, P. S., Bajaj, N., & Auer, D. P. (2013). Diffusion tensor imaging of nigral degeneration in Parkinson's disease: A region-of-interest and voxel-based study at 3 T and systematic review with meta-analysis. *NeuroImage: Clinical*, 3, 481-488. doi:10.1016/j.nicl.2013.10.006
- Schwarz, S. T., Afzal, M., Morgan, P. S., Bajaj, N., Gowland, P. A., & Auer, D. P. (2014). The 'swallow tail' appearance of the healthy nigrosome - a new accurate test of Parkinson's disease: a case-control and retrospective cross-sectional MRI study at 3T. *PLoS One*, 9(4), e93814. doi:10.1371/journal.pone.0093814
- Schwarz, S. T., Mougin, O., Xing, Y., Blazejewska, A., Bajaj, N., Auer, D. P., & Gowland, P. (2018). Parkinson's disease related signal change in the nigrosomes 1-5 and the substantia nigra using T2* weighted 7T MRI. *Neuroimage: Clinical*, 19, 683-689. doi:10.1016/j.nicl.2018.05.027
- Schweser, F., Sommer, K., Deistung, A., & Reichenbach, J. R. (2012). Quantitative susceptibility mapping for investigating subtle susceptibility variations in the human brain. *Neuroimage*, 62(3), 2083-2100. doi:10.1016/j.neuroimage.2012.05.067
- Schweser, F., Robinson, S. D., de Rochefort, L., Li, W., & Bredies, K. (2017). An illustrated comparison of processing methods for phase MRI and QSM: Removal of background field contributions from sources outside the region of interest. *NMR in Biomedicine*, 30(4). doi:10.1002/nbm.3604

- Seppi, K., Schocke, M. F., Esterhammer, R., Kremser, C., Brenneis, C., Mueller, J., . . . Wenning, G. K. (2003). Diffusion-weighted imaging discriminates progressive supranuclear palsy from PD, but not from the Parkinson variant of multiple system atrophy. *Neurology*, *60*(6), 922-927. doi:10.1212/01.wnl.0000049911.91657.9d
- Sethi, S. K., Kisch, S. J., Ghassaban, K., Rajput, A., Rajput, A., Babyn, P. S., . . . Mark Haacke, E. (2019). Iron quantification in Parkinson's disease using an age-based threshold on susceptibility maps: The advantage of local versus entire structure iron content measurements. *Magnetic Resonance Imaging*, *55*, 145-152. doi:10.1016/j.mri.2018.10.001
- Shima, T., Sarna, T., Swartz, H. M., Stroppolo, A., Gerbasi, R., & Zecca, L. (1997). Binding of iron to neuromelanin of human substantia nigra and synthetic melanin: An electron paramagnetic resonance spectroscopy study. *Free Radical Biology and Medicine*, *23*(1), 110-119.
- Shin, C., Lee, S., Lee, J. Y., Rhim, J. H., & Park, S. W. (2018). Non-Motor Symptom Burdens Are Not Associated with Iron Accumulation in Early Parkinson's Disease: a Quantitative Susceptibility Mapping Study. *Journal of Korean Medical Science*, *33*(13), e96. doi:10.3346/jkms.2018.33.e96
- Sian, J., Dexter, D. T., Lees, A. J., Daniel, S., Jenner, P., & Marsden, C. D. (1994). Glutathione-related enzymes in brain in Parkinson's disease. *Annals of Neurology*, *36*(3), 356-361. doi:10.1002/ana.410360306
- Sian-Hulsmann, J., Mandel, S., Youdim, M. B., & Riederer, P. (2011). The relevance of iron in the pathogenesis of Parkinson's disease. *Journal of Neurochemistry*, *118*(6), 939-957. doi:10.1111/j.1471-4159.2010.07132.x
- Sies, H., & Cadenas, E. (1985). Oxidative stress: Damage to intact cells and organs. *Philosophical Transactions of the Royal Society B: Biological Sciences*, *311*(1152), 617-631. doi:10.1098/rstb.1985.0168
- Silvestri, L., & Camaschella, C. (2008). A potential pathogenetic role of iron in Alzheimer's disease. *Journal of Cellular and Molecular Medicine*, *12*(5a), 1548-1550. doi:10.1111/j.1582-4934.2008.00356.x
- Smith, Y., & Parent, A. (1986). Differential connections of caudate nucleus and putamen in the squirrel monkey (*Saimiri sciureus*). *Neuroscience*, *18*(2), 347-371.

- Sofic, E., Riederer, P., Heinsen, H., Beckmann, H., Reynolds, G. P., Hebenstreit, G., & Youdim, M. B. H. (1988). Increased iron (III) and total iron content in post mortem substantia nigra of parkinsonian brain. *Journal of Neural Transmission*, 74(3), 199-205. doi:10.1007/BF01244786
- Sofic, E., Paulus, W., Jellinger, K., Riederer, P., & Youdim, M. B. H. (1991). Selective increase of iron in substantia nigra zona compacta of Parkinsonian brains. *Journal of Neurochemistry*, 56(3), 978-982. doi:10.1111/j.1471-4159.1991.tb02017.x
- Sofic, E., Lange, K. W., Jellinger, K., & Riederer, P. (1992). Reduced and oxidized glutathione in the substantia nigra of patients with Parkinson's disease. *Neuroscience Letters*, 142(2), 128-130.
- Sohmiya, M., Tanaka, M., Aihara, Y., Hirai, S., & Okamoto, K. (2001). Age-related structural changes in the human midbrain: An MR image study. *Neurobiology of aging*, 22(4), 595-601. doi:10.1016/S0197-4580(01)00227-5
- Spatz, H. (1922). On the visualization of iron in the brain, especially in the centers of the extrapyramidal motor system. *Zeitschrift für die gesamte Neurologie und Psychiatrie*, 77, 261-390.
- Springer, E., Dymerska, B., Cardoso, P. L., Robinson, S. D., Weisstanner, C., Wiest, R., . . . Trattinig, S. (2016). Comparison of routine brain imaging at 3 T and 7 T. *Investigative Radiology*, 51(8), 469-482. doi:10.1097/rli.0000000000000256
- Storey, P., Thompson, A. A., Carqueville, C. L., Wood, J. C., de Freitas, R. A., & Rigsby, C. K. (2007). R2* imaging of transfusional iron burden at 3T and comparison with 1.5T. *Journal of Magnetic Resonance Imaging*, 25(3), 540-547. doi:10.1002/jmri.20816
- Strimbu, K., & Tavel, J. A. (2010). What are biomarkers? *Current Opinions in HIV and AIDS*, 5(6), 463-466. doi:10.1097/COH.0b013e32833ed177
- Sulzer, D., & Zecca, L. (2000). Intraneuronal dopamine-quinone synthesis: A review. *Neurotoxicity Research*, 1(3), 181-195.
- Sun, H., Walsh, A. J., Lebel, R. M., Blevins, G., Catz, I., Lu, J. Q., . . . Wilman, A. H. (2015). Validation of quantitative susceptibility mapping with Perls' iron staining for subcortical gray matter. *Neuroimage*, 105, 486-492. doi:10.1016/j.neuroimage.2014.11.010
- Takahashi, H., Watanabe, Y., Tanaka, H., Mihara, M., Mochizuki, H., Takahashi, K., . . . Tomiyama, N. (2018). Comprehensive MRI quantification of the substantia nigra pars

- compacta in Parkinson's disease. *European Journal of Radiology*, 109, 48-56.
doi:10.1016/j.ejrad.2018.06.024
- Takahashi, H., Watanabe, Y., Tanaka, H., Mihara, M., Mochizuki, H., Liu, T., . . . Tomiyama, N. (2018). Quantifying changes in nigrosomes using quantitative susceptibility mapping and neuromelanin imaging for the diagnosis of early-stage Parkinson's disease. *The British Journal of Radiology*, 91(1086), 20180037. doi:10.1259/bjr.20180037
- Thompson, C. B. (1995). Apoptosis in the pathogenesis and treatment of disease. *Science*, 267(5203), 1456-1462. doi:10.1126/science.7878464
- Tse, D. C. S., McCreery, R. L., & Adams, R. N. (1976). Potential oxidative pathways of brain catecholamines. *Journal of Medicinal Chemistry*, 19(1), 37-40.
doi:10.1021/jm00223a008
- Tufekci, K. U., Meuwissen, R., Genc, S., & Genc, K. (2012). Inflammation in Parkinson's disease. *Advances in Protein Chemistry and Structural Biology*, 88, 69-132.
doi:10.1016/b978-0-12-398314-5.00004-0
- Tuite, P. (2016). Magnetic resonance imaging as a potential biomarker for Parkinson's disease. *Translational Research*, 175, 4-16. doi:10.1016/j.trsl.2015.12.006
- Vaillancourt, D. E., Spraker, M. B., Prodoehl, J., Abraham, I., Corcos, D. M., Zhou, X. J., . . . Little, D. M. (2009). High-resolution diffusion tensor imaging in the substantia nigra of de novo Parkinson disease. *Neurology*, 72(16), 1378-1384.
doi:10.1212/01.wnl.0000340982.01727.6e
- Verreyt, N., Nys, G. M. S., Santens, P., & Vingerhoets, G. (2011). Cognitive differences between patients with left-sided and right-sided Parkinson's disease. A review. *Neuropsychology Review*, 21(4), 405-424. doi:10.1007/s11065-011-9182-x
- Walsh, D. O., Gmitro, A. F., & Marcellin, M. W. (2000). Adaptive reconstruction of phased array MR imagery. *Magnetic Resonance in Medicine*, 43(5), 682-690.
- Wang, J. Y., Zhuang, Q. Q., Zhu, L. B., Zhu, H., Li, T., Li, R., . . . Zhu, J. H. (2016). Meta-analysis of brain iron levels of Parkinson's disease patients determined by postmortem and MRI measurements. *Scientific Reports*, 6, 36669. doi:10.1038/srep36669
- Ward, R. J., Zucca, F. A., Duyn, J. H., Crichton, R. R., & Zecca, L. (2014). The role of iron in brain ageing and neurodegenerative disorders. *The Lancet Neurology*, 13(10), 1045-1060.
doi:10.1016/s1474-4422(14)70117-6

- Wharton, S., & Bowtell, R. (2010). Whole-brain susceptibility mapping at high field: A comparison of multiple- and single-orientation methods. *Neuroimage*, *53*(2), 515-525. doi:<https://doi.org/10.1016/j.neuroimage.2010.06.070>
- Windahl, M. S., Petersen, C. R., Christensen, H. E., & Harris, P. (2008). Crystal structure of tryptophan hydroxylase with bound amino acid substrate. *Biochemistry*, *47*(46), 12087-12094. doi:10.1021/bi8015263
- Winkler, A. M. (1988). Dirichlet and Neumann spectrum. *Communications on Pure and Applied Mathematics*, *41*(3), 305-316. doi:10.1002/cpa.3160410304
- World Medical Association Declaration of Helsinki: ethical principles for medical research involving human subjects. (2013). *JAMA*, *310*(20), 2191-2194. doi:10.1001/jama.2013.281053
- Wu, Z., Du, Y., Xue, H., Wu, Y., & Zhou, B. (2012). Aluminum induces neurodegeneration and its toxicity arises from increased iron accumulation and reactive oxygen species (ROS) production. *Neurobiology of Aging*, *33*(1), 199.e191-112. doi:10.1016/j.neurobiolaging.2010.06.018
- Xiong, R., Siegel, D., & Ross, D. (2014). Quinone-induced protein handling changes: Implications for major protein handling systems in quinone-mediated toxicity. *Toxicology and Applied Pharmacology*, *280*(2), 285-295. doi:10.1016/j.taap.2014.08.014
- Xuan, M., Guan, X., Gu, Q., Shen, Z., Yu, X., Qiu, T., . . . Zhang, M. (2017). Different iron deposition patterns in early- and middle-late-onset Parkinson's disease. *Parkinsonism and Related Disorders*, *44*, 23-27. doi:10.1016/j.parkreldis.2017.08.013
- Yamamoto, A., Shin, R. W., Hasegawa, K., Naiki, H., Sato, H., Yoshimasu, F., & Kitamoto, T. (2002). Iron (III) induces aggregation of hyperphosphorylated tau and its reduction to iron (II) reverses the aggregation: Implications in the formation of neurofibrillary tangles of Alzheimer's disease. *Journal of Neurochemistry*, *82*(5), 1137-1147.
- Yang, J., Burciu, R. G., & Vaillancourt, D. E. (2018). Longitudinal progression markers of Parkinson's disease: Current view on structural imaging. *Current Neurology and Neuroscience Reports*, *18*(12), 83. doi:10.1007/s11910-018-0894-7
- Yao, B., Li, T.-Q., Gelderen, P. v., Shmueli, K., de Zwart, J. A., & Duyn, J. H. (2009). Susceptibility contrast in high field MRI of human brain as a function of tissue iron

- content. *Neuroimage*, 44(4), 1259-1266.
doi:<https://doi.org/10.1016/j.neuroimage.2008.10.029>
- Youdim, M. B., Ben-Shachar, D., & Riederer, P. (1993). The possible role of iron in the etiopathology of Parkinson's disease. *Movement Disorders*, 8(1), 1-12.
doi:10.1002/mds.870080102
- Youdim, M. B., Ben-Shachar, D., & Yehuda, S. (1989). Putative biological mechanisms of the effect of iron deficiency on brain biochemistry and behavior. *The American Journal of Clinical Nutrition*, 50(3 Suppl), 607-615; discussion 615-607. doi:10.1093/ajcn/50.3.607
- Yu, F. F., Chiang, F. L., Stephens, N., Huang, S. Y., Bilgic, B., Tantiwongkosi, B., & Romero, R. (2019). Characterization of normal-appearing white matter in multiple sclerosis using quantitative susceptibility mapping in conjunction with diffusion tensor imaging. *Neuroradiology*, 61(1), 71-79. doi:10.1007/s00234-018-2137-7
- Yust-Katz, S., Tesler, D., Treves, T. A., Melamed, E., & Djaldetti, R. (2008). Handedness as a predictor of side of onset of Parkinson's disease. *Parkinsonism and Related Disorders*, 14(8), 633-635. doi:10.1016/j.parkreldis.2008.01.017
- Zafar, K. S., Siegel, D., & Ross, D. (2006). A potential role for cyclized quinones derived from dopamine, DOPA, and 3,4-dihydroxyphenylacetic acid in proteasomal inhibition. *Molecular Pharmacology*, 70(3), 1079-1086. doi:10.1124/mol.106.024703
- Zecca, L., Gallorini, M., Schunemann, V., Trautwein, A. X., Gerlach, M., Riederer, P., . . . Tampellini, D. (2001a). Iron, neuromelanin and ferritin content in the substantia nigra of normal subjects at different ages: Consequences for iron storage and neurodegenerative processes. *Journal of Neurochemistry*, 76(6), 1766-1773.
- Zecca, L., Tampellini, D., Gerlach, M., Riederer, P., Fariello, R. G., & Sulzer, D. (2001b). Substantia nigra neuromelanin: Structure, synthesis, and molecular behaviour. *Molecular Pathology*, 54(6), 414-418.
- Zecca, L., Fariello, R., Riederer, P., Sulzer, D., Gatti, A., & Tampellini, D. (2002). The absolute concentration of nigral neuromelanin, assayed by a new sensitive method, increases throughout the life and is dramatically decreased in Parkinson's disease. *FEBS Letters*, 510(3), 216-220.

- Zecca, L., Youdim, M. B., Riederer, P., Connor, J. R., & Crichton, R. R. (2004). Iron, brain ageing and neurodegenerative disorders. *Nature Reviews Neuroscience*, *5*(11), 863-873. doi:10.1038/nrn1537
- Zhang, J., Zhang, Y., Wang, J., Cai, P., Luo, C., Qian, Z., . . . Feng, H. (2010). Characterizing iron deposition in Parkinson's disease using susceptibility-weighted imaging: An in vivo MR study. *Brain Research*, *1330*, 124-130. doi:10.1016/j.brainres.2010.03.036
- Zheng, W., Nichol, H., Liu, S., Cheng, Y. C., & Haacke, E. M. (2013). Measuring iron in the brain using quantitative susceptibility mapping and X-ray fluorescence imaging. *Neuroimage*, *78*, 68-74. doi:10.1016/j.neuroimage.2013.04.022
- Zucca, F. A., Basso, E., Cupaioli, F. A., Ferrari, E., Sulzer, D., Casella, L., & Zecca, L. (2014). Neuromelanin of the human substantia nigra: An update. *Neurotoxicity Research*, *25*(1), 13-23. doi:10.1007/s12640-013-9435-y
- Zucca, F. A., Segura-Aguilar, J., Ferrari, E., Munoz, P., Paris, I., Sulzer, D., . . . Zecca, L. (2017). Interactions of iron, dopamine and neuromelanin pathways in brain aging and Parkinson's disease. *Progress in Neurobiology*, *155*, 96-119. doi:10.1016/j.pneurobio.2015.09.012

Appendices

Appendix A: Participant Inclusion/Exclusion Criteria

Healthy Controls	Early-stage PD Patients
No contraindications for MRI scanning	No contraindications for MRI scanning
No diagnosis of a movement disorder	Diagnosis of idiopathic PD from a licensed neurologist specializing in movement disorders
No history of: <ol style="list-style-type: none"> 1. Neurological illness 2. Psychiatric illness 3. Neuro-trauma 4. Psychosis or hallucinations 5. Substance abuse (eg. alcohol, drugs) 	No history of (unrelated to PD): <ol style="list-style-type: none"> 1. Neurological illness 2. Psychiatric illness 3. Neuro-trauma 4. Psychosis or hallucinations 5. Substance abuse (eg. alcohol, drugs)
Normal or corrected-to-normal vision	Normal or corrected-to-normal vision
No previous participation in the study	No previous participation in the study
Not currently taking cognitive-enhancing medications including: <ol style="list-style-type: none"> 1. Donepezil 2. Galantamine 3. Rivastigimine 4. Memantine 5. Methylphenidate 	Not currently taking cognitive-enhancing medications including: <ol style="list-style-type: none"> 1. Donepezil 2. Galantamine 3. Rivastigimine 4. Memantine 5. Methylphenidate
No clinical diagnosis of dementia or mild cognitive impairment	No clinical diagnosis of dementia or mild cognitive impairment
	Currently prescribed and taking dopaminergic medication
	PD duration < 5 years from date of diagnosis
	No suspicion of familial form of PD (greater than 2 first degree relatives with PD diagnosis)
	Stable and non-rapidly progressing parkinsonism
	No history of deep brain stimulation treatment or neurological surgery

Appendix B: Consent Form



PENNY A. MACDONALD, MD, PhD, FRCP(C)
Assistant Professor and Movement Disorder Neurologist
Department of Clinical Neurological Sciences and
The Brain and Mind Institute
University of Western Ontario

LETTER OF INFORMATION AND CONSENT FORM

In this consent document, "you" always refers to the study participant. If you are a substitute decision maker (SDM) (i.e. someone who makes the decision of participation on behalf of a participant), please remember that "you" refers to the study patient. If an SDM is needed for this study, you will be asked to review and sign this consent form on behalf of the participant.

Study Title

Distinguishing the roles of ventral and dorsal striatum in cognition

Investigators

Penny A. MacDonald MD, PhD, FRCP(C) in Neurology	Adrian Owen PhD
Hooman Ganjavi MD, PhD, FRCP(C) in Psychiatry	Mel Goodale PhD
Seyed Mirsattari MD, PhD, FRCP(C) in Neurology	Ravi Menon PhD
Sarah Morrow MD, FRCP(C) in Neurology	Stefan Kohler PhD
Jorge Burneo MD, FRCP(C) in Neurology	Paul Gribble PhD
Mary Jenkins MD, FRCP(C) in Neurology	Ingrid Johnsrude PhD
Elizabeth Finger MD, FRCP(C) in Neurology	Ken McRae PhD
Stephen Pasternak MD, FRCP(C) in Neurology	Brian Corneil PhD
Alex Khaw MD, FRCP(C) in Neurology	Robert Bartha PhD
Luciano Sposato MD, PhD, FRCP(C) in Neurology	Jessica Grahn PhD
Jennifer Mandzia MD, PhD, FRCP(C) in Neurology	Ali Kahn PhD
Vladimir Hachinsky MD, FRCP(C) in Neurology	Stuart Fogel PhD
David Spence MD, FRCP(C) in Neurology	Bjorn Hermann PhD
Donald Lee MD, FRCP(C) in Radiology	Chris Fiacconi PhD
Mark Watling MD, FRCP(C) in Psychiatry	Yoshiko Yabe PhD
Sandra Northcott MD, FRCP(C) in Psychiatry	Lorina Naci PhD
Ken Seergobin MSc	

1/11

Version: 12/June/2017
Consent Form

initials: _____

339 Windermere Road
London, Ontario, Canada N6A 5A5
Tel: (519) 685-8500 ext. 33631 • Fax: (519) 663-3753

Sponsoring Agency

The research is funded by a Canada Excellence Research Chair to Dr. Adrian Owen, an Academic Medical Association of Southwestern Ontario Opportunity Fund and Natural Sciences and Engineering Research Council of Canada awarded to Dr. Penny MacDonald.

Purpose

You are being asked to participate in a research project designed to help us understand more about attention, memory, and how people make every day decisions. The study will help show which parts of the brain are involved in these functions. It will also help us to understand whether certain illnesses that affect the brain such as strokes or Parkinson's disease, or obsessive-compulsive disorder change the way people pay attention, remember, and make decisions. Understanding these changes might help us to provide better care for these patients ultimately. We will aim to recruit approximately 200 patients with Parkinson's disease, 200 healthy volunteers, matched in age to PD patients, 200 patients with strokes, 200 patients with neurological or psychiatric disorders that might implicate the striatum (a brain region of interest), and 200 healthy volunteers. The criteria to participate in this study were previously outlined in the recruitment letter that you were given.

Procedures

If you agree, you will be asked to one or two testing sessions at the Brain and Mind Institute or the Roberts Research Institute at the University of Western Ontario. Each session is expected to last approximately 1.5 hours, but may go as long as 3 hours. The first session will begin with a short clinical interview to evaluate your general health. Your heart rate and blood pressure might also be recorded. A screening neurological examination will be performed. You will also be asked to complete a few standard questionnaires to assess aspects of your mood and temperament. In each session, you will next perform a computerized test that is aimed at testing basic aspects of thinking, memory, or problem solving. Explanations of the paper and pencil tests will be provided orally and detailed written instructions will be given prior to the computerized test on each day. You will have the chance to ask questions and will be encouraged to do so before beginning the tests. Practice trials will also be provided so that you will be comfortable with the computerized test and so that you understand thoroughly what you're asked to do.

Your permission is also requested for Dr. MacDonald to review any CT or MRI scans of the brain that you have previously undergone. This will help us better understand the results of the testing.

Experiments involving functional magnetic resonance imaging

During testing, you might perform tests on a computer that are aimed at testing basic aspects of thinking, memory, or problem solving while you are in a magnetic resonance imaging (MRI)

2/11

Version: 12/June/2017
Consent Form

initials: _____

339 Windermere Road
London, Ontario, Canada N6A 5A5
Tel: (519) 685-8500 ext. 33631 • Fax: (519) 663-3753

machine. With MRI, we are able to measure blood flow non-invasively in various parts of your brain as a marker of brain activity while you perform specific thinking functions. We will also collect images of your brain in the MRI to measure different brain structures.

Patients with Parkinson's disease

If you are a patient with Parkinson's disease, you will be tested twice, once while you are taking your Parkinson's medication and once after you have abstained from taking your Parkinson's medication for at least 12 hours on two separate days.

Healthy control participants or patients with neurological (e.g. stroke, epilepsy, multiple sclerosis, multiple systems atrophy, progressive supranuclear palsy, cortico-basal-ganglionic degeneration, Lewy body dementia, ataxia, Huntington's disease, Alzheimer's disease), as well as sleep disorders (e.g. rapid eye movement sleep behavioural disorder or RBD, restless leg disorder and obstructive sleep apnea), or psychiatric disorder (e.g. obsessive-compulsive disorder) other than Parkinson's disease

If you are a non-patient volunteer or a patient with a neurological or psychiatric disorder other than Parkinson's disease, you might perform the tasks once or twice. In all testing sessions, you will take all of your regularly prescribed medications. In some studies, you might also take dopaminergic therapy or a placebo (i.e., cornstarch) in one session or across two sessions.

Patients with addiction (e.g. alcohol, opioids, marijuana)

You will be asked to abstain from all illicit substances as well as alcohol for a minimum of 48 hours prior to testing. Upon arrival on your testing date, you will complete an Crawell Oral Fluid (Saliva) Drug Test and an Alco-Screen Oral Fluid (Saliva) Alcohol Test to confirm compliance with these instructions. In all testing sessions, you will take all of your regularly prescribed medications. In some studies, you might also take dopaminergic therapy or a placebo (i.e., cornstarch) in one session or across two sessions.

Healthy control participants studied while taking dopaminergic therapy

For non-patient volunteers, in some experiments you will perform tasks once while taking a dose of Levocarb or Pramipexole, common medications that are used to treat Parkinson's disease, and once while taking an inactive or *placebo* substance (i.e., cornstarch). The order in which you receive these substances will be randomly determined across participants. You will not be informed of the substance that you are given in either testing session and the experimenter will also be blind to which substance you are given on a particular day. This is done to reduce any effects of expectation that might be induced by knowing that you are receiving active treatment. Levocarb contains 100 mg of levodopa (L-3,4-dihydroxyphenylalanine) and 25 mg of carbidopa. Levodopa is transformed in the brain into dopamine whereas pramipexole mimics dopamine. Dopamine is a neurotransmitter produced

3/11

Version: 12/June/2017
Consent Form

initials: _____

339 Windermere Road
London, Ontario, Canada N6A 5A5
Tel: (519) 685-8500 ext. 33631 • Fax: (519) 663-3753

naturally in the brain that is involved in regulating movement and some aspects of thinking and memory. Carbidopa is a substance that does not cross into the brain but is given to stop the levodopa from being converted to dopamine before it reaches the brain. Carbidopa reduces side effects that can occur due to dopamine being produced in the body rather than in the brain, such as nausea or lowering of blood pressure.

Experiments involving propranolol or atenolol

You might be asked to perform some tasks once while taking a dose of propranolol or atenolol, commonly used to treat high blood pressure, and once while taking an inactive or *placebo* substance (i.e., cornstarch). The order in which you receive these substances will be randomly determined across participants. You will not be informed of the substance that you are given in either testing session and the experimenter will also be blind to which substance you are given on a particular day. This is done to reduce any effects of expectation that might be induced by knowing that you are receiving active treatment. Propranolol and atenolol are beta blockers. Beta blockers compete with the same receptors as adrenaline, slowing the sympathetic nervous system to lower heart rate and blood pressure.

Experiments involving polysomnographic sleep recordings

You might be asked to undergo polysomnographic sleep recordings during either a 3-h daytime nap or 8-h overnight session. Polysomnography (PSG) is a non-invasive technique that uses surface electrodes applied to the scalp and face to measure brain activity during different sleep-wake cycles.

Experiments involving robotic arm manipulation

We will ask you to perform a motor learning task. This will take approximately 40 minutes. You will be asked to grasp the handle of robot arm, and point to visual targets displayed on a virtual-reality display. You will be asked to point to targets one after another. Depending on the phase of the experiment, the robot may be programmed to apply small forces (a few grams) to your hand during movement. The robot will measure the curvature of your movement trajectories (how curved the trajectory of your hand is, as you move to the targets, relative to a straight line) as an index of motor learning.

Experiments involving electroencephalography

You might be asked to undergo electroencephalography (EEG) recordings during either the experimental session. EEG is a non-invasive technique that uses surface electrodes applied to the scalp and face to measure brain activity during rest or during performance of various cognitive tasks.

4/11

Version: 12/June/2017
Consent Form

initials: _____

339 Windermere Road
London, Ontario, Canada N6A 5A5
Tel: (519) 685-8500 ext. 33631 • Fax: (519) 663-3753

Experiments involving audiometric assessment

You may be asked to listen to sounds through headphones and report when you detect the sound and when you can no longer hear the sound. This part is expected to take no longer than 12 minutes.

Experiments involving beat/rhythm discrimination

You may be asked to complete auditory tasks involving discrimination of auditory sequences, and/or tapping during or after listening to auditory sequences. For these tasks, auditory sequences will be presented via headphones at a comfortable intensity level. Tapping will be performed on a computer keyboard or external device (e.g., a drum pad) capable of recording tapping information.

Experiments involving affective processing

You might be asked to view pictures and/or sounds that portray either neutral content (e.g., chairs, glasses) or negatively valenced content, some of which is graphic or disturbing in nature (e.g., guns, threat/attack, body mutilation), or a series of faces. Your psychophysiological responses to these stimuli will be monitored at all times during the task using electromyography (EMG), galvanic skin response (GSR), electrocardiography (ECG), heart rate, blood pressure, and respiration.

Experiments involving virtual reality

You might be asked to interact in real-world situations using a virtual reality head set. During the test, your movements will be tracked using cameras. The virtual reality head set creates a virtual environment that you can see and interact with.

Experiments involving driving simulation

You may be asked to perform driving tasks using a driving simulator. During the test you will be sitting in a cockpit designed to replicate a driver's seat and surrounded by large screens. Tests will involve performing driving tasks (i.e. navigation, turning, etc...).

Benefits

Your participation in this study is of no direct benefit to you.

Risks

If you require treatment for any injuries or illness directly related to procedures implemented during the study, or if you suffer side effects while on study medication, you should contact your study doctor as soon as possible. The necessary medical care will be provided to you at no additional cost to you. You do not waive any legal rights by signing the consent form.

5/11

Version: 12/June/2017
Consent Form

initials: _____

339 Windermere Road
London, Ontario, Canada N6A 5A5
Tel: (519) 685-8500 ext. 33631 • Fax: (519) 663-3753

Participants performing computerized tasks

There are no known physical risks associated with performing computerized tasks. You may find some of the tasks dull or tiring.

Experiments involving functional magnetic resonance imaging

The Food & Drug Administration (USA) has indicated that for clinical diagnosis an 'insignificant' risk is associated with human MRI exposure at the intensities used in this project. Current Canadian guidelines follow the USA guidelines. Although very rare, injury and deaths have occurred in MRI units from unsecured metal objects being drawn at high speeds into the magnet or from internal body metal fragments of which the subject was unaware or had not informed MRI staff. To minimize this latter possibility it is essential that you complete a screening questionnaire. Other remote but potential risks involve tissue burns and temporary hearing loss from the loud noise inside the magnet. The latter can be avoided with ear headphone protection that also allows continuous communication between the subject and staff during the study.

This MRI machine uses a strong magnet and radio waves to make images of the body interior. You will be asked to lie on a long narrow couch for an hour while the machine gathers data. During this time you will be exposed to magnetic fields and radio waves. You will not feel either. You will, however, hear repetitive tapping noises that arise from the magnets that surround you. You will be provided with earplugs or headphones that you will be required to wear to minimize the sound and protect your hearing. The space within the large magnet in which you lie is somewhat confined, although we have taken many steps to relieve the "claustrophobic" feeling. There are no known significant risks with this procedure at this time because the radio waves and magnetic fields, at the strengths used, are thought to be without harm. The exception is if you have a cardiac pacemaker, or a metallic clip in your body (e.g., an aneurysm clip in your brain), have severe heart disease, body piercings, tattoos containing metallic ink or slow release pharmaceutical skin patches.

There is a possibility that you will experience a localized twitching sensation due to the magnetic field changes during the scan. This is not unexpected and should not be painful. However, you can stop the exam at anytime. The magnetism and radio waves do not cause harmful effects at the levels used in the MRI machine. However, because the MR scanner uses a very strong magnet that will attract metal, all metallic objects must be removed from your person before you approach the scanner. In addition, watches and credit cards should also be removed as these could be damaged (these items will be watched for you).

Patients with Parkinson's disease

For Parkinson's patients who are tested off of their Parkinson's medications, you likely will experience an increase in your Parkinson's symptoms. If you do not return to your usual level

6/11

Version: 12/June/2017
Consent Form

initials: _____

339 Windermere Road
London, Ontario, Canada N6A 5A5
Tel: (519) 685-8500 ext. 33631 • Fax: (519) 663-3753

of function after resuming your medication at the conclusion of the testing session, you are invited to contact Dr. MacDonald to discuss your concerns as well as medication strategies for getting back to your usual self.

Participants taking dopaminergic therapy

If you are a non-patient volunteer taking levodopa or pramipexole, there is a potential risk of developing side effects following drug administration. More serious side effects reported are based on chronic use of these medications in patients, and are not expected to develop in this study given the single, low-dose of drug administered. Less serious side effects are largely peripheral effects (e.g., nausea) and should be minimized through co-administration of Carbidopa. Any side effects that do occur are temporary and should quickly subside. In the unlikely situation that your symptoms persist, you are invited to contact the experimenter to discuss your concerns.

Less serious side effects include: mild nausea, dry mouth, loss of appetite; heartburn, diarrhea, constipation; headache, dizziness, drowsiness, blurred vision; sneezing, stuffy nose, cough, other cold symptoms; sleep problems (insomnia), strange dreams, muscle pain, numbness/tingly feelings, skin rash/itching. More serious side effects include: severe allergic reactions; restless muscle movements in your eyes, tongue, jaw, or neck; worsening of tremors (uncontrolled shaking); high fever, stiff muscles, sweating, fast or uneven heartbeats, difficulty breathing, feeling like you might pass out; seizure (convulsions); painful or difficult urination; severe nausea, vomiting, or diarrhea; uneven heart rate or fluttering in your chest; confusion, hallucinations, anxiety, agitation, depressed mood, thoughts of suicide or hurting yourself; unusual or intense urges (e.g., gambling, sexual urges); chest pain or heavy feeling, pain spreading to the arm or shoulder.

Experiments involving propranolol

If you are a volunteer taking propranolol, there is a potential risk of developing side effects following drug administration. More serious side effects reported are based on chronic use of these medications in patients, and are not expected to develop in this study given the single, low-dose of drug administered. Any side effects that do occur are temporary and should quickly subside. In the unlikely situation that your symptoms persist, you are invited to contact the experimenter to discuss your concerns.

Less serious side effects include: fatigue; nausea, vomiting, diarrhea, constipation, stomach cramps; decreased sex drive, impotence, of difficulty having an orgasm; trouble concentrating, sleep problems (insomnia). More serious side effects include: severe allergic reactions; fast, slow, or uneven heartbeats; feeling light-headed or fainting; feeling short of breath even with mild exertion; dilated neck veins, swelling of ankles or feet; nausea, upper stomach pain, itching, loss of appetite, dark urine, clay-coloured stools, jaundice (yellowing of skin or eyes);

7/11

Version: 12/June/2017
Consent Form

initials: _____

339 Windermere Road
London, Ontario, Canada N6A 5A5
Tel: (519) 685-8500 ext. 33631 • Fax: (519) 663-3753

cool pale skin; cold feeling in hands or feet; depression, confusion, hallucinations, slurred speech, headache; seizures; severe skin reaction (blistering or peeling skin)

Experiments involving polysomnographic sleep recording and electroencephalography

The only potential risk is for individuals with extremely sensitive skin. These individuals may have a slight skin irritation where the skin has been gently exfoliated during electrode application. When we apply the electrodes to the surface of the skin, we use a gentle, hypoallergenic medical-grade exfoliant, called NuPrep, to clean the skin where the electrodes will be placed. Any mild irritation to the skin normally lasts less than a few hours.

Experiments involving robotic arm manipulation

The principal potential risk is injury caused by the robotic arm. However, injury is very unlikely and we have implemented a range of safety precautions that are widely used for the prevention of injury in studies of human motor control involving robots. A number of safety precautions have been implemented with respect to the robot linkage. In addition to minimizing the applied force, we test for forces at the endpoint. If forces exceed 10 N all forces are immediately set to zero. Additional vendor supplied algorithms limit the workspace over which forces may be applied. Moreover, all experimental protocols were tested in full prior to the experiment. Both you and the experimenter have a switch that instantaneously deactivates the robot. In studies over the past 20 years using this setup at both Western and McGill we have not had a single injury or adverse event.

Experiments involving affective processing

There is the possibility of emotional and/or mental distress resulting from viewing images with extremely graphic, violent, frightening, disturbing, and/or emotionally distressing content and listening to sounds that portray equally upsetting or distressing emotional content. There is also a small possibility that some of the recording electrodes may produce mild skin irritation.

Experiments involving virtual reality

Virtual reality can be disorienting and cause dizziness. The only potential risk is for individuals to develop nausea and vomiting during the task. Before any testing begins, you will undergo a period of acclimatization involving slow movements and interactions in the virtual environment to ensure you are comfortable with performing the task.

Experiments involving driving simulation

Much like virtual reality, the driving simulator can also be disorienting that may lead to nausea and vomiting. Before any testing begins, you will undergo a period of acclimatization involving slow movements and interactions in the virtual environment to ensure you are comfortable with performing the task.

8/11

Version: 12/June/2017
Consent Form

initials: _____

339 Windermere Road
London, Ontario, Canada N6A 5A5
Tel: (519) 685-8500 ext. 33631 • Fax: (519) 663-3753

Confidentiality

The investigators will maintain all information collected in this study strictly confidential, shared only with individuals directly involved in this study, except as may be required by court order or by law. To further ensure your confidentiality, information collected from you will be devoid of any unique personal identifier and will be filed under an anonymous subject number. If any publication or presentation results from this research, you will not be referred to by name and no potentially identifying information will be released. The information collected in the course of this study is kept on file in a secure location for no less than 25 years. If you decide you do not want this information to be kept on file, simply advise the research team of your wishes, and your record will be destroyed.

Consent to Use and Disclose Information for Research subjects

Representatives of the University of Western Ontario Health Sciences Research Ethics Board might be granted direct access to your medical records. A representative of the University of Western Ontario Health Sciences Research Ethics Board might contact you or might require access to your study-related records to monitor the conduct of the research. By signing the consent, you also permit the principal investigator to use and disclose health information about yourself for the purposes of this study.

Incidental Findings

The tests you undergo in this study are not intended to diagnose or monitor any medical conditions you may have. Nevertheless, if information that might be relevant to your care is discovered incidentally, this information will be communicated to you, and at your request, to your physician.

Compensation

You will receive \$20-50 depending on the length (1.5hrs vs. 3hrs) and type (behavioural only vs. behavioural with an MRI component) of study in which you are taking part. This is to compensate you for the time and inconvenience associated with your participation. You will also be reimbursed for parking costs.

Voluntary Participation/Withdrawal from the Study

Your participation in this research is completely voluntary. You may refuse to continue performing the tasks in this study at any time without any consequences. You may refuse to participate, refuse to answer any questions or withdraw from the study at any time with no effect on your future care. You do not waive any of your legal rights by signing the consent form. If the research investigators find it necessary, and/or in your best interest, you will be asked to withdraw from the study. In the event that you withdraw from the study for any reason, you will receive compensation for the sessions that you attended, even if you did not complete the entire session. Your cost of parking will also be reimbursed.

9/11

Version: 12/June/2017
Consent Form

initials: _____

339 Windermere Road
London, Ontario, Canada N6A 5A5
Tel: (519) 685-8500 ext. 33631 • Fax: (519) 663-3753

Contact Information

If you have any questions or concerns regarding the study, you may contact the principle investigator. If you wish to speak to a neutral individual who is not involved in the study at all and who will answer any questions about your rights as a research participant or about the conduct of the study, you may contact Dr. David Hill, Scientific Director, Lawson Health Research Institute (519) 667-6649.

Results

If you're interested in obtaining the results of the study, we will gladly provide you with a summary of our findings once the research is complete. Please let the investigator know if you would like a summary of the results mailed or emailed to you.

10/11

Version: 12/June/2017
Consent Form

initials: _____

339 Windermere Road
London, Ontario, Canada N6A 5A5
Tel: (519) 685-8500 ext. 33631 • Fax: (519) 663-3753

Consent Form

Distinguishing the roles of ventral and dorsal striatum in cognition

Principle Investigator: Penny A. MacDonald, MD, PhD

I (_____) have read the Letter of Information and Consent form and have had the nature of the study explained to me and I agree to participate. All questions have been answered to my satisfaction. I have been provided a copy of the Recruitment/Information Letters and the Consent form. I freely and voluntarily consent to participate in this study.

Signature of participant

Date

Your signature on this form indicates that you are acting as a substitute decision maker(s) for the participant and the study has been explained to you and all your questions have been answered to your satisfaction. You agree to allow the person you represent to take part in the study. You know that the person you represent can leave the study any time.

Signature of substitute decision maker
(if applicable)

Relationship to Participant

Date

Signature of investigator

Date

I have discussed this clinical research study with the participant using a language that is understandable and appropriate. I believe that I have fully informed this participant of the purpose, duration etc. of this research study and its possible benefits and risks and I believe the participant understood this explanation.

Signature of person assisting in consent process

Date

11/11

Version: 12/June/2017
Consent Form

initials: _____

339 Windermere Road
London, Ontario, Canada N6A 5A5
Tel: (519) 685-8500 ext. 33631 • Fax: (519) 663-3753

Appendix C: Health & Demographics Questionnaire

Please print and fill out this form as accurately as possible and bring it with you to your first appointment session. If you are attending your appointment with another participant, please ensure you both have your own personal copies filled out.

1. Basic Demographic Information

Date of Birth: _____ Age: _____

Weight: _____ Height: _____

Sex: _____ Handedness: _____

First language: _____ Other languages: _____

Level of Education and total years (e.g. 4 years high school, 4 years university, etc.)

Occupation: _____

2. Health-Related Information

A. Smoking History (please circle): Never Smoker Ex-Smoker Current Smoker

If current smoker, indicate how many years and how many cig/day: _____

If ex-smoker, indicate year that you quit; how many years smoking; how many cig/day:

B. Alcohol History

Average number of drinks per week: _____

Has there ever been heavy alcohol consumption? (please circle) Yes No

If yes, when, for how long, and estimate your weekly alcohol consumption during that time:

C. Other Drug History

Have you ever taken street drugs or other drugs that were not prescribed by a physician? (please circle)

Yes No

If yes, when, what drugs, how frequently and over what period of time?

D. Eye Glasses (only if applicable)

What is the prescription of your eye glasses? _____

Without the aid of glasses are you able to see near objects well? (please circle) Yes No

Without the aid of glasses are you able to see far objects well? (please circle) Yes No

E. Parkinson's Disease (only if applicable)

What year were you diagnosed with Parkinson's disease? _____

Which side of the body is *more* affected? _____

3. Previous Medical Problems

Have you had any major health problems, or do you have any chronic, ongoing medical conditions such as high blood pressure, high cholesterol, diabetes, thyroid problems, multiple sclerosis or epilepsy? Have you had any strokes, heart attacks/ heart surgeries, significant head trauma, or cancer? If you've had cancer, what kind and what treatments did you receive (e.g. chemotherapy)? Have you ever had more than one seizure? Answer in the space below.

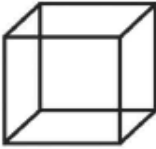
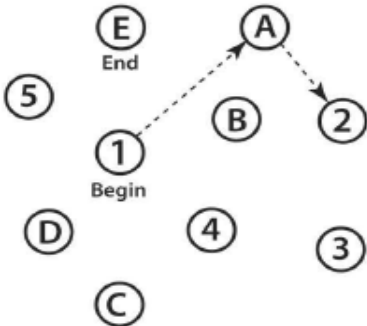
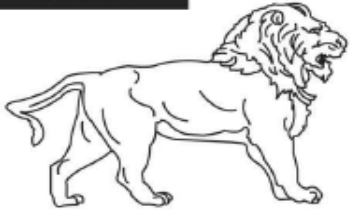
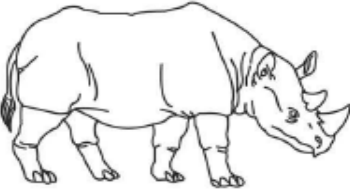
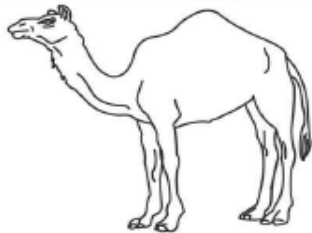
4. Family Medical Problems

Is there anyone in your family with a neurological or serious psychiatric illness such as PD, Huntington's, epilepsy, strokes at a young age (< 50 for men and < 60 for women)? Is there anyone who had trouble walking or with balance, needing a wheelchair or a walker at a young age? Any family members with dementia (such as Alzheimer's), schizophrenia, bipolar/manic depression, or severe depression or anxiety requiring hospitalization or close follow up by a psychiatrist? Answer in the space below.

5. Current Medication

Please list any medications you are currently taking, what they are treating for specifically, and the prescribed dosage.

Appendix D: Montreal Cognitive Assessment

MONTREAL COGNITIVE ASSESSMENT (MOCA) Version 7.1 Original Version					NAME : Education : Sex :	Date of birth : DATE :			
VISUOSPATIAL / EXECUTIVE		 Copy cube		Draw CLOCK (Ten past eleven) (3 points)		POINTS			
		<input type="checkbox"/>		<input type="checkbox"/>		___/5			
NAMING		 <input type="checkbox"/>		 <input type="checkbox"/>		 <input type="checkbox"/>		___/3	
MEMORY		Read list of words, subject must repeat them. Do 2 trials, even if 1st trial is successful. Do a recall after 5 minutes.		FACE	VELVET	CHURCH	DAISY	RED	No points
		1st trial	2nd trial						
ATTENTION		Read list of digits (1 digit/ sec). Subject has to repeat them in the forward order		<input type="checkbox"/> 2 1 8 5 4				___/2	
		Subject has to repeat them in the backward order		<input type="checkbox"/> 7 4 2					
LANGUAGE		Repeat : I only know that John is the one to help today. <input type="checkbox"/> The cat always hid under the couch when dogs were in the room. <input type="checkbox"/>						___/2	
		Fluency / Name maximum number of words in one minute that begin with the letter F		<input type="checkbox"/> _____ (N ≥ 11 words)				___/1	
ABSTRACTION		Similarity between e.g. banana - orange = fruit		<input type="checkbox"/> train - bicycle		<input type="checkbox"/> watch - ruler		___/2	
DELAYED RECALL		Has to recall words WITH NO CUE		FACE	VELVET	CHURCH	DAISY	RED	Points for UNCUED recall only
		Category cue							
Optional		Multiple choice cue							
ORIENTATION		<input type="checkbox"/> Date		<input type="checkbox"/> Month		<input type="checkbox"/> Year		<input type="checkbox"/> Day	
		<input type="checkbox"/> Place		<input type="checkbox"/> City				___/6	
© Z.Nasreddine MD		www.mocatest.org		Normal ≥ 26 / 30		TOTAL		___/30	
Administered by: _____						Add 1 point if ≤ 12 yr edu			

Appendix E: Montreal Cognitive Assessment Evaluation Scale

MoCA Version August 18, 2010 © Z. Nasreddine MD www.mocatest.org

Montreal Cognitive Assessment (MoCA) Administration and Scoring Instructions

The Montreal Cognitive Assessment (MoCA) was designed as a rapid screening instrument for mild cognitive dysfunction. It assesses different cognitive domains: attention and concentration, executive functions, memory, language, visuoconstructional skills, conceptual thinking, calculations, and orientation. Time to administer the MoCA is approximately 10 minutes. The total possible score is 30 points; a score of 26 or above is considered normal.

1. Alternating Trail Making:

Administration: The examiner instructs the subject: *"Please draw a line, going from a number to a letter in ascending order. Begin here [point to (1)] and draw a line from 1 then to A then to 2 and so on. End here [point to (E)]."*

Scoring: Allocate one point if the subject successfully draws the following pattern:

1 –A- 2- B- 3- C- 4- D- 5- E, without drawing any lines that cross. Any error that is not immediately self-corrected earns a score of 0.

2. Visuoconstructional Skills (Cube):

Administration: The examiner gives the following instructions, pointing to the **cube**: *"Copy this drawing as accurately as you can, in the space below"*.

Scoring: One point is allocated for a correctly executed drawing.

- Drawing must be three-dimensional
- All lines are drawn
- No line is added
- Lines are relatively parallel and their length is similar (rectangular prisms are accepted) A point is not assigned if any of the above-criteria are not met.

3. Visuoconstructional Skills (Clock):

Administration: Indicate the right third of the space and give the following instructions: *"Draw a **clock**. Put in all the numbers and set the time to 10 past 11"*.

Scoring: One point is allocated for each of the following three criteria:

- Contour (1 pt.): the clock face must be a circle with only minor distortion acceptable (e.g., slight imperfection on closing the circle);
- Numbers (1 pt.): all clock numbers must be present with no additional numbers; numbers must be in the correct order and placed in the approximate quadrants on the clock face; Roman numerals are acceptable; numbers can be placed outside the circle contour;
- Hands (1 pt.): there must be two hands jointly indicating the correct time; the hour hand must be clearly shorter than the minute hand; hands must be centred within the clock face with their junction close to the clock centre.

A point is not assigned for a given element if any of the above-criteria are not met.

4. Naming:

Administration: Beginning on the left, point to each figure and say: *“Tell me the name of this animal”*.

Scoring: One point each is given for the following responses: (1) lion (2) rhinoceros or rhino (3) camel or dromedary.

5. Memory:

Administration: The examiner reads a list of 5 words at a rate of one per second, giving the following instructions: *“This is a memory test. I am going to read a list of words that you will have to remember now and later on. Listen carefully. When I am through, tell me as many words as you can remember. It doesn’t matter in what order you say them”*.

Mark a check in the allocated space for each word the subject produces on this first trial. When the subject indicates that (s)he has finished (has recalled all words), or can recall no more words, read the list a second time with the following instructions: *“I am going to read the same list for a second time. Try to remember and tell me as many words as you can, including words you said the first time.”*

Put a check in the allocated space for each word the subject recalls after the second trial. At the end of the second trial, inform the subject that (s)he will be asked to recall these words again by saying, *“I will ask you to recall those words again at the end of the test.”*

Scoring: No points are given for Trials One and Two.

6. Attention: Forward Digit Span:

Administration: Give the following instruction: *“I am going to say some numbers and when I am through, repeat them to me exactly as I said them”*. Read the five number sequence at a rate of one digit per second.

Backward Digit Span:

Administration: Give the following instruction: *“Now I am going to say some more numbers, but when I am through you must repeat them to me in the backwards order.”* Read the three number sequence at a rate of one digit per second.

Scoring: Allocate one point for each sequence correctly repeated, (*N.B.*: the correct response for the backwards trial is 2-4-7).

Vigilance:

Administration: The examiner reads the list of letters at a rate of one per second, after giving the following instruction: *“I am going to read a sequence of letters. Every time I say the letter A, tap your hand once. If I say a different letter, do not tap your hand”*.

Scoring: Give one point if there is zero to one errors (an error is a tap on a wrong letter or a failure to tap on letter A).

Serial 7s:

Administration: The examiner gives the following instruction: *“Now, I will ask you to count by subtracting seven from 100, and then, keep subtracting seven from your answer until I tell you to stop.”* Give this instruction twice if necessary.

Scoring: This item is scored out of 3 points. Give no (0) points for no correct subtractions, 1 point for one correction subtraction, 2 points for two-to-three correct subtractions, and 3 points if the participant successfully makes four or five correct subtractions. Count each correct subtraction of 7 beginning at 100. Each subtraction is evaluated independently; that is, if the participant responds with an incorrect number but continues to correctly subtract 7 from it, give a point for each correct subtraction. For example, a participant may respond “92 – 85 – 78 – 71 – 64” where the “92” is incorrect, but all subsequent numbers are subtracted correctly. This is one error and the item would be given a score of 3.

7. Sentence Repetition:

Administration: The examiner gives the following instructions: *“I am going to read you a sentence. Repeat it after me, exactly as I say it [pause]: **I only know that John is the one to help today.**”*

Following the response, say: *“Now I am going to read you another sentence. Repeat it after me, exactly as I say it [pause]: **The cat always hid under the couch when dogs were in the room.**”*

Scoring: Allocate 1 point for each sentence correctly repeated. Repetition must be exact. Be alert for errors that are omissions (e.g., omitting “only”, “always”) and substitutions/additions (e.g., “John is the one who helped today;” substituting “hides” for “hid”, altering plurals, etc.).

8. Verbal fluency:

Administration: The examiner gives the following instruction: *“Tell me as many words as you can think of that begin with a certain letter of the alphabet that I will tell you in a moment. You can say any kind of word you want, except for proper nouns (like Bob or Boston), numbers, or words that begin with the same sound but have a different suffix, for example, love, lover, loving. I will tell you to stop after one minute. Are you ready? [Pause] Now, tell me as many words as you can think of that begin with the letter F. [time for 60 sec]. Stop.”*

Scoring: Allocate one point if the subject generates 11 words or more in 60 sec. Record the subject’s response in the bottom or side margins.

9. Abstraction:

Administration: The examiner asks the subject to explain what each pair of words has in common, starting with the example: *“Tell me how an orange and a banana are alike”*. If the subject answers in a concrete manner, then say only one additional time: *“Tell me another way in which those items are alike”*. If the subject does not give the appropriate response (*fruit*), say, *“Yes, and they are also both fruit.”* Do not give any additional instructions or clarification. After the practice trial, say: *“Now, tell me how a train and a bicycle are alike”*. Following the response, administer the second trial, saying: *“Now tell me how a ruler and a watch are alike”*.

Do not give any additional instructions or prompts.

Scoring: Only the last two item pairs are scored. Give 1 point to each item pair correctly answered. The following responses are acceptable:

Train-bicycle = means of transportation, means of travelling, you take trips in both;
Ruler-watch = measuring instruments, used to measure.

The following responses are **not** acceptable: Train-bicycle = they have wheels; Ruler-watch = they have numbers.

10. Delayed recall:

Administration: The examiner gives the following instruction: *“I read some words to you earlier, which I asked you to remember. Tell me as many of those words as you can remember.”* Make a check mark for each of the words correctly recalled spontaneously without any cues, in the allocated space.

Scoring: **Allocate 1 point for each word recalled freely without any cues.**

Optional: Following the delayed free recall trial, prompt the subject with the semantic category cue provided below for any word not recalled. Make a check mark (√) in the allocated space if the subject remembered the word with the help of a category or multiple-choice cue. Prompt all non-recalled words in this manner. If the subject does not recall the word after the category cue, give him/her a multiple-choice trial, using the following example instruction,

“Which of the following words do you think it was, NOSE, FACE, or HAND?”

Use the following category and/or multiple-choice cues for each word, when appropriate:

FACE: category cue: part of the body multiple choice: nose, face, hand

VELVET: category cue: type of fabric multiple choice: denim, cotton, velvet

CHURCH: category cue: type of building multiple choice: church, school, hospital

DAISY: category cue: type of flower multiple choice: rose, daisy, tulip

RED: category cue: a colour multiple choice: red, blue, green

Scoring: **No points are allocated for words recalled with a cue.** A cue is used for clinical information purposes only and can give the test interpreter additional information about the type of memory disorder. For memory deficits due to retrieval failures, performance can be improved with a cue. For memory deficits due to encoding failures, performance does not improve with a cue.

11. Orientation:

Administration: The examiner gives the following instructions: “Tell me the date today”. If the subject does not give a complete answer, then prompt accordingly by saying: *“Tell me the [year, month, exact date, and day of the week].”* Then say: *“Now, tell me the name of this place, and which city it is in.”*

Scoring: Give one point for each item correctly answered. The subject must tell the exact date and the exact place (name of hospital, clinic, office). No points are allocated if subject makes an error of one day for the day and date.

TOTAL SCORE: Sum all sub-scores listed on the right-hand side. Add one point for an individual who has 12 years or fewer of formal education, for a possible maximum of 30 points. A final total score of 26 and above is considered normal.

UPDRS Protocol

Ask at the start *“which arm/hand do you have most difficulty with?”*

Always start with **LESS** impaired side

Only model for a few seconds, then stop

“This is subject (PD/CTRL #), session #, (on/off) medication.”

1. Film face at rest for a few seconds
2. Ask patient to speak one-two sentences (for dysarthria)
 - *“Today is a very nice day outside”*
 - *“I am at the University for an experiment”*
3. Evaluate resting tremor
 1. hands relaxed on thighs
 2. with cognitive stressing *“Close your eyes and name the months of the year backward from December”*
4. Evaluate tone
 - a. Bilateral upper extremities
5. Evaluate postural tremor
 - a. Hands outstretched
 - b. Fingertips apposed (forming wings with arms ensuring fingers are not touching)
6. Evaluate action tremor
 - a. Finger-to-nose (finger target should be arms-length away and in same position)
7. Evaluate bradykinesia
 - a. Finger taps (pinching) *“Big and fast”*
 - b. Hand opening-closing movements *“Big and fast”*
 - c. Pronation-supination movements *“Fast as you can”*
 - d. Toe-tapping (minimum 3 inches off ground)
8. Ask patient to rise from the chair without the assistance of his/her arms (arms crossed over chest) *“Fold your arms across and chest and stand up”*
9. Evaluate gait, ask to walk up and down hallway 2-3 times, with turns
10. Pull test *“Try to maintain your balance and limit yourself to one step backwards”*

Appendix G: Covariate Analysis for Age and Sex

QSM: $2 \times 2 \times 2$ RM-ANCOVA p -values for Age and Sex covariate main effects and interactions of the SNc, SNr, and VTA. Significant values after Benjamini-Hochberg correction are shown in bold font.

Main Effect	Age	Sex
SNc	.923	.453
SNr	.002 *	< .001 *
VTA	.948	.663

Interaction	Hemisphere*Age	Hemisphere*Sex
SNc	.086	.672
SNr	.830	.717
VTA	.150	.794

Interaction	Scanner*Age	Scanner*Sex
SNc	.405	.388
SNr	.599	.149
VTA	.338	.362

Interaction	Hemisphere*Scanner*Age	Hemisphere*Scanner*Sex
SNc	.072	.838
SNr	.268	.874
VTA	.001 *	.071

QSM 3T: 2×2 RM-ANCOVA p -values for Age and Sex covariate main effects and interactions of the SNc, SNr, and VTA. Significant values after Benjamini-Hochberg correction are shown in bold font.

Main Effect	Age	Sex
SNc	.427	.477
SNr	.059	.062
VTA	.202	.678

Interaction	Hemisphere*Age	Hemisphere*Sex
SNc	.011	.780
SNr	.555	.577
VTA	.073	.316

QSM 7T: 2×2 RM-ANCOVA p -values for Age and Sex covariate main effects and interactions of the SNc, SNr, and VTA. Significant values after Benjamini-Hochberg correction are shown in bold font.

Main Effect	Age	Sex
SNc	.551	.885
SNr	.007	< .001 *
VTA	.459	.873

Interaction	Hemisphere*Age	Hemisphere*Sex
SNc	.970	.617
SNr	.334	.859
VTA	.124	.978

R2*: 2 × 2 × 2 RM-ANCOVA *p*-values for Age and Sex covariate main effects and interactions of the SNc, SNr, and VTA. Significant values after Benjamini-Hochberg correction are shown in bold font.

Main Effect	Age	Sex
SNc	.153	.626
SNr	.238	.564
VTA	.838	.625

Interaction	Hemisphere*Age	Hemisphere*Sex
SNc	.799	.122
SNr	.641	.286
VTA	.740	.095

Interaction	Scanner*Age	Scanner*Sex
SNc	.090	.074
SNr	.245	.848
VTA	.744	.382

Interaction	Hemisphere*Scanner*Age	Hemisphere*Scanner*Sex
SNc	.528	.340
SNr	.791	.817
VTA	.991	.011

R2* 3T: 2 × 2 RM-ANCOVA *p*-values for Age and Sex covariate main effects and interactions of the SNc, SNr, and VTA. Significant values after Benjamini-Hochberg correction are shown in bold font.

Main Effect	Age	Sex
SNc	.994	.292
SNr	.081	.674
VTA	.667	.620

Interaction	Hemisphere*Age	Hemisphere*Sex
SNc	.815	.851
SNr	.608	.288
VTA	.333	.875

R2* 7T: 2 × 2 RM-ANCOVA *p*-values for Age and Sex covariate main effects and interactions of the SNc, SNr, and VTA. Significant values after Benjamini-Hochberg correction are shown in bold font.

Main Effect	Age	Sex
SNc	.038	.251
SNr	.687	.721
VTA	.712	.347

Interaction	Hemisphere*Age	Hemisphere*Sex
SNc	.542	.119
SNr	.675	.456
VTA	.813	.006

Appendix H: ROC Curve Analyses of Left and Right Hemisphere of the SNc

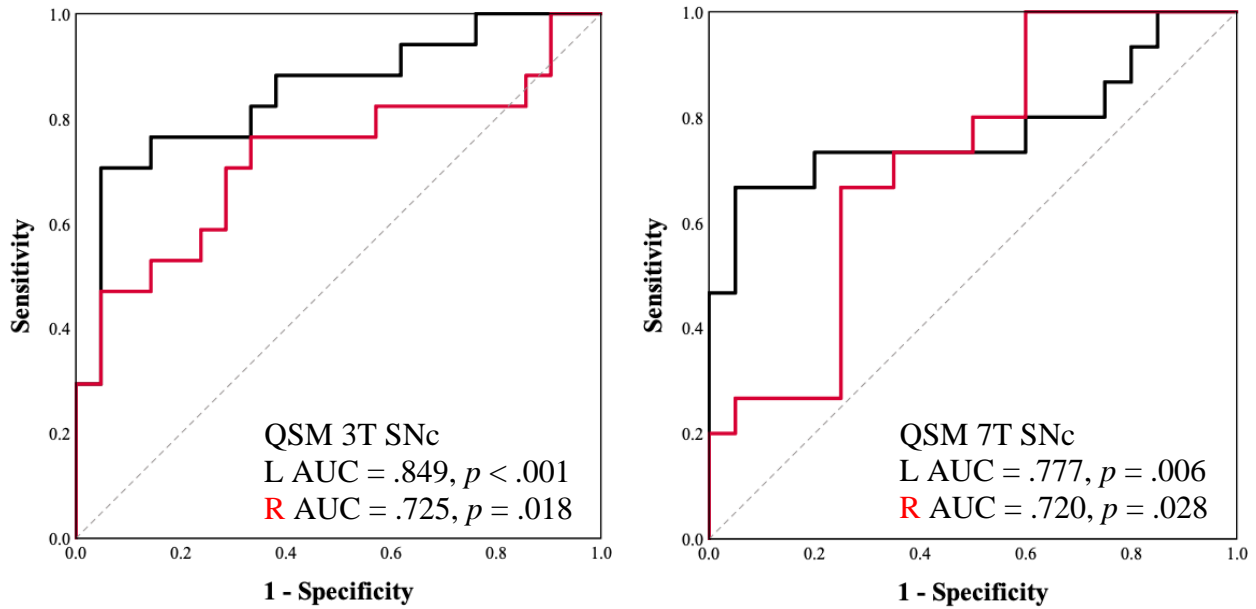


Figure S1. ROC Curves for Left and Right Hemisphere of the SNc for QSM at 3T and 7T. Left (black) and right (red) hemisphere shown with AUCs and respective p values reported. $n_{CT} = 21$, $n_{PD} = 17$.

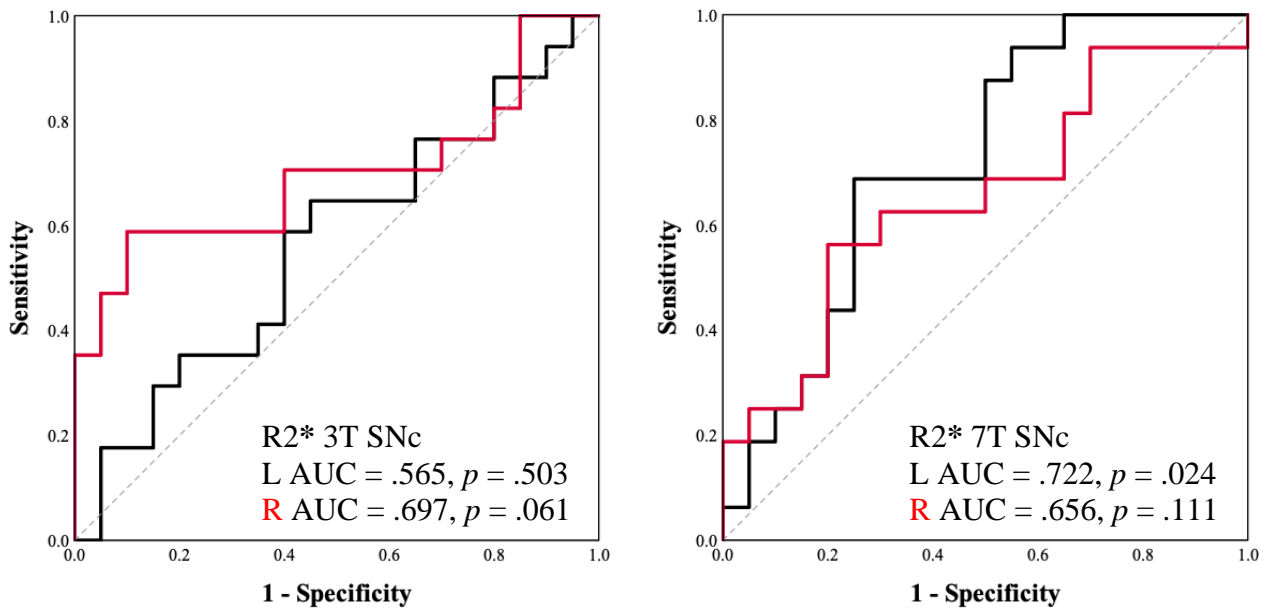



Figure S2. ROC Curves for Left and Right Hemisphere of the SNc for R2* at 3T and 7T. Left (black) and right (red) hemisphere shown with AUCs and respective p values reported. $n_{CT} = 21$, $n_{PD} = 17$.

Left hemisphere appears to have higher AUC values than right hemisphere likely due to our sample having more PD patients who were *right* body side affected suggesting the *left* hemisphere would be more affected. QSM still boasts larger AUCs than R2* relaxometry.

Appendix I: Ethics Approval

	<h1 style="margin: 0;">Western Research</h1>	<p style="margin: 0;">Research Ethics</p>																								
<p style="margin: 0;">Western University Health Science Research Ethics Board HSREB Amendment Approval Notice</p>																										
<p>Principal Investigator: Dr. Penny MacDonald Department & Institution: Schulich School of Medicine and Dentistry/Clinical Neurological Sciences, London Health Sciences Centre</p>																										
<p>Review Type: Full Board HSREB File Number: 102018 Study Title: Distinguishing the roles of ventral and dorsal striatum in cognition (REB #18517) Sponsor: Canadian Excellence Research Chair</p>																										
<p>HSREB Amendment Approval Date: December 18, 2015 HSREB Expiry Date: November 29, 2016</p>																										
<p>Documents Approved and/or Received for Information:</p> <table border="1" style="width: 100%; border-collapse: collapse;"> <thead> <tr> <th style="text-align: left;">Document Name</th> <th style="text-align: left;">Comments</th> <th style="text-align: left;">Version Date</th> </tr> </thead> <tbody> <tr> <td>Amendment</td> <td>List of changes to ethics protocol and consent form</td> <td>2015/11/19</td> </tr> <tr> <td>Revised Western University Protocol</td> <td>Marked version of updated ethics protocol</td> <td>2015/11/19</td> </tr> <tr> <td>Instruments</td> <td>UPPS-P Impulsive Behavior Scale</td> <td>2015/11/19</td> </tr> <tr> <td>Instruments</td> <td>Domain Specific Risk Taking Scale DOSPRT</td> <td>2015/11/19</td> </tr> <tr> <td>Instruments</td> <td>Behavioral Inhibition/Approach Scale BIS/BAS Scale</td> <td>2015/11/19</td> </tr> <tr> <td>Revised Letter of Information & Consent</td> <td></td> <td>2015/11/19</td> </tr> <tr> <td>Revised Western University Protocol</td> <td></td> <td>2015/11/19</td> </tr> </tbody> </table>			Document Name	Comments	Version Date	Amendment	List of changes to ethics protocol and consent form	2015/11/19	Revised Western University Protocol	Marked version of updated ethics protocol	2015/11/19	Instruments	UPPS-P Impulsive Behavior Scale	2015/11/19	Instruments	Domain Specific Risk Taking Scale DOSPRT	2015/11/19	Instruments	Behavioral Inhibition/Approach Scale BIS/BAS Scale	2015/11/19	Revised Letter of Information & Consent		2015/11/19	Revised Western University Protocol		2015/11/19
Document Name	Comments	Version Date																								
Amendment	List of changes to ethics protocol and consent form	2015/11/19																								
Revised Western University Protocol	Marked version of updated ethics protocol	2015/11/19																								
Instruments	UPPS-P Impulsive Behavior Scale	2015/11/19																								
Instruments	Domain Specific Risk Taking Scale DOSPRT	2015/11/19																								
Instruments	Behavioral Inhibition/Approach Scale BIS/BAS Scale	2015/11/19																								
Revised Letter of Information & Consent		2015/11/19																								
Revised Western University Protocol		2015/11/19																								
<p>The Western University Health Science Research Ethics Board (HSREB) has reviewed and approved the amendment to the above named study, as of the HSREB Initial Approval Date noted above.</p>																										
<p>HSREB approval for this study remains valid until the HSREB Expiry Date noted above, conditional to timely submission and acceptance of HSREB Continuing Ethics Review.</p>																										
<p>The Western University HSREB operates in compliance with the Tri-Council Policy Statement Ethical Conduct for Research Involving Humans (TCPS2), the International Conference on Harmonization of Technical Requirements for Registration of Pharmaceuticals for Human Use Guideline for Good Clinical Practice Practices (ICH E6 R1), the Ontario Personal Health Information Protection Act (PHIPA, 2004), Part 4 of the Natural Health Product Regulations, Health Canada Medical Device Regulations and Part C, Division 5, of the Food and Drug Regulations of Health Canada.</p>																										
<p>Members of the HSREB who are named as Investigators in research studies do not participate in discussions related to, nor vote on such studies when they are presented to the REB.</p>																										
<p>The HSREB is registered with the U.S. Department of Health & Human Services under the IRB registration number IRB 00000940.</p>																										
<p>_____ Ethics Officer, on behalf of Dr. Joseph Gilbert, HSREB Chair</p>																										
<p>Ethics Officer to Contact for Further Information: Erika Beale <input type="checkbox"/> Nicole Kanko <input type="checkbox"/> Grace Kelly <input checked="" type="checkbox"/> Mira Mehrotra <input type="checkbox"/> Viki Tran <input type="checkbox"/></p>																										
<p><small>This is an official document. Please retain the original in your files.</small></p>																										
<p>Western University, Research, Support Services Bldg., Rm. 5150 London, ON, Canada N6G 1G9 t: 519.661.3036 f: 519.850.2465 www.uwo.ca/research/ethics</p>																										

Curriculum Vitae

Name: Erind Alushaj

Education: Western University
London, ON, Canada
2017 - 2019 M.Sc.

University of Toronto
Toronto, ON, Canada
2012 – 2016 B.Sc.

Honours and Awards: Frederick Banting and Charles Best Canada Graduate Scholarship Masters
2018-2019
Parkinson Society Southwestern Ontario Graduate Student Scholarship
2018-2019
Canadian Association for Neuroscience Meeting Travel Award 2019
Canadian Psychological Association Certificate of Academic Excellence
(Honours Thesis) 2016
Vincent Bladen In-course Scholarship 2014-2015
A.D. Allen Memorial Scholarship 2013-2014
F.A. Urquhart Entrance Scholarship 2012-2013
Governor General's Bronze Academic Medal 2012-2013
University of Toronto Scholar In-course Awards 2012-2016
Honours/Dean's List Awards 2012-2016

Related Work Experience: Behavioural Neuroscience Research Volunteer 2016-2017
University of Toronto, LiMBiC Lab

Neuroscience Co-op Student 2014-2015
St. Michael's Hospital, Schweizer Lab

Neuroscience Lab Assistant 2013-2014
University of Toronto, Niemeier Lab

Publications:
Nguyen D, **Alushaj E**, Erb S & Ito R. (2019) Dissociative effects of dorsomedial striatum D1 and D2 receptor antagonism in the regulation of anxiety and learned approach-avoidance conflict resolution. *Neuropharmacology*, 146, 222-230. <https://doi.org/10.1016/j.neuropharm.2018.11.040>